# Benchmarking the ignition prediction capability of B-RISK using furniture calorimeter and room-size experiments

by

**Shahriar Sazegara**

Supervised by

Associate Professor Michael Spearpoint

Greg Baker (BRANZ Ltd & SP Fire Research AS)

March 2016

A thesis submitted in partial fulfilment of the requirements for the degree of

Master of Engineering in Fire Engineering

Department of Civil and Natural Resources Engineering

University of Canterbury

Christchurch, New Zealand

# ABSTRACT

A fire zone model called B-RISK has been developed and part of this work is to benchmark its capability to predict item ignition in multi-object compartment fire simulations. A series of fire experiments have been conducted which measured single item ignition times under the furniture calorimeter and in the ISO 9705 room. These experiments used mock-up furniture items created from three common materials found in most households in New Zealand. B-RISK uses the flux time product (FTP) method to predict ignition of items based on radiation received using the point source model (PSM). This thesis presents an analysis of the B-RISK predictions compared to the experimental measurements. Due to the mathematical formulation of the PSM and FTP method, it is found that the predicted ignition time is sensitive to the distance between the radiative source and the item. Predicted ignition times of armchairs constructed of PU foam were within 14% of the ISO 9705 room experimental results. However for the furniture calorimeter experiments it is found that to get reasonable predicted ignition times for the mock-up armchair and TV items there is a need to account for the burner flame movement by adjusting the radial distance. Direct flame contact was required to ignite the mock-up cabinetry items and B-RISK was unable to successfully predict this ignition time.

Deputy Vice-Chancellor's Office
Postgraduate Office

UNIVERSITY OF CANTERBURY
*Te Whare Wānanga o Waitaha*
CHRISTCHURCH NEW ZEALAND

# Co-Authorship Form

This form is to accompany the submission of any thesis that contains research reported in co-authored work that has been published, accepted for publication, or submitted for publication. A copy of this form should be included for each co-authored work that is included in the thesis. Completed forms should be included at the front (after the thesis abstract) of each copy of the thesis submitted for examination and library deposit.

Please indicate the chapter/section/pages of this thesis that are extracted from co-authored work and provide details of the publication or submission from the extract comes:

*Some of the content of Chapter 3 was extracted from the co-authored work: Baker, G B, Collier, P C, Wade, C A, Spearpoint, M.J., Fleischmann, C.M., Frank, K. and Sazegara, S A comparison of a priori modelling predictions with experimental results to validate a design fire generator submodel. San Francisco, CA, USA: 13th International Fire and Materials Conference 2013, 28-30 Jan 2013.*

Please detail the nature and extent (%) of contribution by the candidate:

*My contribution was being involved with setting up the experiments and taking part in the review of the final paper. The extent of the contribution was 15% overall.*

**Certification by Co-authors:**

If there is more than one co-author then a single co-author can sign on behalf of all
The undersigned certifys that:

- The above statement correctly reflects the nature and extent of the candidate's contribution to this co-authored work
- In cases where the candidate was the lead author of the co-authored work he or she wrote the text

Name: *Shahriar Sazegara* Signature:  Date: *30/03/16*

Name: *Michael Spearpoint* Signature:  Date: *30 Mar 2016*

*(on behalf of all other co-authors)*

# ACKNOWLEDGEMENTS

The author would like to offer sincere thanks to the following people and organisations that have assisted with this research, including:

Supervisors associate Professor Mike Spearpoint and Greg Baker for generously giving their time, knowledge and guidance throughout my research.

The University of Canterbury and Fire Engineering programme, including other academic staff Professor Andy Buchanan, Professor Charley Fleischman and Dr Tony Abu.

The Foundation for Research, Science and Technology for providing funding for the project

BRANZ Ltd for providing the project itself; with special thanks to Colleen Wade and Peter Collier of BRANZ Ltd for their support.

Finally, my wife Saji and family for the continuous motivation they have provided throughout my studies and life.

# Table of Contents

## List of Figures

# List of Tables

# NOMENCLATURE

| | | |
|---|---|---|
| $c$ | specific heat of the material | (kJ/kg K) |
| $FTP$ | The Flux Time Product | ($kWs^{1/n}m^2$) |
| $h_c$ | Convective heat transfer coefficient | ($kW/m^2$ K) |
| $k$ | Thermal conductivity | (W/m K) |
| $n$ | The flux time product index | ( - ) |
| $\dot{Q}$ | Heat release rate of fire | (kW) |
| $\dot{q}^{"}$ | Radiant heat flux | ($kW/m^2$) |
| $\dot{q}^{"}_{cr}$ | Critical heat flux | ($kW/m^2$) |
| $\dot{q}^{"}_{fl}$ | Flaming item heat flux | ($kW/m^2$) |
| $R$ | Distance from point source to target | (m) |
| $T_o$ | Ambient temperature | (K) |
| $t$ | Time | (s) |
| $t_{ig}$ | Time-to-ignition | (s) |
| $\Delta H_C$ | Heat of combustion | (kJ/kg) |
| $\Delta H_{C,eff}$ | The effective heat of combustion | (MJ/kg) |

## Greek Symbols

| | | |
|---|---|---|
| $\alpha$ | Thermal diffusivity | $(k/\rho c)$ $(m^2/s)$ |
| $\rho$ | Density | $(kg/m^3)$ |
| $\varepsilon$ | Emissivity | ( - ) |
| $\sigma$ | Stefan-Boltzmann Constant | $(5.67x10^{-11}$ $kW/m^2$ $K^4)$ |
| $\theta$ | Angle between normal to target and line of sight from target to point source location | (radians) |
| $\lambda_r$ | Radiative fraction | ( - ) |

## List of abbreviations

| | |
|---|---|
| ISO | International Organisation for Standardisation |
| NI | No ignition |
| SD | Standard deviation |
| DFG | Design Fire Generator |
| HRRPUA | Heat release rate per unit area |

# Chapter One

# INTRODUCTION

## 1.1 Background

The fire growth process in compartments is of interest to fire engineers, with insight into the being obtained from experiments and models. Fire engineers make extensive use of computer simulations to design buildings for fire safety in which there are generically two types of fire models in common use; zone models and field models. The focus of this thesis is two-zone fire models where a compartment is divided into two specific zones; a hot upper layer and a cool lower layer. For each zone, conservation equations of mass and energy are solved and predictions made of layer height, average zone temperature, average zone species concentrations, etc. Depending on their capabilities, fire zone models can also be used to investigate other phenomena within the compartment such as ignition of linings and flame spread, detector activation, and the performance of smoke control systems, etc.

In New Zealand, BRANZFIRE was one of the first zone models which was commonly used by fire engineers and building officials. It was a deterministic two-zone model developed by the BRANZ Ltd [1] for predicting compartment conditions during fire. BRANZFIRE could predict layer heights and temperatures within the compartment as well as the ignition of a wall lining and its associated upward flame spread. The program output also included species concentrations, visibility, wall temperature and tenability assessment.

BRANZ and the University of Canterbury have developed B-RISK a novel quantitative risk assessment software tool, which is based on its predecessor BRANZFIRE [2]. B-RISK

produces modelling outputs that allows fire practitioners to assess the fire safety performance of a building in a probabilistic manner and also has the capability to visualise its geometry and output using Smokeview [3]. Included within B-RISK is a design fire generator (DFG) [4] submodel, which can generate ignition times for single and multiple combustible items within a compartment during a fire. Each item created in the DFG submodel has geometric, chemical, ignition and heat release rate (HRR) properties assigned to it.

The process of determining the degree to which a model or simulation is an accurate representation of the real world from the perspective of its intended users is often termed 'benchmarking'. Part of developing the B-RISK fire zone model is to benchmark its capability to predict item ignition and in order to do this a series of experiments were conducted at BRANZ in which single item ignition times under the furniture calorimeter and in the ISO 9705 room were measured. These single item experiments were used as a precursor to a series of multiple item experiments carried out in the ISO room as described elsewhere by Baker *et al.* [4]. The focus of this research project is to compare the measured ignition times from the single item and multi-item ignition experimental data with DFG submodel predictions from B-RISK. For this research B-RISK version 2013.0.15.28139 is used.

## 1.2 B-RISK benchmarking by others

A guide has been published by Wade [5] which presents comparisons between B-RISK (version 2013) model predictions with experiments. The benchmark examples presented in this guide are spilt in to 10 main cases, which includes:

- Single room with a single vent conditions. Multi room scenarios where looking at the upper layer hot gases and temperatures within the different room from the origin of fire.

- A number of other case studies in this benchmark guide looks at the fire growth on surface lining. This includes both the fire spread on surface lining in the ISO 9705 room and in the large room.
- Other case studies in this guides explores the post-flashover fire in single compartment and glass fracture compared to the B-RISK model.
- Also in this guide there are case studies benchmarking the (active fire systems) sprinkler and smoke detectors activation times.
- Finally, there are two case studies looking at smoke density and spill plumes capacity of B-RISK when it is compared to the experiments.

Other research has been conducted by Shah [6] to benchmark the DFG submodel in B-RISK. The work includes modelling a free burning single workstation which included desktops, a computer with monitor and keyboard, an office chair, a sled base chair and side panels. The other experiment was a compartment fire containing four workstations. Both single and multiple (four) workstations were based on experimental data from the National Institute of Standards and Technology (NIST) fire laboratory by Madrzykowski and Walton [7]. The NIST report used for this project included three cone calorimeter tests for each item sample. The results included ignition properties of the items and combustion properties such as the heat of combustion, soot yield and $CO_2$ yield. The geometry of the items such as length, width and height were calculated to replicate the NIST workstation set up. Shah's research compared the HRR; the item-to-item fire spread sequences and the time line between the DFG output and the NIST experimental results. The research concluded that the simulation of a single workstation in the DFG calculated is 3.2 MW peak HRR compared to the 3.3 MW from the experimental result. The DFG simulation of multiple (four) workstations in B-RISK results moderately match with the experiment. The item-to-item fire spread sequence of the

experiment were similar to the DFG simulation, however the time line comparison does not match due to the slow fire spread and unavailability of detailed information from the NIST report.

## 1.3 Objectives

The objectives of this research are to explore the capabilities and limitations by benchmarking or comparing the ignition prediction capability of B-RISK using furniture calorimeter and room-size experiments. In order to achieve the objectives the following tasks were required:

- Document the furniture calorimeter and multi-item ISO 9705 room experiments and process the experimental results.

- Conduct a number of computer simulations for the furniture calorimeter and multi-item ISO 9705 room experiments.

- Compare the results from the modelling with the experiments to benchmark the ignition prediction capability of the DFG submodel within B-RISK.

## 1.4 Outline of thesis

This thesis describes the processes undertaken and the results found for the ignition prediction capability of B-RISK model for items in a compartment effected by fire.

Chapter 1 provides an introduction to the research that has been conducted and outlines the objectives and methodology used in the research project.

Chapter 2 gives a review of the theory of ignition and previous research done relevant B-RISK benchmarking.

Chapter 3 describes the experimental setup of this research. The details and reasons for the use of three key materials are discussed. Mock-items design philosophy are given and details for the fire source used for series of experiments is given. This chapter also outlines the experiments which took place at BRANZ and were broken into four phases: cone calorimeter, furniture calorimeter single-item in the ISO 9705 room and multi-item in the ISO 9705 room.

Chapter 4 compares the experimental data with predictions made by the B-RISK model.
The model inputs such as geometry and different HRR for the gas burner item are closely scrutinised and their results discussed.

Chapter 5 summarises all of the findings from the research and makes conclusions as to the appropriateness of B-RISK in prediction ignition of items.

Chapter 6 presents further work and recommendations to BRANZ about the level of accuracy, limitations and potential improvements within the DFG submodel of B-RISK.

## 1.5 Methodology

In order to benchmark the software, a series of experiments were completed by joint effort from University of Canterbury and BRANZ [4], the series is shown in Figure 1. These experiments involved constructing a number of mock-up room furniture items and setting up experimental testing room for different fire spread scenarios.

The three main materials nominated for the series of experiments were: medium density fibreboard (MDF) a commonly used material for residential cabinetry, non-fire retarded flexible polyurethane (PU) foam commonly used material for furniture in New Zealand and acrylonitrile butadiene styrene (ABS) commonly used as hard plastic casing for electronic goods.

This author has conducted a serious of computer simulations of the furniture calorimeter and the multi-item room experiments. The experimental results (Phase 1-4) will be used as input data to benchmark the DFG submodel within the software. The following sections outline the project.

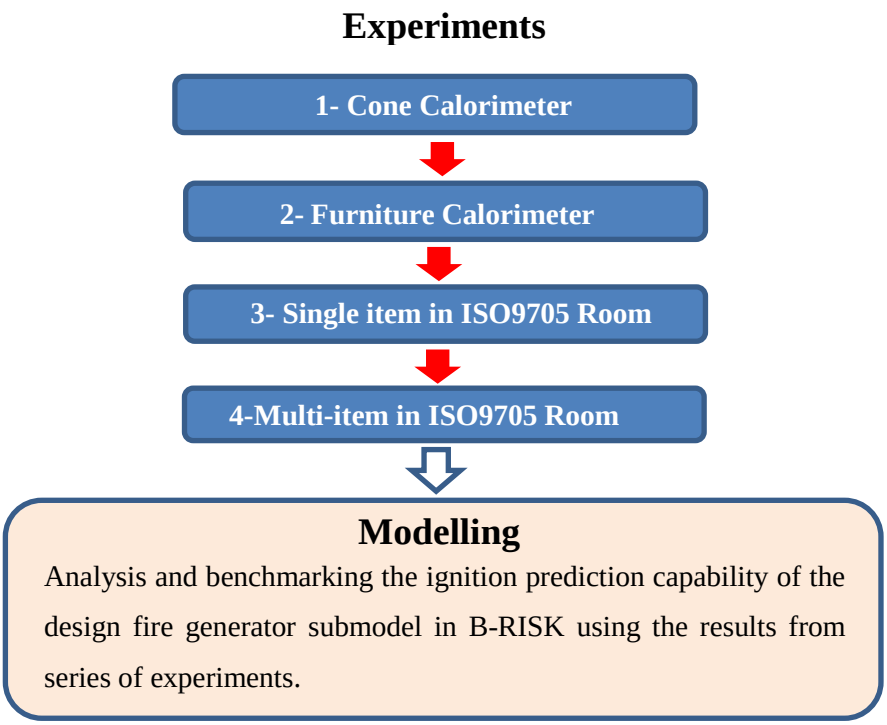


**Figure 1**. The sequence of experiments followed by B-RISK modelling is shown above

# Chapter Two

# THEORY

## 2.1 Theoretical Background

Before going into details of the method chosen for modelling the ignition properties and radiation model in the DFG submodel within B-RISK, there are some definitions worth a brief review. When the material is heated, it decomposes and releases combustible by-products known as pyrolyzates. Ignition is assumed to occur when the surface reaches a material dependent temperature defined as the ignition temperature $T_{ig}$.

This research only considered the ignition of three materials as defined in Section 3.1 caused by both piloted and auto ignition. Both piloted and auto ignition occurs when a material is heated with an ignition source present. For Piloted the ignition source can be a spark, an electric arc, small flame and so on. For Auto the ignition is via radiation from a burner, a radiating panel, remote flame or hot gas layer.

### 2.1.1 Thermal thickness

For a specimen to be classified as thermally thick sample [8], the heated layer has to be less than the physical depth so that an increasing physical thickness of the specimen will not influence the time-to-ignition for a given set of conditions. For a specimen to be classified as a thermally thin sample the temperature gradient through the material is negligible. The specimen's backing or substrate can become an important factor in influencing the time of ignition.

Drysdale [9] recommended that the characteristic thermal conduction length ($\sqrt{\alpha\, t}$) could be used as an indicator of the depth of the heated layer of a thick material, where α is the thermal diffusivity of the material and t is exposure time. Heat losses from the rear face of a material would be negligible if $L_o > 4x\sqrt{\alpha\, t}$, which indicates "semi-infinite behaviour" – thermally thick. $L_o$ is the physical thickness of the specimen. A thermally thin material could be defined as one with $L_o < \sqrt{\alpha\, t}$. "Thermal thickness" increases with $\sqrt{t}$, and for a sufficiently long exposure time, a physically thick material will no longer behave as a semi-infinite solid, and begin to show behaviour that is neither "thick" nor "thin".

### 2.1.2 The critical heat flux ($\dot{q}''_{cr}$) and the ignition temperature ($T_{ig}$)

The critical heat flux, $\dot{q}''_{cr}$ is a theoretical lower limit for the incident flux necessary to create the conditions for ignition. The critical heat flux is extrapolated from experimental correlation by making the time to ignition equal to infinity. Therefore critical heat flux is dependent on the kind of model used for correlating the ignition data. It is equal to the heat loss from the surface at ignition, as below this irradiance level the surface temperature will never reach the ignition temperature, $T_{ig}$ with the important assumptions; the material is chemically inert, homogenous, and is opaque. In relating the critical heat flux and the ignition temperature of the material, it is assumed there is no heat conduction into the material. The equation of energy balance can be expressed as follows:

$$\varepsilon.\dot{q}''_{cr} = h_c\left(T_{ig} - T_\infty\right) - \varepsilon\sigma\left(T^4{}_{ig} - T^4{}_\infty\right) \qquad (1)$$

The above theoretical concept and assumptions were developed and used by researchers in developing the time-to-ignition models, which one of the models was developed into the DFG submodel within B-RISK as discussed below.

## 2.2 Modeling Target Ignition

The ignition properties for each item in the DFG submodel are an essential input to the fire spread procedure in B-RISK. The method for choosing ignition properties for the DFG submodel has been described in detail by Baker *et al.* [10], from which a number of processes were established and the flux time product (FTP) method was selected.

The FTP approach is a simple way to predict piloted ignition when a combustible material is subjected to a time-changing incident radiation flux. The method initially defined by Smith and Satija [11] and then was further developed by other researchers [12-15]. Work by Shields *et al.* [16] generalised the FTP method to include thermal thickness for different materials. They also related time-to-ignition, $t_{ig}$, to the effective flux, $\left(\dot{q}^{"} - \dot{q}^{"}_{cr}\right)$, for a material under an apparatus such as cone calorimeter, expressed by:

$$FTP = t_{ig}\ (\dot{q}^{"} - \dot{q}^{"}_{cr})^{n} \qquad (2)$$

where $\dot{q}^{"}$ is the incident radiation flux, $\dot{q}^{"}_{cr}$ is the critical heat flux (kW/m$^2$) and $n$ is a parameter called the FTP index. The FTP index depends upon the thermal thickness and can take positive values that gives reasonable results where conventionally when $n$ = 1 the material is regarded as thermally thin and when $n$ = 2 the material is thermally thick.

Equation (2) can be rearranged to give a linear relationship between the external heat flux $\dot{q}^{"}$, and the reciprocal of the time-to-ignition, $t_{ig}$, to the power of 1/$n$ such that

$$\dot{q}^{"} = (FTP)^{\frac{1}{n}} / \ t_{ig}{}^{\frac{1}{n}} + \dot{q}^{"}_{cr} \qquad (3)$$

By plotting $1/t_{ig}{}^{\frac{1}{n}}$ on the x-axis versus $\dot{q}^{"}$ on the y-axis, $FTP^{\frac{1}{n}}$ and $\dot{q}^{"}_{cr}$ can be determined. Though the FTP model originally applied only to piloted ignition, Baker *et al.* [10] developed

an empirical auto-ignition approximation to accommodate this ignition mode into DFG submodel.

## 2.3 Modeling Radiation

In B-RISK, radiation is modelled to determine when a secondary (target) item will ignite following exposure to radiation from either an initial burning item or from the underside of the hot upper layer. The focus of this thesis is to investigate the former of the two mechanisms. Based on the research by Fleury *et al.* [17] he investigated six different radiation models and found that a spherical model, also known as the Point Source Model (PSM) [18] provided the best theoretical match with his experimental results. Moreover the PSM was relatively insensitive to changes in the input variables of radiative fraction and mean flame height.

Fleury's research similarly looked at selecting the most appropriate model in terms of ease of implementation into B-RISK. Joined with this was the ease of application by the end-user. Where other examined models such a rectangular planar model, are very complex models and would be difficult to program into B-RISK software such that could be applied in a user-friendly and timely manner by the end-user. Operating such a complex model would have required a high level of information about the fire, target position and target orientation relative to the fire. Most of fire zone models such as B-RISK are used by industry practitioners for design purposes, where the exact locations and orientations of objects within rooms are either unknown or could change. The PSM model assumes radiation is emitted isotropically from a point, therefore is not orientation specific and always assumes the maximum heat flux at a given location. This is of great importance in design purposes. The mathematical formulation is

$$\dot{q}''_{fl} = \dot{Q}\,\lambda_r cos\theta / 4\pi R^2 \qquad (4)$$

The PSM equation (4) although simple compared to other model researched by Fleury was further simplified by removing the angle$\theta$. The simplification of the PSM model was done for ease the calculation process in the DFG submodel algorithm. The revised mathematical formulation is:

$$\dot{q}_{fl}^{"} = \dot{Q}\ \lambda_r / 4\pi R^2 \qquad (5)$$

where $\dot{q}_{fl}^{"}$ (kW/ $m^2$) is the heat flux from the flaming item received by the target, $\dot{Q}$ (kW) is the heat output from the burning item, λr is the radiative fraction and $R$ (m) is the radial distance from the centre of the burning item to the nearest point of secondary item in the horizontal plane.

In the DFG to calculate $R$, each side of the secondary item is divided into ten equal length sections, with each section having a nominated target point. The distance between the point source and the divided sections (points) on each side of the secondary item is calculated and the nearest distance between two points is used. Therefore each item in the DFG submodel needs to have target ignition properties in order to ignite as a secondary item. The PSM estimates the heat flux that items not yet ignited receive from one or more burning items, which in turn is the incident flux parameter, $\dot{q}^{"}$, by which the FTP method then calculates when the item has received sufficient radiative heat to ignite.

# Chapter Three

# EXPERIMENTS

## 3.1 Materials

The three combustible materials used in the single item experiments and the subsequent multiple item experiments [4] described here, were: a 100 mm thick non-fire retarded flexible polyurethane (PU) foam with a nominal density of $\rho_{PU} = 32$ kg/m$^3$ typically used material for furniture in New Zealand, 3 mm thick acrylonitrile butadiene styrene (ABS) with a nominal density of $\rho_{ABS} = 1050$ kg/m$^3$ which used as hard plastic casing for electronic goods and 18 mm thick medium density fibreboard (MDF) with a nominal density of $\rho_{MDF} =$ 620 kg/m$^3$ commonly used material for residential cabinetry. Prior to commencing the experiments all the materials were conditioned at 23 ± 2 °C and the relative humidity was 50 ± 5%, in accordance with AS/NZS 3837. [19]

## 3.2 Items

The furniture calorimeter and the ISO 9705 room experiments involved a number of mock-up armchair, television and wooden furniture "items" as shown in Figure 2 made from the PU, ABS and MDF materials respectively. The design, geometry and material used for these items were purposely kept simple for the following reasons: (a) B-RISK represents items in a cuboid (rectangular prism) shapes; (b) allow for future replicates to be easily constructed; and (c) minimise additional factors that would complicate comparisons with the DFG predictions (e.g. fabric cover for the PU foam or paint finish on the MDF surface).

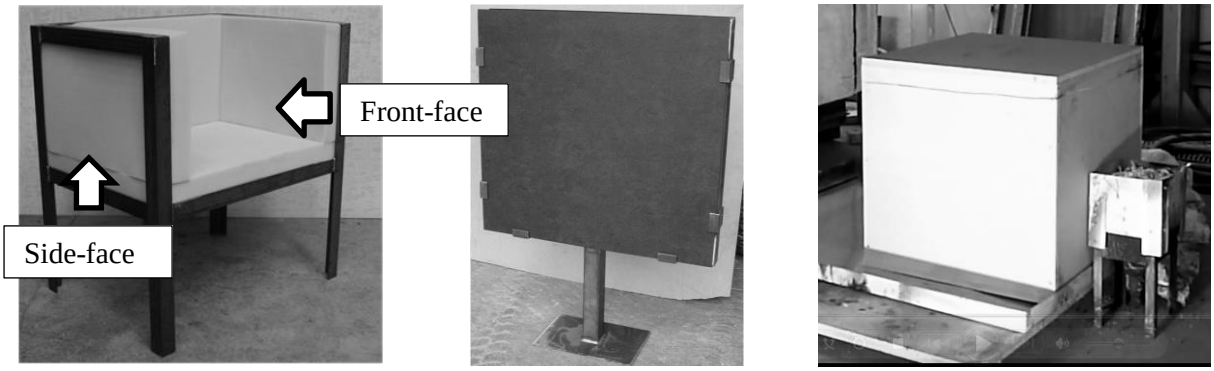


(a) (b) (c)

**Figure 2.** Mock-up furniture items: (a) PU foam armchair; (b) ABS TV; (c) MDF cube.

The mock-up armchair shown in Figure 2 (a) was constructed of a steel angle frame and filled with five equal size blocks of PU foam. Each block was 600 × 400 × 100 mm thick, two blocks made the seat, one for back and the two for each side. A steel mesh was used to support the seat of the armchair. The armchair dimensions were 900 mm high × 800 mm wide × 600 mm deep, the bottom surface of the armchair seat was 400 mm above the floor. The average weight of PU foam was 3.72 kg for the armchair.

The mock-up TV shown in Figure 2 (b) was constructed from a 50 × 50 mm steel square hollow section frame with a 300 mm high stand and a 675 wide × 635 mm high 'screen', which was covered with the ABS plastic sheets on the front and back. The plastic sheets were held in place with steel edge cleats and restricted horizontally and diagonally with light-gauge metal wires. The mock-up TV had an average of ≈ 2.76 kg of ABS plastic. The MDF hollow cube shown in Figure 2 (c) was constructed from six pieces of MDF with total measurements of 600 × 600 × 600 mm, each piece was mechanically fixed with three screws per edge to their neighbouring pieces. Each cube had an average weight of 22.7 kg.

## 3.3 Ignition Source

The ignition source used for the furniture calorimeter and ISO 9705 room experiments was a standard ISO 9705 set to a rate of heat release (RHR) of 100 kW propane gas burner. The burner was 170 mm square with a height of 145 mm. Propane gas was supplied through a metal gas inlet pipe at the bottom of the burner. The top of the burner (base of fire) was 300 mm above the floor. The burner was typically positioned so that the centre of it was 300 mm away from the surface of each item although in some experiments this distance was varied as discussed later.

## 3.4 Cone Calorimeter

The cone calorimeter was developed for bench-scale fire testing of various products and is able to ignite (both auto and pilot), heat release rate, mass loss and smoke measurement [20]. The constant heat flux provided by the conical electrical heater is up to 100 $kW/m^2$ with uniform over the surface.

The cone calorimeter was designed to test specimen in both horizontal and vertical orientation. Figure 3 shows the general view of the cone calorimeter.

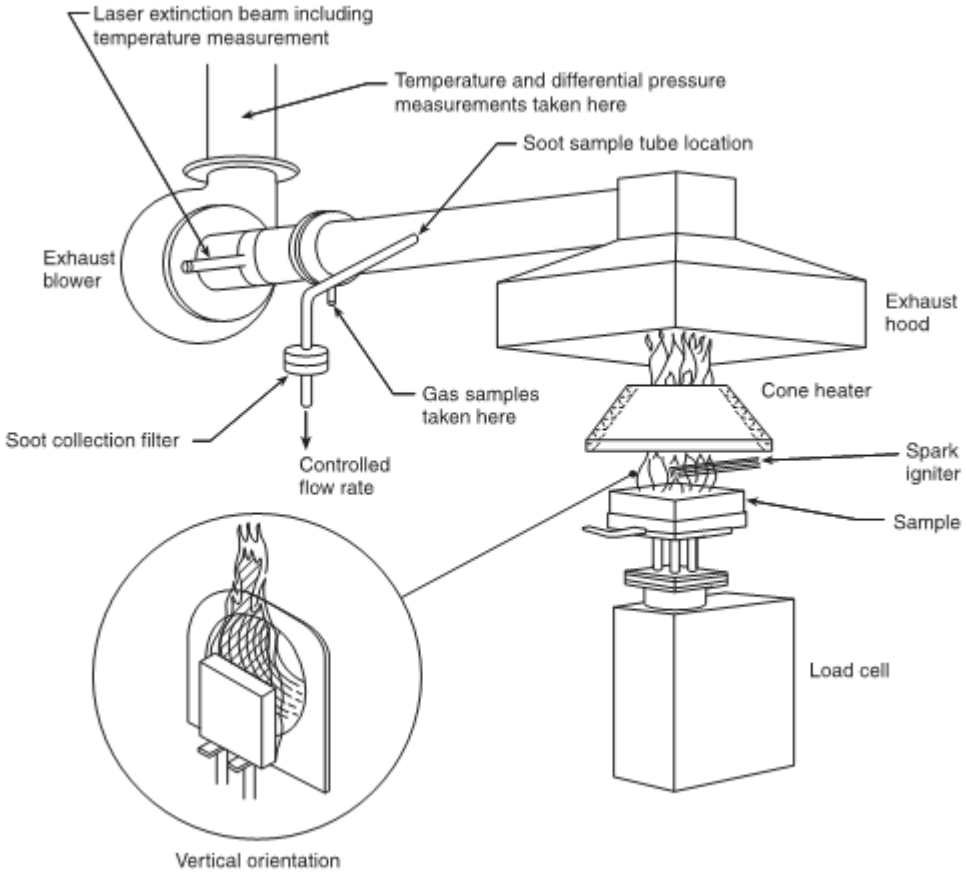


**Figure 3.** The cone calorimeter apparatus [20]

For the first set of experiments for benchmarking the DFG software a series of cone calorimeter experiments were carried out in the horizontal orientation to obtain the thermal properties of the three materials. Three samples of 100 × 100 mm × 50 mm thick PU foam, 100 × 100 mm × 3 mm thick ABS and 100 × 100 mm × 18 mm thick MDF were tested at each radiation level. The materials were exposed to heat fluxes, $\dot{q}''$ (kW/m$^2$) ranging between 10 and 70 kW/m$^2$ where Figures 4-6 shows each set of triplicate experiments. Also Table 1 shows the range of heat flux each material was exposed to under the cone calorimeter apparatus. The ignition times $t_{ig}$ (s) for both piloted and auto-ignition modes were recorded. In Table 1 The data is presented as the average of each triplicate sample ignition time (s) with the same heat flux plus/minus two standard deviations, and rounded down to the nearest 0.5 s. The notation NI means that no ignition occurred after 900 s exposure, and shaded boxes

indicate that no testing was conducted. The data from piloted ignition is analysed using the FTP method where a best-fit trend (solid) line is shown in Figures 4-6.

**Table 1.** Cone calorimeter ignition data

| $\dot{q}''$ (kW/m²) | $t_{ig}$(s) | | | | | |
|---|---|---|---|---|---|---|
| | PU foam | | ABS | | MDF | |
| | Pilot | Auto | Pilot | Auto | Pilot | Auto |
| **10** | 199.5±62.0 | | NI | | | |
| **15** | 59.0±19.5 | | NI | | | |
| **20** | 12.0±1.0 | NI | 195.5±22.0 | NI | 198.0±6.5 | |
| **25** | 7.5±0.0 | | | | | |
| **35** | | 109.0±49.0 | 50.0±3.0 | 162.0±108.0 | 66.0±1.5 | NI |
| **40** | | 93.5±24.5 | | | 52.5±4.0 | NI |
| **50** | | 45.0±4.5 | 22.5±0.5 | 34.5±1.0 | 34.5±1.0 | 45.0±8.5 |
| **60** | | 4.0±1.5 | 16.0±1.5 | 24.0±4.0 | 24.0±0.0 | 31.0±3.0 |
| **70** | | | | | | 26.0±2.0 |

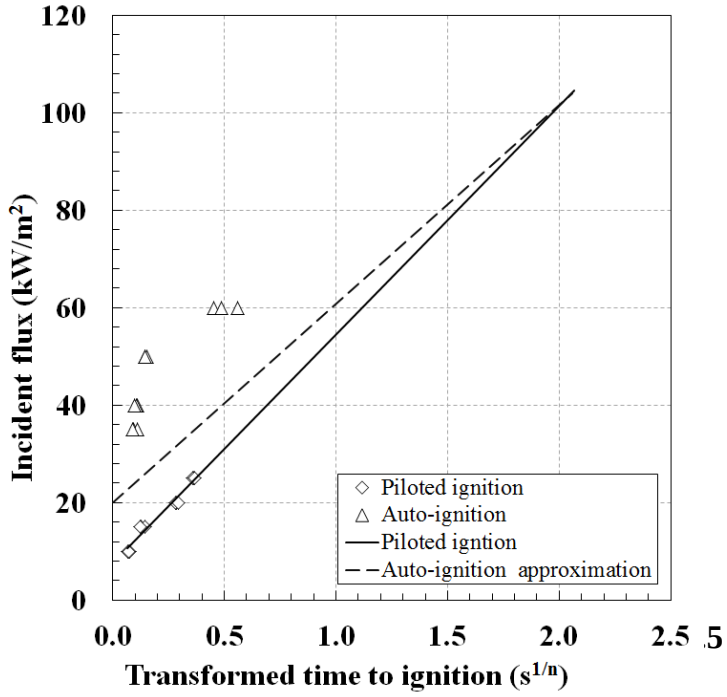


**Figure 4.** FTP analysis of the cone calorimeter experiments: PU Foam

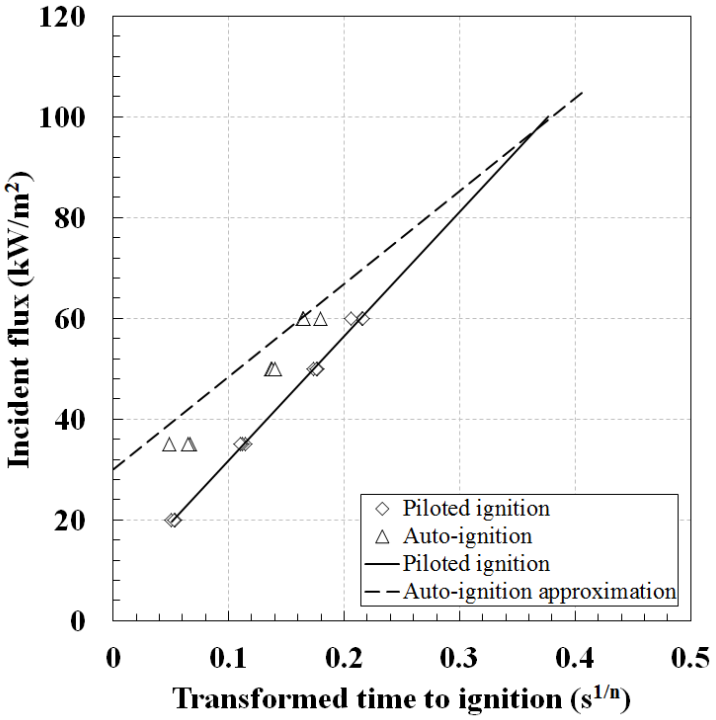


**Figure 5.** FTP analysis of the cone calorimeter experiments: ABS

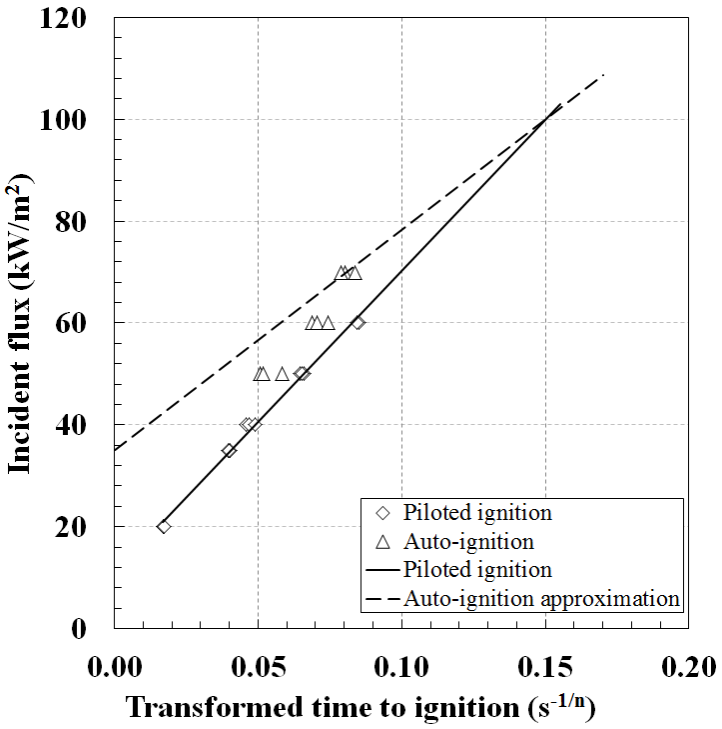


**Figure 6.** FTP analysis of the cone calorimeter experiments: MDF.

The empirical approximation by Baker *at el.* [10] is also used to derive comparable target ignition data for the auto-ignition mode shown in Figures 4-6 by the broken line.

The auto-ignition approximation consists of drawing a line between two assumed points, and $\dot{q}''_{cr}$ the value for $t_{ig}$ at which the piloted- and auto-ignition times converge, and then deriving the representative auto-ignition properties for each material. Figure 4 shows the empirical approximation auto-ignition trend lines fits as well it can for the PU-foam, ABS and MDF experimental data recorded.

The initial observation in Figures 4-6 indicates that the auto-ignition empirical approximation under-predicts the cone calorimeter results for ABS and MDF, but over-predicts for PU-foam. However when applying the empirical approximation method, as discussed by Baker *et al.* [4], changes to the incident flux $\dot{q}''$ to a point where $t_{ig}$(auto) = $t_{ig}$ (piloted) is not sensitive to the assumed value. For example if the selected incident flux value is increased by

50% the FTP value increases by less than 5%. Such minor changes in FTP values are insignificant as whole for the approximation of the auto-ignition properties. Furthermore the sensitivity of the $\dot{q}''_{cr}$ value intercept on the y-axis is in such way that, if the DFG predicts shorter ignition times than the experiments then increasing the assumed $\dot{q}''_{cr}$ value will increase the predicted ignition times. Table 2 shows the target ignition parameters for the three materials.

**Table 2.** Target ignition properties for PU foam, ABS and MDF.

| **Target ignition parameters** | **PU foam** | | **ABS** | | **MDF** | |
|---|---|---|---|---|---|---|
| | Pilot | Auto | Pilot | Auto | Pilot | Auto |
| **FTP ($kW.s^{1/n}.m^2$)** | 2210 | 1666 | 19242 | 11348 | 4038 | 2678 |
| $\boldsymbol{n}$ | 2 | 2 | 1.8 | 1.8 | 1.3 | 1.3 |
| **Critical flux $\dot{q}''_{cr}$ ($kW/m^2$)** | 7.5 | 20 | 7.1 | 30 | 10.8 | 35 |

Other parameters obtained from the cone calorimeter experiments were the effective heat of combustion $\Delta H_{C,eff}$ (MJ/kg) and the average peak measured values across the three experiments for each material to get the heat release rate per unit area HRRPUA ($kW/m^2$). The summarised results for the three materials are shown in Table 3.

**Table 3.** Average heat of combustion and HRRPUA data for PU foam, ABS and MDF.

| | PU Foam | ABS | MDF |
|---|---|---|---|
| $\Delta \boldsymbol{H}_{\boldsymbol{C,eff}}$ (MJ/kg) | 25 | 29 | 12.2 |
| $\boldsymbol{HRRPUA}$ (kW/m$^2$) | 459 | 1077 | 252 |

The results generated from the cone calorimeter experiments were used in the DFG as the input data for the target ignition properties and fire chemistry parameters for each material

## 3.5 Furniture Calorimeter

The furniture calorimeter is used to determine the burning behaviour of real size items such as furniture and mattresses. The items' geometry, orientation and key features of ignition can be measured [21].

The collected data includes HRR, mass loss and species production for each item under the furniture calorimeter device as shown in Figure 7.

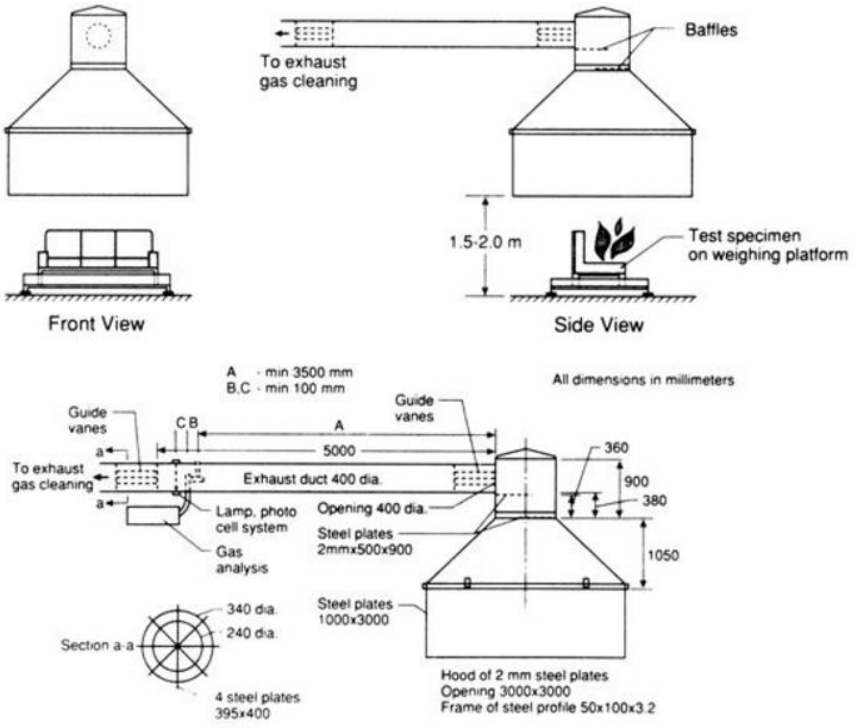


**Figure 7.** The Furniture Calorimeter Figure by Briggs, (http://goo.gl/bb7Vu0)

For the furniture calorimeter experiments, both the gas burner and mock-up items were placed beneath the 3.0 × 3.0 m hood. The armchair experiments were conducted in two different arrangements: Arm–A was with the front-face oriented towards the burner and Arm–B was with the side-face oriented towards the burner as indicated in Figure 2(a). These arrangements were investigated to correspond to the multi-item compartment fire experiments [4] that took place subsequently.

The initial burning item, i.e., the ignition source for each experiment was the propane gas burner and each of the three mock-up furniture items/arrangements were tested three times for repeatability purposes. The experiments obtained the ignition time from visual observation as shown in Table 4.

**Table 4.** Ignition times for items under the furniture calorimeter.

| **Item** | **Ignition time (s)** | | | **Mean** | **Standard deviation** |
|---|---|---|---|---|---|
| | **Expt 1** | **Expt 2** | **Expt 3** | | |
| **Arm–A** | 278 | 582 | 789 | 550 | 257 |
| **Arm–B** | 75 | 105 | 85 | 88 | 15 |
| **ABS TV** | 225 | 276 | 303 | 268 | 40 |
| **MDF Cube** | 57 | 62 | 51 | 57 | 6 |

The results from the Arm–A experiments show ignition times in the order of several minutes with a wide variation. During the Arm–A2 experiment for example it was observed that the asymmetric air movement and turbulence in the laboratory resulting from the extract hood and laboratory layout caused instability of the burner flame. As such, the flames fluctuated

about their vertical axis during the experiment which then affected the radiation exposure to the PU foam. Figure 8 shows a photograph from the Arm–A2 experiment where the flames are shifted to the right at that particular instant. This movement of the flames was coupled with the fact that the armchair faced the burner which meant only a relatively small vertical surface area of PU foam closest to the radiation received by the flames from the burner, again shown in Figure 8, which is one possible explanation for the long ignition times.

**Figure 8.** Photograph from Arm–A2 furniture calorimeter experiment.

The actual point of ignition in fact in the Arm-A experiments was the vertical side corner. This suggests that the correct configuration for the radial distance parameter R is the diagonal distance, which in this case is 424 mm, rather than the minimum distance of 300 mm. The average $t_{ig}$ for the Arm-A experiments from Table 4 is 550 s, which equates to an equivalent radial distance value of R' ≈ 330 mm when the auto ignition FTP dataset from Table 2 for PU foam is used in the PSM calculation from Eqn. (5) and the FTP calculation from Eqn. (2).

Considering the geometry of the propane gas burner, the virtual origin of this equivalent radial distance is within the perimeter boundary of the burner and is not an unrealistic representation of the burner flame position during the Arm-A experiments.

Since in the Arm–B experiments the armchair had a side face oriented towards the burner, a larger surface area of PU foam was closest when compared to the Arm–A experiments. This would have resulted in a larger amount of pyrolyzates being produced. The ignition times for these experiments were much shorter with a narrower range compared with the Arm–A results. In addition, the larger area of PU foam exposed to the radiation meant ignition was likely less sensitive to any flame movement.

For the multiple item experiments [4] the ABS TV was placed on the top of an MDF cube to represent the TV being on a cabinet. However, in order to gather experimental data and ignition times for the single items under the furniture calorimeter, the ABS TV was positioned on the ground and parallel to the burner to be consistent with the single item armchair and MDF cube experiments.

Initially the MDF cube experiments began with the burner centrally positioned at 300 mm from a parallel edge of the cube, similar to the armchair and ABS TV arrangements. However, no ignition occurred after running the burner for 50 minutes. In fact this experimental observation is entirely consistent with the auto ignition FTP dataset in Table 1 for the MDF material. The PSM calculation from Eqn. (3) and the FTP calculation from Eqn. (1) indicate that the radial distance would need to be less than ~260 mm before ignition was possible, i.e., the threshold where $\dot{q}''_{fl} = \dot{q}''_{cr}$ . The MDF cube was then progressively shifted closer to the burner and the experiment repeated until ignition was achieved. It was not until the propane burner was sitting flush against the MDF cube, as shown in Figure 1(c), that

ignition finally occurred. Two further MDF cube experiments followed the same arrangement to get the three ignition times given in Table 4.

## 3.6 ISO 9705 room

The ISO 9705 [22] room is a standard size compartment used in reaction-to-fire testing. It is 2.4 m × 3.6 m × 2.4 m high with a single opening in one of the 2.4 m long walls that is 0.8 m wide and 2.0 m high as shown in Figure 9.

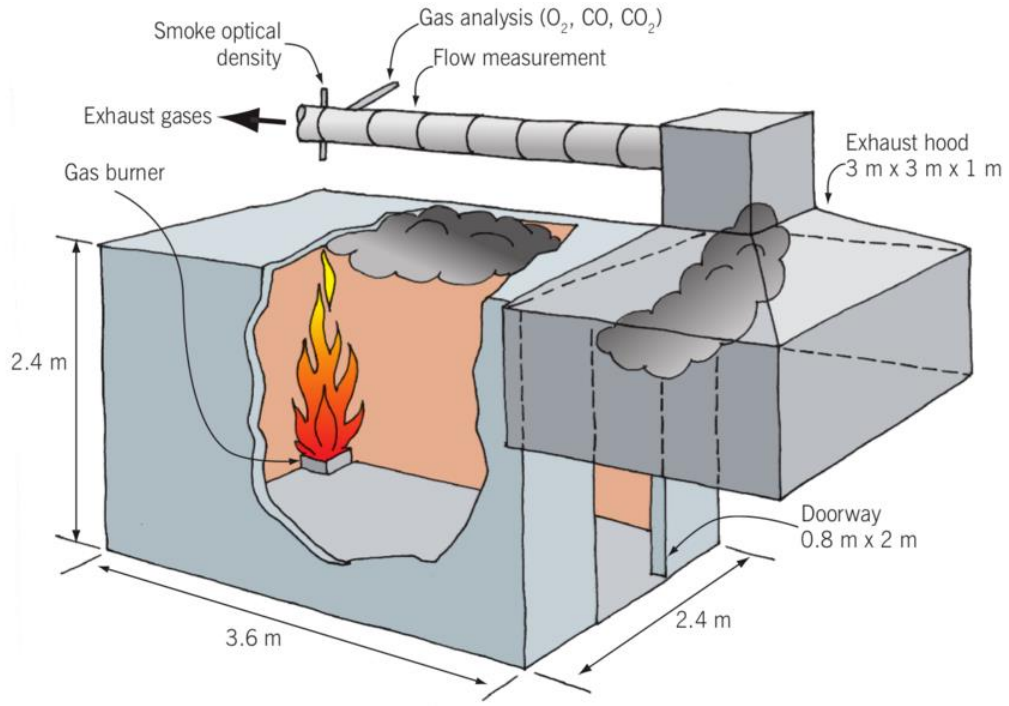


**Figure 9.** ISO 9705 room figure by Collier, 2006 (http://goo.gl/pNa7IB)

It was originally intended that the series of single item ISO 9705 room experiments was going to be for all three mock-up items however due to the restricted time schedule to complete coursed out the multiple item experiments and the availability of the fire laboratory at BRANZ the only single item compartment experiments were the two armchair arrangements as shown in Figure 9. Furthermore given the proposed layout of items in the multiple item experiments and the results already obtained from the furniture calorimeter experiments it was clear that the most important ignition times were those of the armchairs.

For the Arm–A arrangement the armchair and burner were located mid-way and 200 mm away from the 3.6 m wall as shown in Figure 9 with the middle of burner 300 mm away from the front surface of the armchair. For the Arm–B set of experiments the armchair and burner were located in the top corner furthest from the opening with the middle of burner 300 mm away from the 3.6 m wall and 300 mm from the side surface of the armchair. The back of Arm-B was 300 mm away from the back wall.

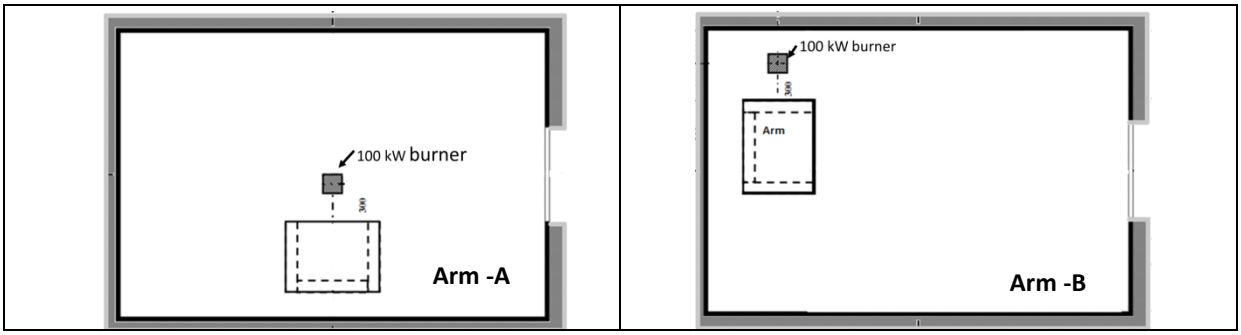


**Figure 10**. Two different ignition scenarios (Arm-A and Arm-B) in the ISO 9705 room.

The ignition time for each of the three repeats of the room experiments is given in Table 5. The ignition times for the Arm–A set of ISO 9705 room experiments exhibited both shorter ignition times and reduced uncertainty in comparison to the Arm–A experiments under the furniture calorimeter. Similarly, the ignition times for the three Arm–B ISO 9705 room experiments were shorter than the Arm–B experiments under the furniture calorimeter, although the results exhibited a marginal increase in uncertainty.

**Table 5.** Ignition times for items in ISO 9705 room.

| Item | Ignition time (s) | | | Mean | Standard deviation |
|---|---|---|---|---|---|
| | Expt 1 | Expt 2 | Expt 3 | | |
| **Arm–A** | 75 | 42 | 30 | 49 | 23 |
| **Arm–B** | 45 | 27 | 42 | 38 | 10 |

The earlier ignition times for both Arm−A and Arm−B in the compartment compared to the furniture calorimeter could possibly result from an observed greater degree of burner flame stability inside the compartment. It is unlikely that traditional compartment effects, i.e., radiation from the hot gas layer and heated boundary surfaces, would have been a contributor and given the relatively short ignition times any radiation feedback from the boundaries is likely to be insignificant in any case compared to the flame radiation. What is clear is that the ignition times from the ISO 9705 room experiments indicates that the orientation of the armchairs relative to the burner was not as influential as with the furniture calorimeter experiments. However, it is possible to propose specific theories as to the difference between the Arm-A and Arm-B ignition results in the ISO 9705 room. The quantity of PU foam exposed to flame radiation in the Arm-B configuration is greater than the Arm-A layout, which may contribute to faster ignition times for the former, along with the possibility that the proximity of wall surfaces in the Arm-B case, may have introduced localized compartment enhancement.

## 3.7 Multiple item in the ISO 9705 room

For the final set of experiments initially two multi-item compartment fire scenarios were planned to take place in the ISO 9705 Room compartment with each scenario to be replicated three times for repeatability purposes. Each Scenario had a typical residential furniture layout filled with the items used for previous experiments. Prior to commencing experiment the main raw materials were relocated from the conditioned room to the fire laboratory to be weighed. This included 6 pieces of PU foam for each armchair, the MDF cube and two sheets of the ABS plastic for the mock-up TV.  After assembling each item they were placed in the

ISO room in the exact location as per the scenario layouts. Each experiment had a chart that included the scenario, the number of the experiment and the date. The measurements for time of ignition for each item was recorded by participant observation with use of stop-watch and two sets of video camera recoding each experiment. The bigger (main) camera was about 3 m away from the door opening on a tripod. The smaller webcam was boxed with fire rated wool and the front of the screen was protected with a fire rated glass and placed at the doorway of the ISO 9705 room at a 45° degree angle facing upwards in the compartment. A digital photo camera was used to record different stages of each experiment. The BRANZ fire laboratory used the Large Scale Heat Release (LSHR) software version Window 95 to collect the relevant species and gas analysis. The software was calibrated before each experiment.

Although the LSHR software was used to collect a range of data from each experiment instead the only measurement of particular interest for this thesis are the ignition times of the items for each experiment.

### 3.7.1 Scenario A

Scenario A (first scenario) had 4 MDF cubes. 2 Arm chairs and ABS mock-up television with the propane burner set in the middle of the room. The exact location of each item in relation to each other and the compartment is shown in Figure 11. The first item ignited in all three experiments was Arm-1.The ignition time for second item varied from each experiment. The ignition sequence for each of the three room experiments for scenario A is shown in Table 6. The ignition times shaded in grey are estimated only, as the precise ignition of these items was not possible via observation.

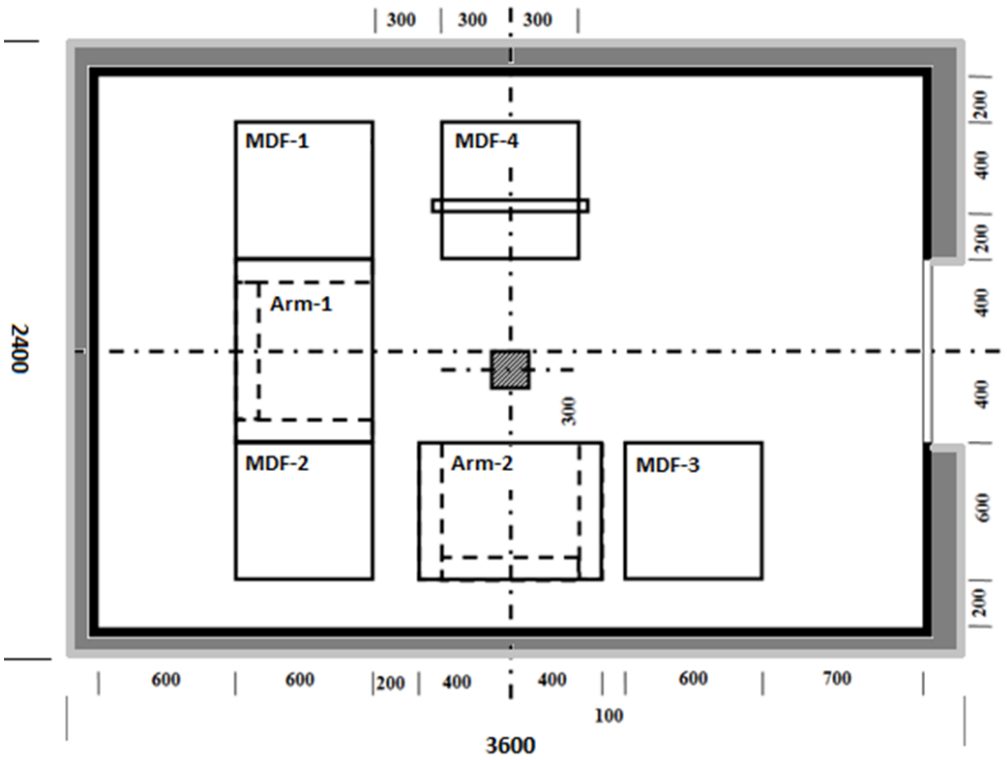


**Figure 11**. The layout items for Scenario A in the ISO room compartment.

**Table 6**. Ignition times for items for scenario-A in the ISO room compartment.

| Item | Ignition time (s) | | |
|---|---|---|---|
| | **Experiment-1** | **Experiment-2** | **Experiment-3** |
| **Arm-1** | 49 | 60 | 34 |
| **Arm-2** | 171 | 205 | 213 |
| **MDF-1** | ≈ 150-160 | ≈ 160-170 | ≈ 125-135 |
| **MDF-2** | ≈ 175-180 | ≈ 210-220 | 173 |
| **MDF-3** | ≈ 175-180 | ≈ 210-220 | ≈ 220-230 |
| **MDF-4** | 184 | 268 | 283 |
| **TV** | 154 | 270 | 280 |


**Figure 12**. Scenario A-1 in the ISO room just before the experiment.

**Figure 13-** Scenario A-1 in the ISO room during the experiment.


**Figure 14-** Scenario A-1 flash-over in the ISO room.

**Figure 15**. Scenario A-1 After the experiment in the ISO room.

### 3.7.2 Scenario-B

Scenario-B had 5 MDF cubes, 3 Arm chairs and ABS mock-up television with the propane burner set in the top right corner of the room as shown in Figure 16. During the first

experiment (B-1) as shown in Figure 18 the foam on the Arm-3 has shrunk deformed smouldering away, this continued for 30 minutes without ignition. Therefore the first experiment (B-1) was stopped as the Armchair (Arm-3) next to the burner did not ignite.

The second experiment followed the same trend and was stopped after 30 minutes. It was then that it was decided to amend the room layout in order to achieve ignition and item to item fire spreads.

This was surprising as the Arm-B as a single item in the ISO room ignition time ranged between 27-45 seconds. The main possible reason for ignition not occurring was the air-flow being altered via the three MDF cubes (i.e. MDF-3, MDF-5 and MDF-4) facing the upper 3.6m wall.

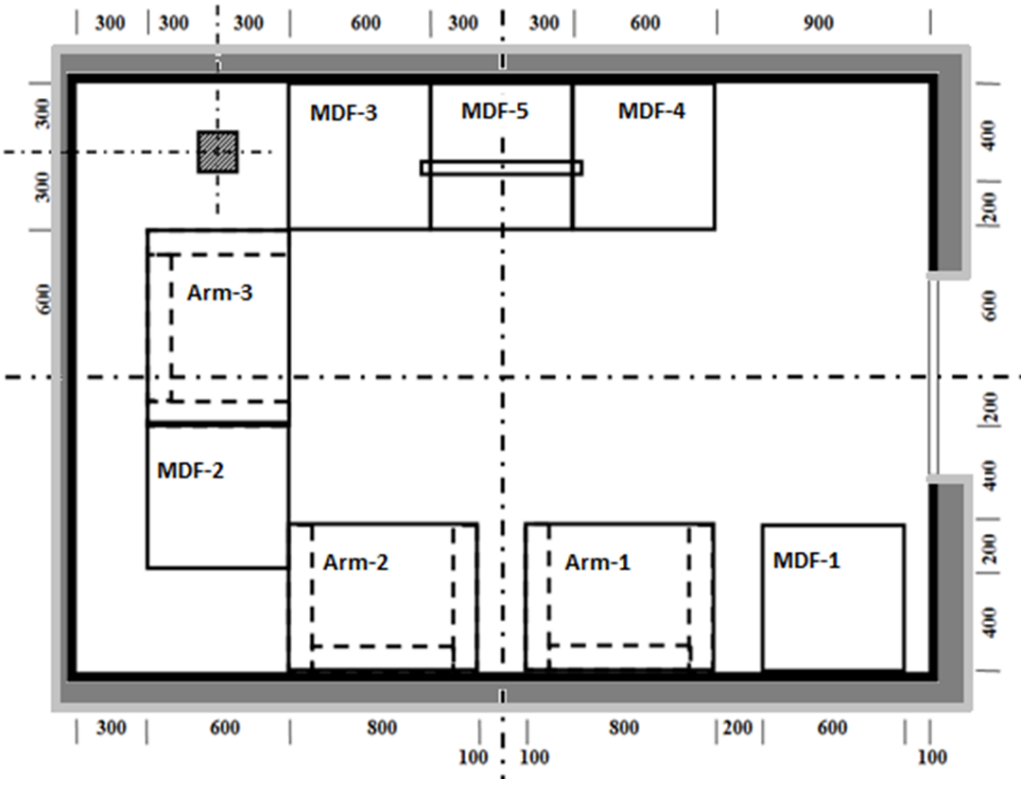


**Figure 16-** The layout items for Scenario-B in the ISO Room compartment.

**Figure 17.** Scenario B-1 in the ISO room just before the experiment.


**Figure 18.** Scenario B-1 in the ISO room during the experiment.

### 3.7.3 Scenario-C

Then first amended scenario C-1 had the edge of the burner sitting right under the edge of the (Arm-3) as shown in Figures 19-20, which resulted in the ignition of Arm-3 instantly,

however this did not lead into spread and ignition of other items particularly Arm-2. Figure 21 shows how Arm-3 foam was almost burned out and no other items such as MDF-2 and Arm-2 were ignited. The ABS sheet on the mock up TV melted and deformed but ignition did not occur. The experiment was stopped after 30 minutes, which at that point the entire foam from Arm-3 was burned and chance of ignition occurring after that was very low. After the experiment as shown in Figure 22 the foam on Arm-2 and Arm-1 was slightly charred from the radiation from the burning Arm-3 and hot upper layer and possible feedback from the wall. The melted ABS sheet on the TV frame shown the right hand side. Both MDF-3 and MDF-2 was charred on exposed side.

The second experiment C-2 followed the same trend. The combination of the radiation from the Arm-3 burning with the hot upper later and feedback from the walls was not enough for the ignition of other items within the compartment to occur. This resulted in further amended to the item layout cratering a new scenario.

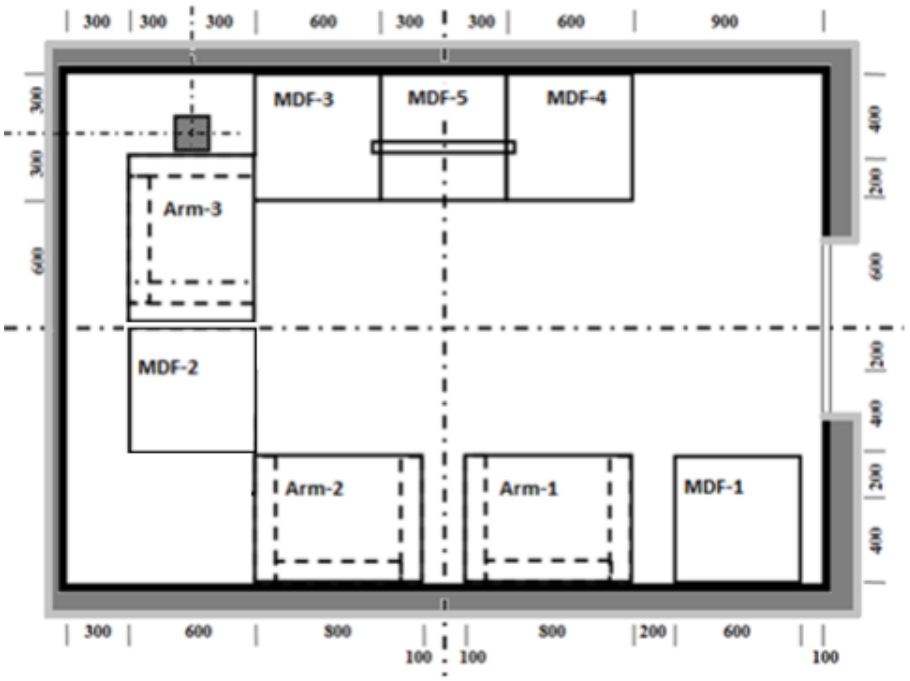


**Figure 19**. The layout items for Scenario-C in the ISO Room compartment.

**Figure 20.** Scenario C-1 Shows the gas burner was shifted 215 mm to the left right under the edge of Arm-3.


**Figure 21.** Scenario C-1 during the experiment.

**Figure 22.** Scenario C-1 After the experiment.

### 3.7.4 Scenario-D

The room layout was amended for the 2nd time, with both Arm-2 and Arm-1 as shown in Figures 23-24 moved up towards the middle of the room by 600 mm. This allowed the lower front corner of Arm-3 and top left corner of Arm-2 almost touching each other so the fire spread between the two armchairs could occur. Therefore there would be a higher possibility for the ignition of the remaining items in the compartment.

These changes allowed three replicate experiments for scenario-D where item to item fire spread was successful.

The ignition sequence for each of the three room experiments for scenario D is shown in Table 7. Similar to scenario A, the ignition times shaded in grey are estimated only.

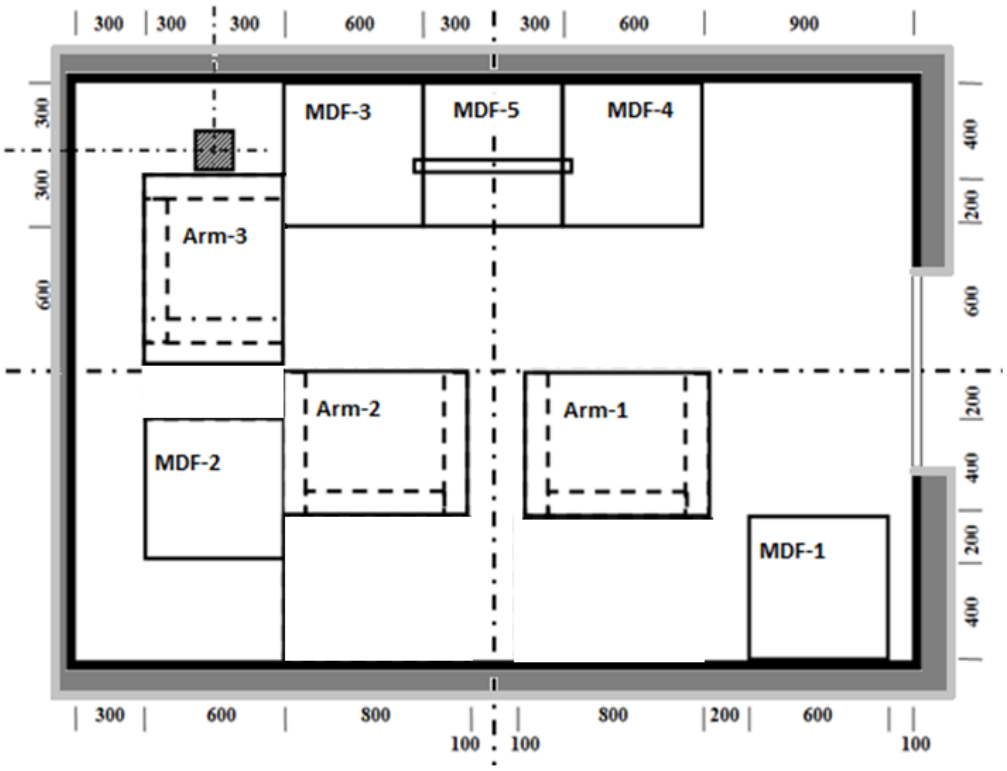


**Figure 23-** The layout items for Scenario D in the ISO Room compartment.

**Figure 24-** Scenario D-1 shows the amdneded layout with both Arm-2 and Arm-1 shifted towards the middle of ISO room just before the experiment.


**Figure 25**. Scenario D-1 in the ISO room during the experiment.


**Figure 26.** Scenario D-1 flash-over in the ISO room.

**Figure 27.** Scenario D-1 After the experiment in the ISO room.

**Table 7.** Ignition times for items for scenario-D in the ISO room compartment.

| Item | Ignition time (s) | | |
|---|---|---|---|
| | **Experiment-1** | **Experiment-2** | **Experiment-3** |
| **Arm-1** | 219 | 220(214) | ≈217-222 |
| **Arm-2** | 205 | 204 | ≈198-204 |
| **Arm-3** | ≈ 15-25 | ≈ 15-25 | ≈15-25 |
| **MDF-1** | ≈220-240 | ≈205-215 | ≈220-250 |
| **MDF-2** | ≈ 200-210 | ≈ 185-195 | ≈ 195-225 |
| **MDF-3** | ≈ 205-225 | ≈ 195-200 | ≈ 200-220 |
| **MDF-4** | ≈ 205-225 | ≈ 195-200 | ≈ 220-240 |
| **MDF-5** | ≈ 205-225 | ≈ 195-200 | ≈ 220-240 |
| **TV** | 222 | 223 | 217 |

Total of 10 experiments were conducted for the multi item ISO room experiments. As per previous stages, the ignition times were collected from all the experiments.

.

# Chapter Four

# MODELLING

## 4.1 Design Fire Generator Submodel

This Chapter highlights the ignition prediction capability of the design fire generator submodel (DFG) in B-RISK. The collected data from the series of experiments as previously detailed in Chapter Three will be used to compare the results obtained from the B-RISK predictions. This includes the HRR from the gas burner and other items are used as inputs for each particular experiment for each single item in B-RISK.

### 4.1.1 Input specifications

The ignition predictions from B-RISK are not impacted by the compartment boundary properties, nor the combustion properties of the item (other than the radiative fraction) as the ignition times are simply the result of direct radiation using the PSM and FTP formulations, as defined by Eqn. (2) and Eqn. (5). However, to demonstrate the broader functionality of the model, both the furniture calorimeter and single item in ISO 9705 Room experiments are modelled in B-RISK.

### 4.1.2 Geometry

The furniture calorimeter experiments have been modelled in B-RISK as a rectangular shape domain with dimensions 6.6 m long × 4.4 m wide × 4.4 m high. Three of the domain boundaries are left open to represent the fire laboratory. A wall is located on the fourth boundary to represent the front of the ISO room. The burner and the single item are placed in front of the wall. The solid ceiling boundary of the modelled domain has a 2.4 × 2.4 m horizontal opening above both items representing the furniture calorimeter hood. Figure 28

shows the view of the modelled domain in Smokeview. The material selected for the walls, ceiling and floor was “concrete, light-weight” form the B-RISK database with a thermal conductivity of 0.21 W/m.K, a density of 800 kg/m$^3$ and specific heat of 880 J/kg.K. The simulated walls and ceiling are 162 mm thick and the floor is a 150 mm thick light-weight concrete slab. These steps created a simulation similar to the free burning furniture calorimeter experiments.

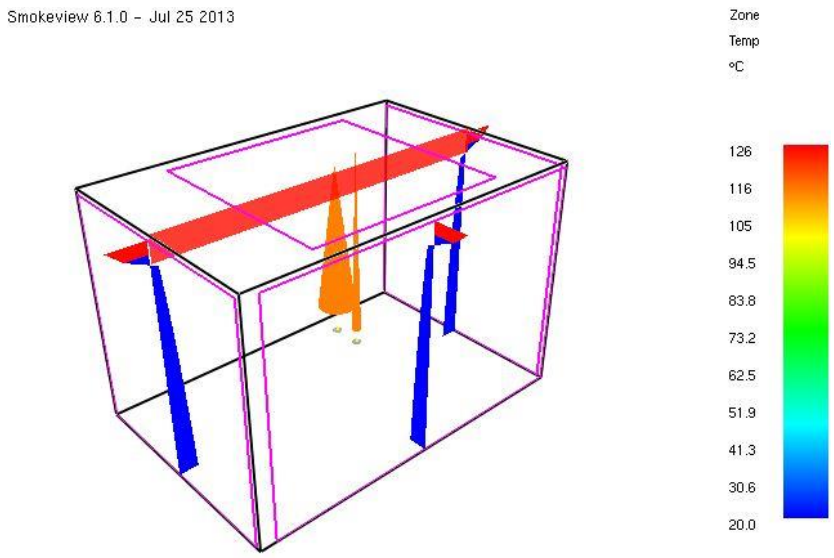


**Figure 28.**The furniture calorimeter representation in Smokeview during simulation.

The ISO 9705 room is modelled as a 3.6m long × 2.4 m wide × 2.4 m high compartment with a 0.8 m wide × 2 m high opening to the outside used as a single ventilation in the front wall to replicate the experiments. Again a light-weight concrete material is selected for the wall, ceiling and floor similar to the construction materials in the BRANZ ISO room.

In modelling of both the furniture calorimeter and ISO room experiments the length, width and height of items and their distance from the burner are specified to replicate the experiments.

### 4.1.3 Combustion and ignition properties

The combustion and ignition properties of an item such as heat of combustion and HRRPUA are taken from the cone calorimeter results. Since the ignition of the mock-up furniture items in the experiments were by auto-ignition then the auto-ignition properties are used for inputs into B-RISK.

In order to determine ignition times, values for soot and $CO_2$ yield are not required and so these were not measured during the cone calorimeter experiments. However B-RISK requires values for these properties when performing its simulations so appropriate values are selected from the SFPE Handbook [12] for similar representative materials as shown in Table 8. The soot yield, $CO_2$ yield and radiant loss fraction $\chi_R$, found from the ratio of the radiative heat of combustion (kJ/g) to the net heat of complete combustion per unit mass of fuel consumed (kJ/g), are taken from Table 3-4.16 of the SFPE Handbook [12]. The latent heat of gasification is selected from Table 3-4.9 of the SFPE Handbook.

**Table 8.** Combustion and ignition properties.

| | **Propane burner** | **Polyurethane (flexible) foam GM23** | **PMMA** | **Wood (Douglas fir)** |
|---|---|---|---|---|
| **Soot yield (g/g)** | 0.024 | 0.227 | 0.022 | 0.015 |
| **$CO_2$ yield (g/g)** | 2.85 | 1.51 | 2.12 | 1.32 |
| **Radiant loss fraction** | 0.3 | 0.31 | 0.30 | 0.29 |
| **Latent heat of gasification (kJ/g)** | N/A | 2.7 | 1.6 | 1.8 |

Note: The latent heat of gasification (kJ/g) for the burner was not required as an input in the model.

### 4.1.3 Gas burner

Each B-RISK simulation included a representation of the 100 kW gas burner. The simulations were set up so that the first item (burner) ignites immediately and then the secondary item (mock-up furniture) is ignited by radiation from the burner item. Initially the heat release rate from the burner was defined by an instantaneous steady-state output of 100 kW (Figure 29). However the burner heat release rate was subsequently derived from the measured gas flow in the experiments to evaluate the sensitivity of the ignition predictions. For example Figure 29 shows the modeled output heat release rate from the burner for Arm–B1 and TV–1 in which the gas flow to the burner in the experiments exhibited a ramp-up delay or some fluctuation before settling into a steady-state flow.

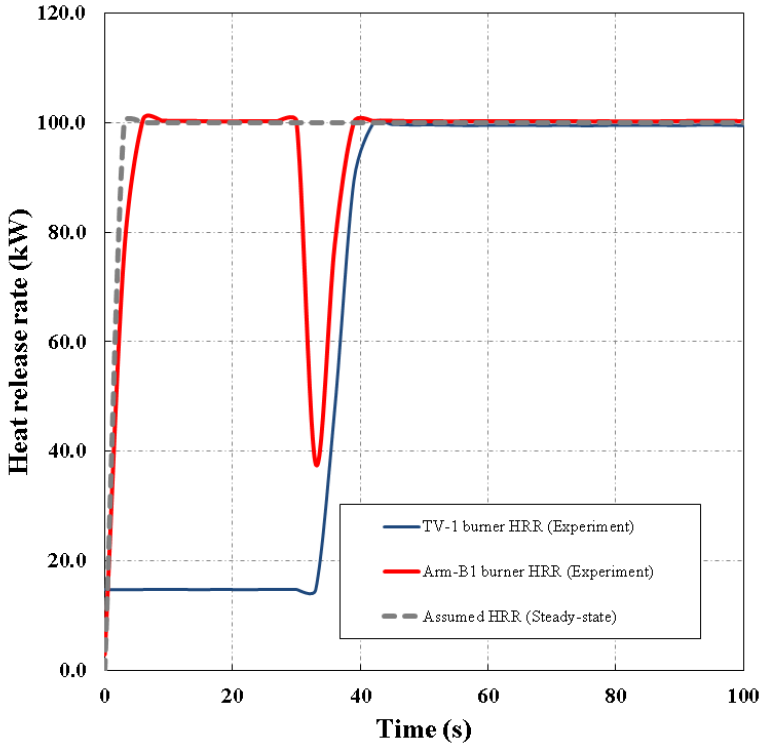


**Figure 29.** Assumed steady-state vs experiment gas burner HRR for Arm–B1 and TV–1.

### 4.1.4 Items HRR for the furniture calorimeter experiments

As previously mentioned in Chapter Three, a total of 12 furniture calorimeter tests were conducted, three tests for each single item. The PU foam armchair-A, the PU foam armchair-B, the ABS TV and the MDF cube. Figures 30-34 shows the three HRR curves that were measured for each test including the average. The 100 kW gas burner input was removed by deducting 100 from the output data. For each simulation the actual HRR curve from the test was used as the input for each item in the modelling. The representative HRR average curve for each set of experiments was used as input for the modelling of the multiple experiments. In the case of Figure 33 the HRR curves have been offset by approximately 3000 s which is an approximate time –shift to allow for the larger radiation source that would be present in the modelling of the experiments.

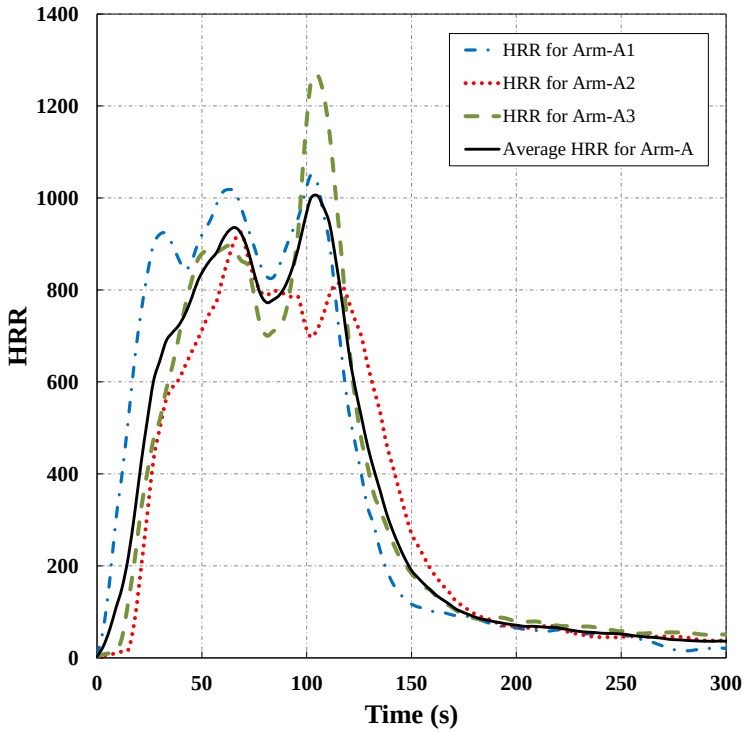


**Figure 30.** Furniture calorimeter experiment HRR for Arm-A

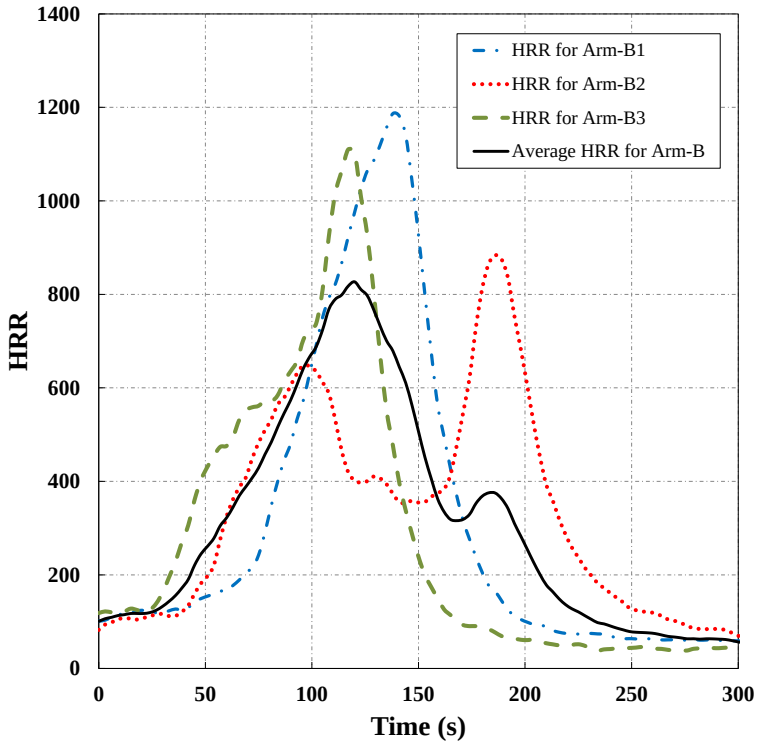


**Figure 31.** Furniture calorimeter experiment HRR for Arm-B

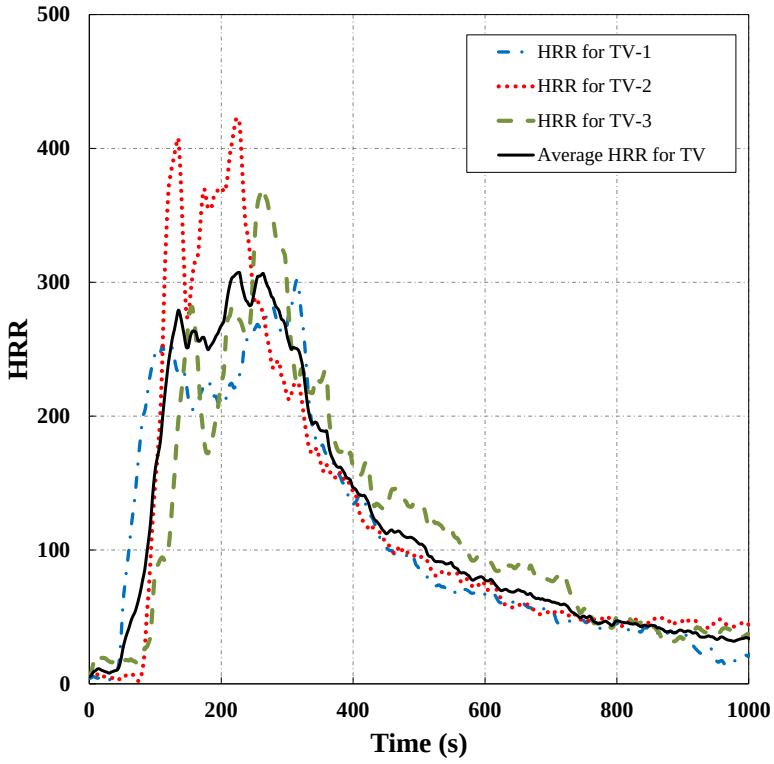


**Figure 32.** Furniture calorimeter experiment HRR for TV used

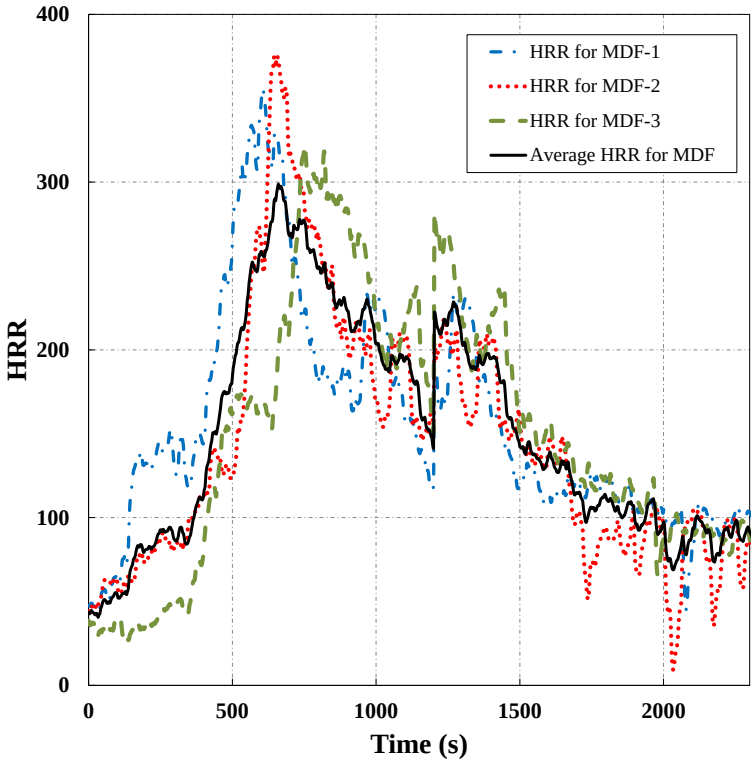


**Figure 33.** Furniture calorimeter experiment HRR for MDF

All the average HRR curves from each single item under the furniture calorimeter is shown in Figure 34 to give an overview and comparison of all the HRR used in the simulations.

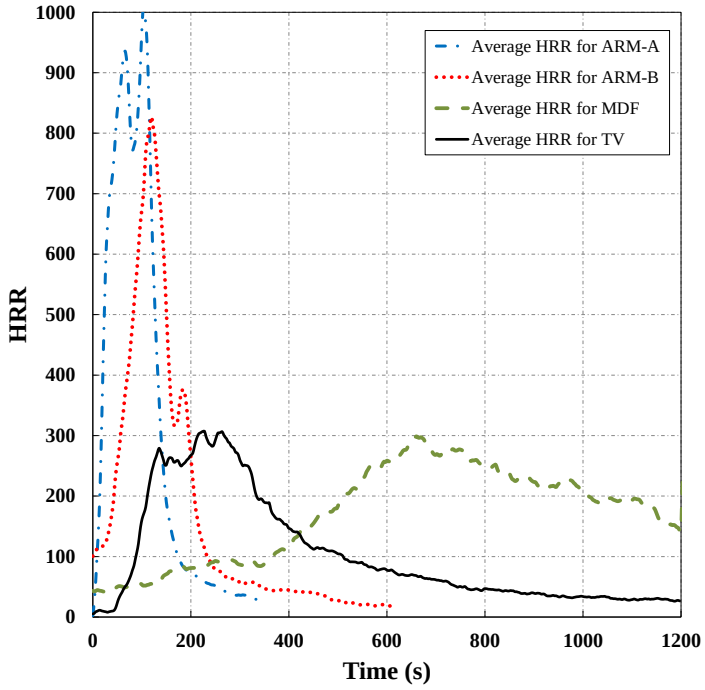


**Figure** 34. Average HRR for all items under the furniture calorimeter experiment

## 4.2 Furniture calorimeter comparison

In order to replicate the furniture calorimeter experiments in B-RISK, first set an assumed steady state output of 100kW is used to replicate the burner. Afterward simulations were run using the HRR output from the gas flow burner for each experiment as inputs. This also included a process of varying the radial distance to get a better match between experiment and prediction for each of the simulations.

Finally, a set of simulations were run by using the actual HRR output from the gas burner for each of the experiment as detailed in Section 0, based on oxygen consumption calorimetry (OCC). This is used instead of the HRR from the gas flow which is fundamentally constant during the experiments, to investigate its influence on the simulations compared experiments.

### 4.2.1 Arm-A

For the initial simulation, the burner is given a steady-state output of 100 kW which results in representative ignition time of 44 s for the Arm–A experiments. Simulations are then carried out in which the measured burner heat release rate from each experiment is specified as the simulated burner item. The results varied from each other and also compared with the steady-state burner simulation although the predicted ignition times were at least 50% shorter than the experimental results. In order to investigate the effect of the fluctuation of the burner flame on ignition times, the radial distance parameter, *R*, in Eqn. (3) was varied to get a better agreement between the experiments and the predictions, as an approximate representation of the varying distance of the gas burner flame from the PU foam of the mock-up armchair. All the other parameters in the calculations were kept constant. Figure 35 shows the ignition time results for the 300 mm baseline distance between the Arm–A surface and centre of the burner

and when the distance is increased by 10 mm then the ignition time is delayed by 33 s. By adding 20 mm to the baseline distance the ignition time is delayed by 116 s. These changes in distances are up to 10% of the radial distance between the burner and the surface of secondary item; however this level of variation has a significant impact on the ignition time. This is due to the mathematical formulation of the PSM method used in the DFG submodel. As the radial distance increases, the radiation received by the armchair decreases, which in turn means that the time to ignition increases at an exponential rate. Therefore the 30 mm addition to the baseline line distance shows an agreement to within -7.4% on average, relative to the experimental value, with the best agreement at 14%.

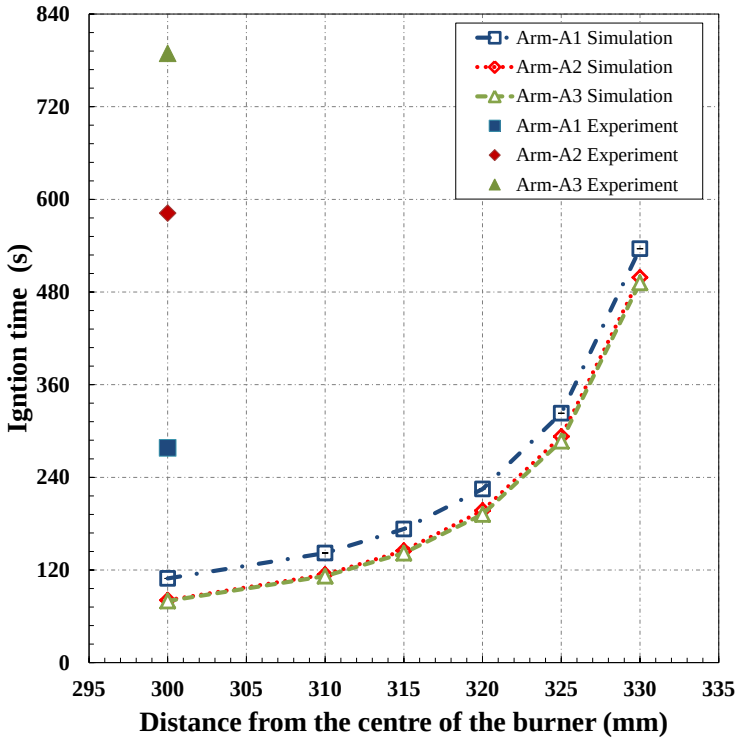


**Figure 35.** Measured and predicted ignition times for Arm–A triplicate experiments.

### 4.2.2 Arm-B

The Arm–B ignition time generated from B-RISK using the assumed steady-state of 100 kW for the burner is also 44 s., matching that for the Arm-A configuration. This is due to way

that B-RISK defines the items as being simple cuboid shapes. In the model the minimum distance to both Arm–A and Arm–B are identical and hence the ignition times are also identical irrespective of the armchair item orientation to the burner. In a similar manner to the Arm–A modelling, using the measured HRR from the burner in each experiment improved the predictions when compared to the observed ignition times. The ignition times generated were more accurate in relation to the experimental results as shown in Table 4 compared to Arm–A ignition times. Again the process of varying the radial distance to get a better match between experiment and prediction showed that a greater radial distance between the item and the burner gives a longer ignition time. Figure 36 shows that the simulated results are closer to the experimental results where an increase of 10 mm in the radial distance displays an agreement across the three experiments within +16% deviation on average, with the best agreement at +8%.

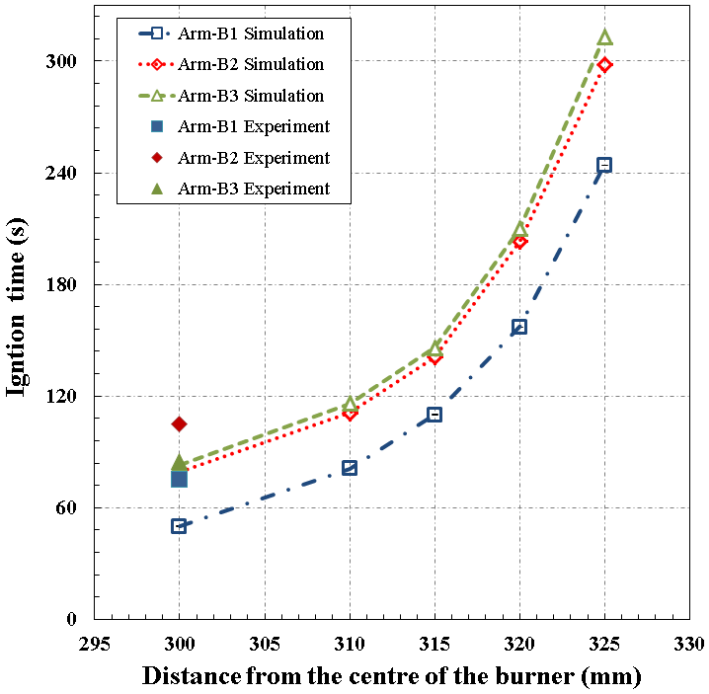


**Figure 36.** Measured and predicted ignition times for Arm–B triplicate experiments.

### 4.2.3 ABS TV

The predicted ignition time using the assumed steady-state of 100 kW for the burner is 64 s. Once more the output heat release rate for each of the experiments used as an input for the burner in B-RISK gave better results, however Figure 37 illustrates how the DFG submodel under-predicted the ignition time compared to the experimental results. The radial distance adjustment improved the comparison of the ignition times and a 30 mm increase gives average predictions to within +13% on average across the three experiments with the best agreement at +3%.

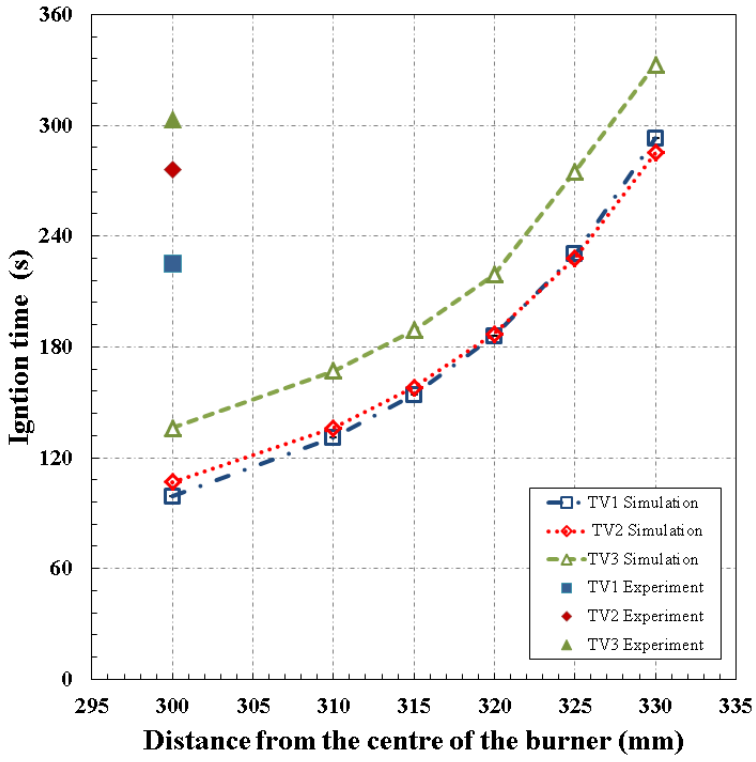


**Figure 37.** Measured and predicted ignitions time for ABS TV triplicate experiments.

### 4.2.4 MDF cube

For consistency and to assess the outcome, each MDF cube experiment was modelled at the 300 mm initial distance from the burner similar to the experiments which resulted in no simulated ignition of the target item. In relation to Eqn. (1) and (3), this is due to the PSM

radiation at 300 mm being less than the critical heat flux for MDF. Using both an assumed steady-state and the experimental HRR from the burner as input made no difference to the prediction that ignition does not occur. Following the revised experimental procedure, the MDF cube was simulated in close proximity the burner, i.e., a nominal radial distance of 100 mm. The predicted ignition time from the steady-state burner input is 7 s. The results for the predicted ignition times from the model are significantly shorter as shown in Figure 38. A sensitivity analysis of the radial distance shows that an additional distance of 100 mm (i.e., radial distance increasing from 100 to 200 mm) is needed to obtain correspondence to within -15% on average of the experimental measurements with the best agreement at -2%.

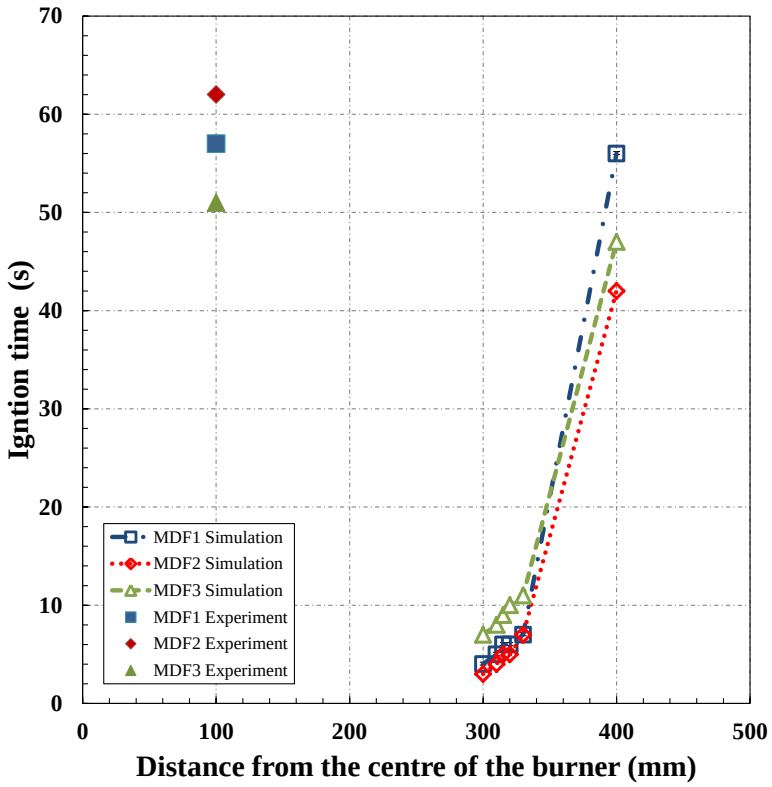


**Figure 38.** Ignition time for MDF triplicate experiments vs varying radial distance.

To assess whether varying the auto-ignition properties of the MDF makes any difference to the predicted ignition times, a sensitivity analysis using the empirical approximation

proposed by Baker *et al.* [5] is made as shown in Figure 39 and Table 9. However using these revised properties does not change the predicted ignition time significantly. This is due to the fact that the PSM flame radiation at an offset of 100 mm is ~240/m$^2$ kW so varying $\dot{q}''_{cr}$ by the amounts indicated in Table 6 will only affect ignition times by a few seconds. In reality, an incident heat flux of this magnitude is extrapolating the PSM/FTP correlation well beyond the experimental cone calorimeter radiation maximum value of 70 kW/m$^2$ (as shown in Table 1) and hence well beyond the range of validity for the PSM/FTP correlation.

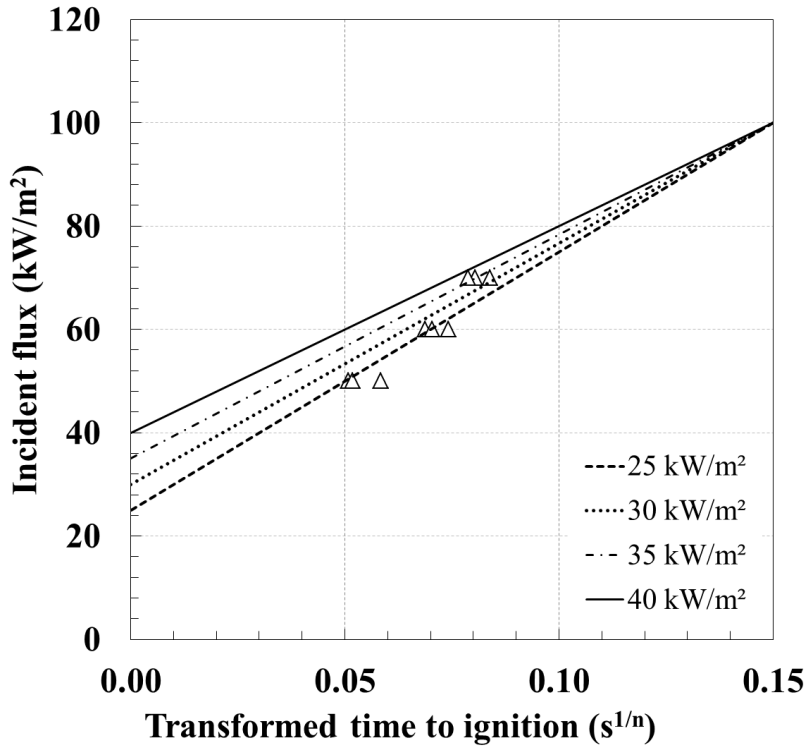


**Figure 39.** Auto-ignition FTP plot for MDF with critical heat flux ranging from $\dot{q}''_{cr}$ = 25 kW/m$^2$ to $\dot{q}''_{cr}$ = 40 kW/m$^2$.

**Table 9.** Revised MDF auto-ignition properties

| **Target ignition data** | **MDF** | | | |
|---|---|---|---|---|
| $\dot{q}''_{cr}$ **(kW/m$^2$)** | 25 | 30 | 35 | 40 |
| $n$ | 1.3 | 1.3 | 1.3 | 1.3 |
| $FTP$ **(kWs$^{1/n}$m$^2$)** | 3225 | 2949 | 2678 | 2414 |

Since from the experimental arrangement it could be argued that the direct flame contact was a piloted ignition scenario the piloted ignition properties given in Table 2 obtained from the cone calorimeter experiment are used. No significant changes in ignition time are obtained when the MDF cube is simulated in close proximity to the burner for the piloted and auto-ignition properties and the predicted piloted ignition times are on average 37% shorter than the auto-ignition times at the previously identified 200 mm radial best fit. Although shorter ignition times using piloted ignition properties when compared to using auto-ignition properties are to be expected, it means predictions are even poorer when assessed against the experimental measurements. However a combination of piloted data and applying the radial distance $R$ = 200 mm predicated much better agreement between the experiments and the experiments.

By placing the MDF cube in close proximity to the burner in the experiments meant that direct radiation was no longer the primary ignition mechanism but instead ignition was through direct flame contact. Therefore the MDF cube experiment modelled in B-RISK is no longer assessing the capability of the PSM and FTP methods and so it is not surprising to see that the predictions for ignition times do not match the experimental results.

## 4.3 Oxygen consumption HRR input in the DFG Submodel

The HRR output from the OCC is used as input in the DFG submodel within B-RISK for this section. Where a set of simulation tested using the HRR for the burner derived from the OCC for each experiment. This is a 30 s average value which is based on Oxygen consumption. Therefore the results suggest different HRR for the gas flow burner output. These results are not as constant as the HRR for the gas flow burner is essentially constant during the experiment.

### 4.3.1 HRR output for the OCC gas burner

The HRR output from the OCC burner was subsequently set to the measured experimental output to evaluate the impact on of the ignition predictions. Figure 40 shows the output heat release rate from the burner for Arm–A2 and TV–1 when compared with the experiment measured gas flow HRR. The fluctuations are typical of the HRR for the burner derived from the OCC that include Oxygen consumption for all of the furniture calorimeter experiments. Some of the output results from the experiments exhibited systematically lower values than the assumed steady state or measured HRR gas flow while others had higher values as shown in Figure 40.

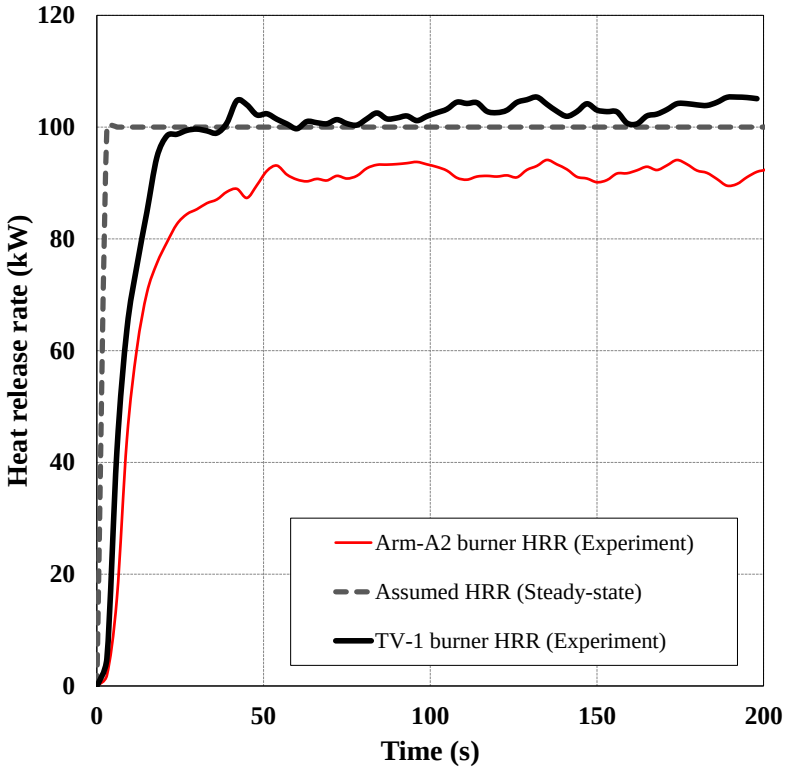


**Figure 40.** Assumed steady-state vs experiment HRR derived from OCC for Arm–A2 and TV–1.

### 4.3.2 Furniture calorimeter comparison applying HRR derived by OCC output

#### 4.3.2.1 Arm- A

Simulations were carried out in which the measured burner HRR derived by OCC from each experiment is specified for the simulated burner item with the DRG submodel input. The results varied from each other and also compared with the HRR from gas flow burner simulation however the predicted ignition times were still at least 50% shorter than the experimental results. The same sensitivity analysis explored earlier was carried out on the distance of the gas burner from the armchair but with the new gas burner input. Figure 41 shows the ignition time results for the 300 mm baseline distance between the Arm–A surface and centre of the burner and when the distance is increased by 10 mm then the ignition time is delayed by 28 s. By adding 20 mm to the baseline distance the ignition time is delayed by 112 s. These changes in distances are less than 10% of the radial distance between the burner and the surface of secondary item; however this level of variation has a significant impact on the ignition time. Therefore the 20 mm addition to the baseline line distance shows an agreement with the experimental results to within 7% on average, with the best agreement at 1% and the worst at 28%.

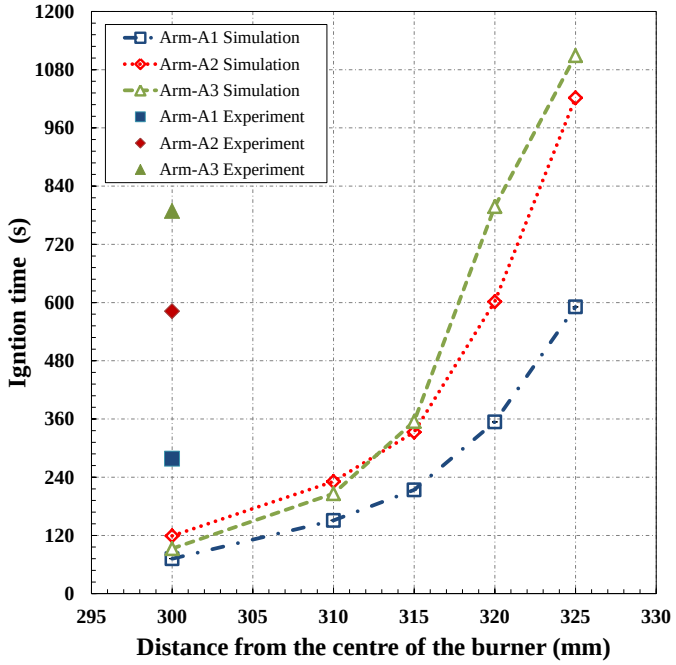


**Figure 41**. Measured and predicted ignition times for Arm-A triplicate experiments.

#### 4.3.2.2 Arm- B

Once more similar to the Arm–A modelling, using the measured HRR derived by OCC from the burner in each experiment improved the predictions when compared to the observed ignition times. The ignition times generated from this analysis were similarly in closer range to the experimental results as shown in Table 4 compared to Arm–A ignition times. Once more the process of using the measured HRR derived by OCC showed that a greater radial distance between the item and the burner gives an even longer ignition time. Figure 42 shows that the simulated results are closer to the experimental results where the increase of 10 mm in the radial distance displays an agreement across the three experiments within 11% on average, with the best agreement at 20% and the worst at 54%.

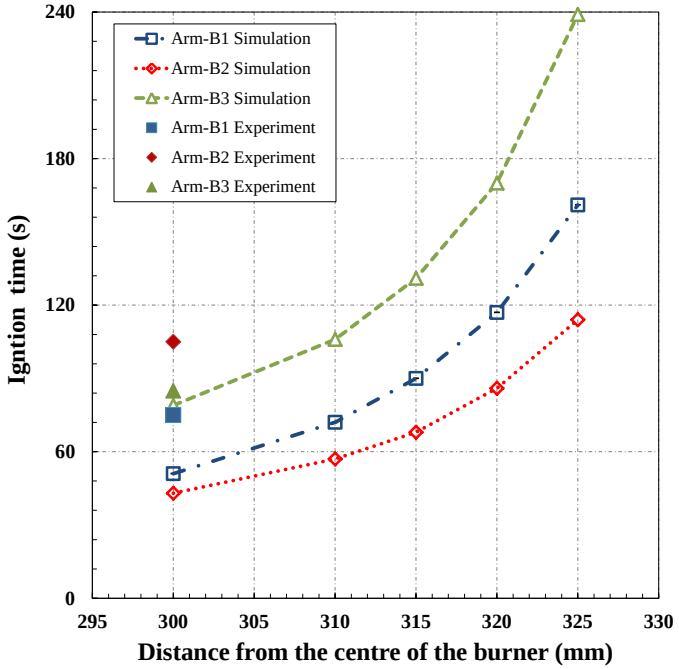


**Figure 42**. Measured and predicted ignition times for Arm-B triplicate experiments.

#### 4.3.2.3 ABS TV

Again the output HRR derived by OCC for each of the experiments used as an input for the burner in B-RISK had better agreement with the experimental results, though Figure 43 still illustrates how the DFG submodel under-predicted the ignition time compared to the experimental results. Once more the radial distance sensitivity adjustment improved the ignition times and a 30 mm increase gives average predictions to within 1% across the three experiments with the best agreement at 3% and worst at 32%.

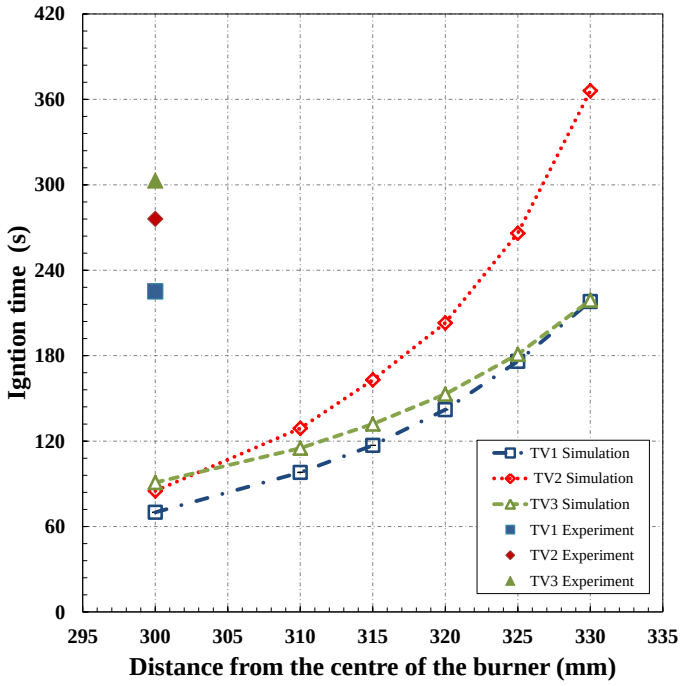


**Figure 43.** Measured and predicted ignitions time for ABS TV triplicate experiments.

#### 4.3.2.4 MDF cube

For consistency with the above sensitively assessment using the experimental HRR derived by OCC as input, the MDF yet again made no difference to the prediction given that ignition does not occur when modelled at 300 mm away from the burner. The MDF cube was simulated with it placed against the burner HRR derived by OCC as the input as shown in Figure 44. Again a sensitivity analysis of the radial distance shows that an additional distance of 90 mm is needed to obtain correspondence to within 22% on average of the experimental measurements with the best agreement at 2% and the worst at 35%.

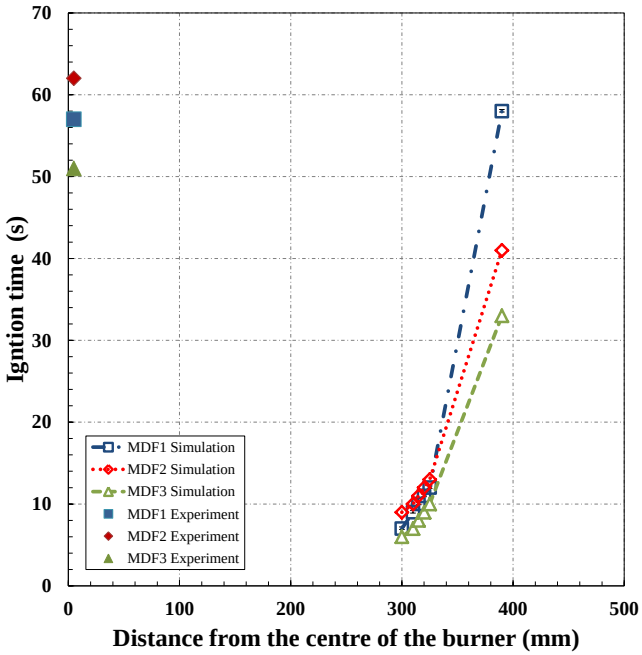


**Figure 44.** Ignition time for MDF triplicate experiments vs radial distance sensitively simulation assessment.

As mentioned previously, placing the MDF cube directly against the burner in the experiments meant that indirect radiation was no longer the primary ignition mechanism but instead ignition was through direct flame contact.

Therefore the MDF cube experiment modelled using the burner output with HRR derived by OCC as input in B-RISK as a sensitivity analysis is outside the validity range of the PSM and FTP methods and so a comparison of the predictions for ignition times with the experimental results is not an appropriate approach.

### 4.3.3 Summary of the furniture calorimeter comparison

A summary comparison of actual ignition times from the experiments and corresponding predictions from B-RISK are shown in Figure 45 for the furniture calorimeter. The data presented in each graph includes the results for the assumed steady-state 100 kW input, the measured heat release rate from the gas burner and the HRR derived by OCC output for each

experiment. Figure 45 (a) – (d) for the furniture calorimeter also includes the best radial distance adjustment that is closest to the equality line.

The ignition time for furniture items displays better comparison between the experiments and predictions when the measured burner data was used rather than assuming a steady-state output.

The ignition time for furniture items displayed better comparison between the experiments and predictions when the measured burner with Oxygen consumption data was used rather than constant gas burner or steady-state output for the furniture calorimeter.

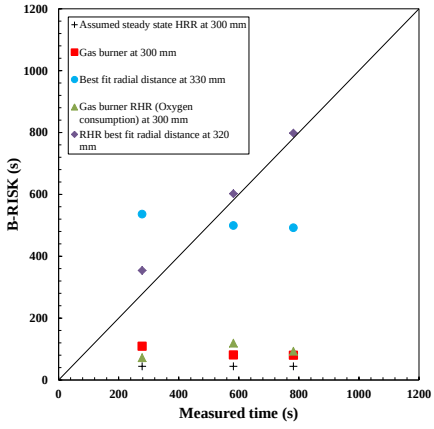


(a) Arm-A ignition times under the furniture calorimeter.

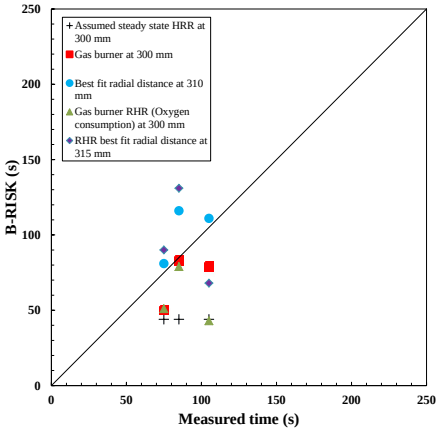


(b) Arm-B ignition times under the furniture calorimeter.

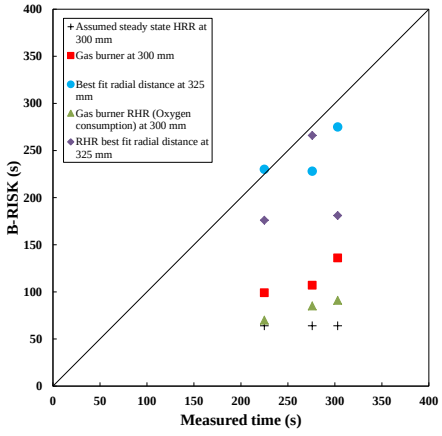


(c) ABS TV ignition times under the furniture calorimeter.

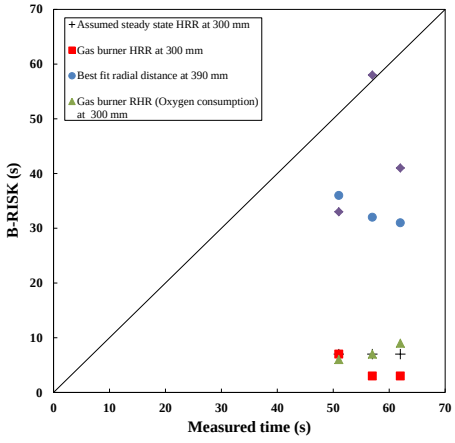


(d) MDF cube ignition times under the furniture calorimeter.

**Figure 45**. Furniture calorimeter experiment vs predicted ignition time of B-RISK.

## 4.4 Single Item in ISO 9705 room

In order to replicate the single item experiments in an ISO 9705 room in B-RISK, to the furniture calorimeter simulations, an assumed steady state output of 100kW is used. The following section describes comparisons between the experiments considering each individual input.

### 4.4.1 Single items HRR in the ISO 9705 room experiments

As mentioned previously in Chapter Three, a total of 6 single items tests were conducted in the ISO 9705 room, three for each of the PU foam armchair-A and the PU foam armchair-B. The Figures 39-40 shows the three measured HRR curves for each test. Similar to the furniture calorimeter tests the 100 kW gas burner input was removed. For each simulation the HRR curve from the test was used as the input for each item in the modelling. The average HRR for each test is also shown in Figures 39-40.

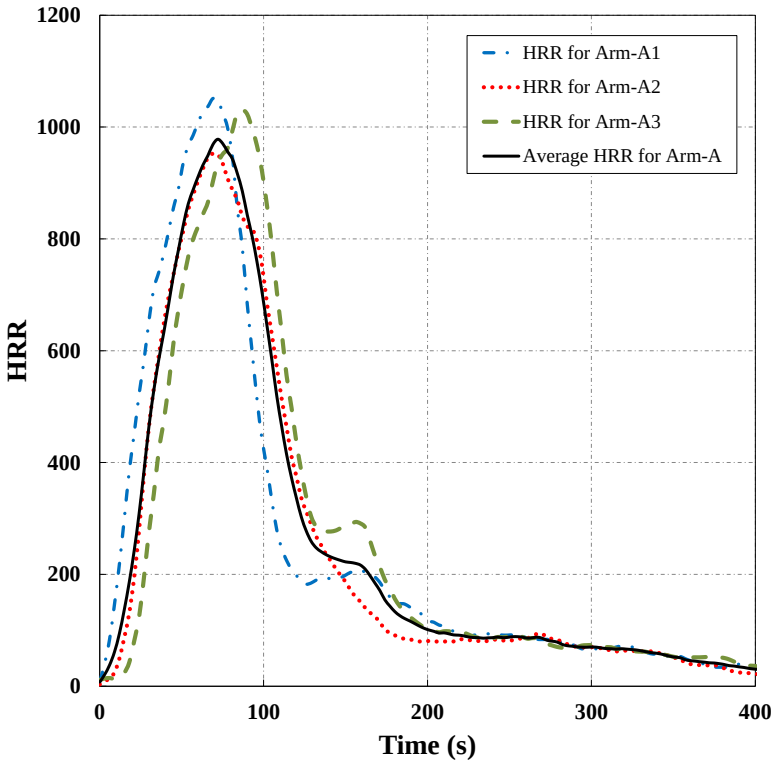


**Figure 46.** Single item ISO 9705 room experiment HRR for Arm-A

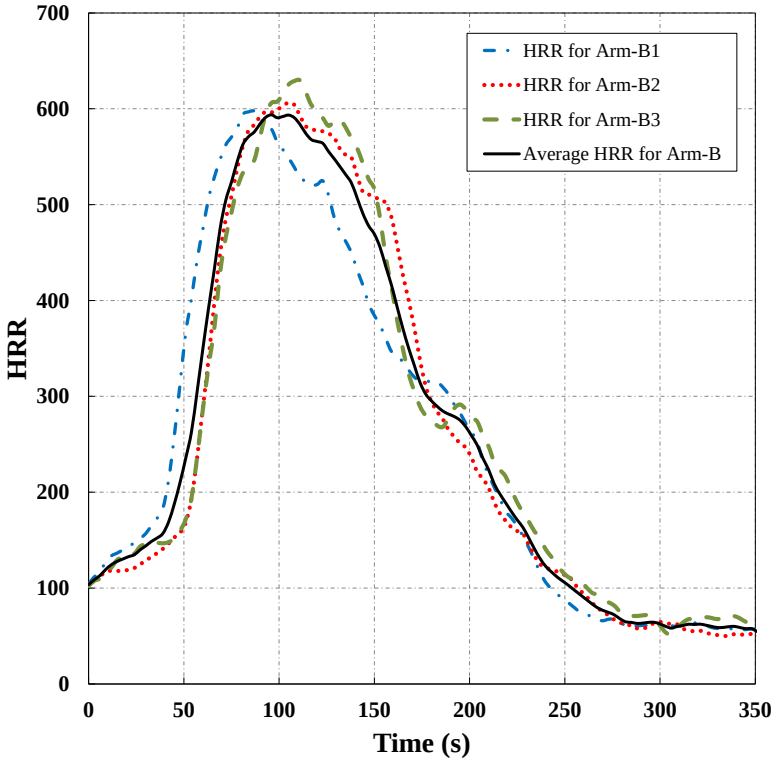


**Figure 47.** Single item ISO 9705 room experiment HRR for Arm-B

### 4.4.2 Single Item in ISO 9705 room comparison

The predicted ignition times for the armchair using the assumed steady state burner are again 44 s irrespective of the orientation, matching the furniture calorimeter predictions. The armchair ignition times using the measured burner output show an improved agreement with

the experimental results. The results show that B-RISK under and over-predicts the ignition time for Arm–A to within 14% average compared to the experiments. For the Arm–B orientation B-RISK over-predicts the ignition time by around 28% on average. Given that the flame in the ISO room was observed to be more stable than for the furniture calorimeter experiments the radial distance sensitivity is not applied.

### 4.4.3 Single –item in ISO 9705 room comparison with RHR inputs

Once more, the armchair ignition times using the measured burner output with Oxygen consumption as input showed an improved agreement with the experimental results. The results show that B-RISK under and over-predicts the ignition time for Arm–A to within 7% average compared to the experiments. For the Arm–B orientation B-RISK over-predicts the ignition time by around 42% on average. As mentioned previously above given that the flame in the ISO room was observed to be more stable than for the furniture calorimeter experiments the radial distance sensitivity was not applied.

### 4.4.4 Summary of the single items in the ISO 9705 room comparison

A summary comparison of actual ignition times from the experiments and corresponding predictions from B-RISK are shown in Figure 48 for the ISO 9705 room experiments. The data presented in each graph includes the results for the assumed steady-state 100 kW input, the measured HRR from the gas burner and HRR derived by OCC output for each experiment.

Predicted ignition times using the steady-state burner in the ISO 9705 room gives 44 s for both scenarios and an average ignition of 43 s or within 5% of the experimental measured values using the actual measured burner output.

Furthermore the radial distance sensitivity analysis was not applied for ISO room experiments as the results from the simulation deemed sufficiently close to the experimental results.

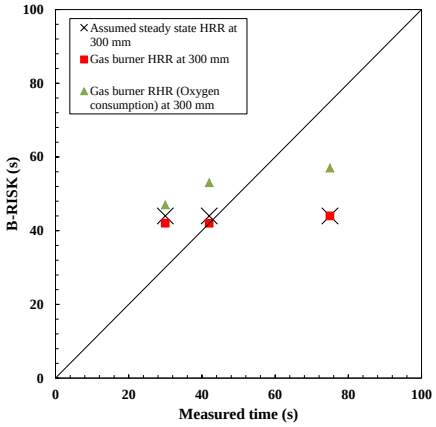


(e) Arm-A ignition times in ISO 9705 room.

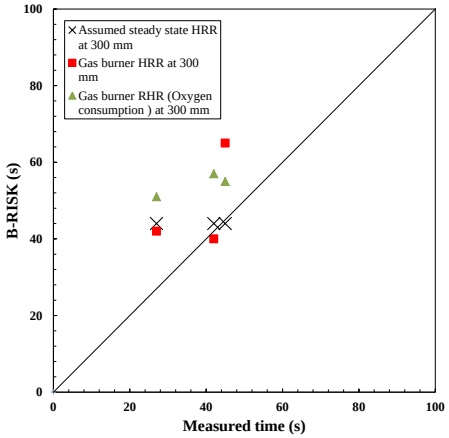


(f) Arm-B ignition times in ISO 9705 room.

**Figure 48**. ISO 9705 room experiment vs predicted ignition time of B-RISK.

## 4.5 Multi–item ISO 9705 room comparison

The final set of simulations was used as benchmark for the multi-item ignitions within the originally planned multi-item compartment fire scenarios. These simulations emphasised the importance of the ignition of the first and second items. This was due to the complexity of recording the ignition sequence for the rest of the items via observation of the experiments, where it was not possible to observe the exact ignition time of the remaining items.

Initially, only the first and second items ignited in each experiment are simulated. Then the full scenario replicated to see if additional items in the room changes the sequence and ignition time for each of the other items. However, there were no changes in the sequence or ignition time of the first two items as a result of adding other items within the compartment. Therefore the full scenario A and scenario B was simulated.

### 4.5.1 Items HRR in the ISO 9705 room Multi–item experiments

#### 4.5.1.1 Scenarios A

In order to model the three experiments for Scenario A, the HRR output from the burner for each of the triplicate experiment is used as input for the burner of each simulation. When selecting the heat release rate for each item, the average heat release rate input for Arm-A (single item in the ISO 9705 room) as shown in Figure 46 is used for both Arm-1 and Arm-2 in Scenario A. The average heat release rate input for the TV (Furniture calorimeter experiment HRR for TV) as shown in Figure 32 is used for all the room scenarios. To finish the average heat release rate input for the MDF cube (Furniture calorimeter experiment HRR for MDF) as shown in Figure 33 is used for all the MDF cubes (i.e. MDF-1,2,3 and 4). The layout items for Scenario A populated in B-Risk is shown in Figure 49 below.

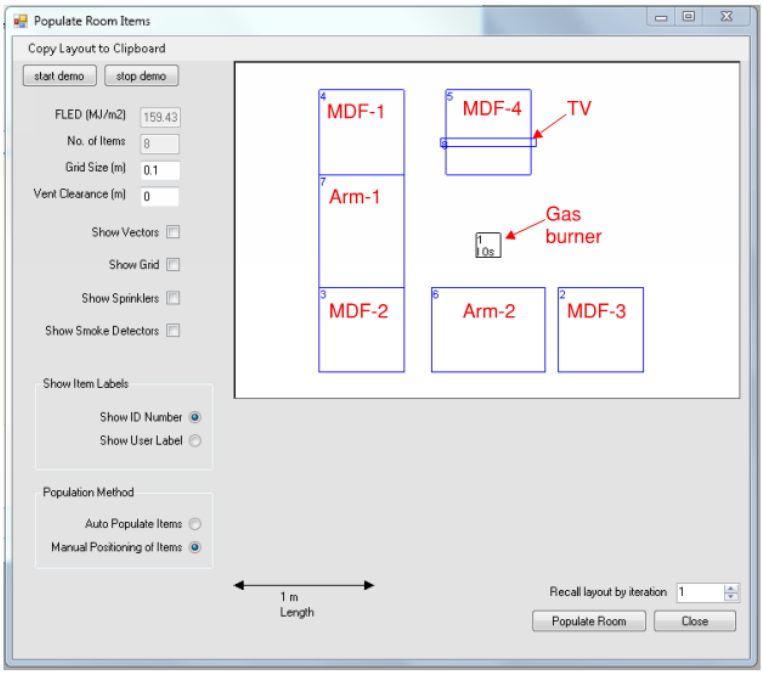


**Figure 49.** Scenario A populate room items in B-Risk

#### 4.5.1.2 Scenarios B

Similarly, to model the three experiments for scenario B the heat release rate output from the burner for each of the triplicate experiments is used for each simulation. Selecting the heat

release rate for each item, the average heat release rate input for Arm-B (single item in the ISO 9705 room) as shown in Figure 47 is used for Arm-3. This is due to the orientation of the burner to the armchair which is in the same location and orientation of the single item test in the ISO 9705 room. However for the other armchairs in scenario B (Arm-1 and Arm-2), the average heat release rate input for Arm-A (single item in the ISO 9705 room) as shown in Figure 46 is used. The rest of the heat release rate inputs are used the same as explained above for scenario A. The layout items for Scenario B populated in B-Risk is shown in Figure 50 below.

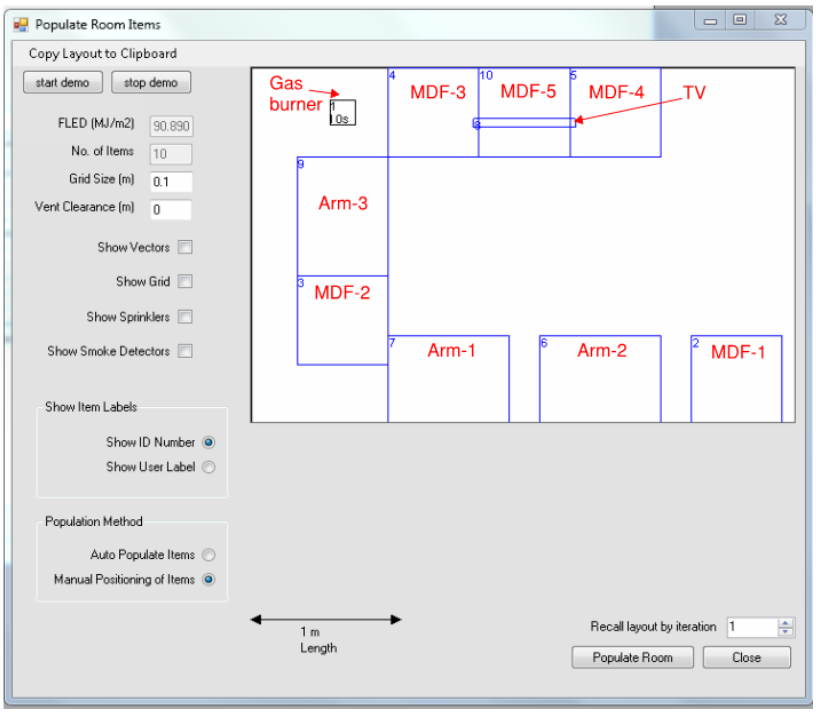


**Figure 50.** Scenario B populate room items in B-Risk

### 4.5.2 Multi–item in ISO 9705 room comparison

#### 4.5.2.1 Scenarios A

The ignition sequence for each of the three Scenario A experiments is recorded in Table 10, along with the modelling predictions for each of the experiments using the HRR inputs from

Section 4.5.1.1. As previously mentioned in Chapter Three the shaded grey entries are estimates only, where it was not possible to observe exactly when ignition occurred.

The development of the fire for all three experiments is driven by the ignition of the two armchairs and their ignition was observed during the experiments. The DFG submodel makes a reasonably accurate predation of the ignition of the first two armchairs although the order is the other way around. The DFG submodel predicted the first experiment relatively close by over predicting only by 12s. The reason for the delayed ignition times for the other two experiments was most likely due to the ABS sagging onto the top of MDF-4 and therefore receiving less radiation if the ABS had remained in a vertical orientation. As mentioned previously during all the experiments it was virtually impossible to accurately observe when the MDF cubes ignited, however the DFG submodel on average over predicted the ignition of the MDF cubes modelled in the compartment.

**Table 10** Ignition times comparison for Scenario A in the compartment room

| Item | Ignition time (s) | | | | | |
|---|---|---|---|---|---|---|
| | Model-1 | Experiment-1 | Model-2 | Experiment-2 | Model-3 | Experiment-3 |
| Arm-1 | 102 | 49 | 104 | 60 | 95 | 34 |
| Arm-2 | 67 | 171 | 69 | 205 | 60 | 213 |
| MDF-1 | 139 | ≈ 150-160 | 141 | ≈ 160-170 | 132 | ≈ 125-135 |
| MDF-2 | 125 | ≈ 175-180 | 127 | ≈ 210-220 | 118 | 173 |
| MDF-3 | 120 | ≈ 175-180 | 122 | ≈ 210-220 | 113 | ≈ 220-230 |
| MDF-4 | 163 | 184 | 165 | 268 | 155 | 283 |
| TV | 166 | 154 | 168 | 270 | 158 | 280 |

#### 4.5.2.2 Scenarios B

Contrasting to Scenario A, there was no ignition of any items for each of the two Scenario B experiments as previously detailed in Chapter Three. However the modelling predictions and

ignition sequences for each of the two experiments using the HRR inputs from Section 4.5.1.2. are recoded in Table 11.

**Table 11** Ignition times comparison for Scenario B in the compartment room

| Item | Ignition time (s) | | | |
|---|---|---|---|---|
| | Model-1 | Experiment-1 | Model-2 | Experiment-2 |
| **Arm-1** | **249** | **NI** | **209** | **NI** |
| **Arm-2** | **280** | **NI** | **240** | **NI** |
| **Arm-3** | **153** | **NI** | **113** | **NI** |
| **MDF-1** | **347** | **NI** | **307** | **NI** |
| **MDF-2** | **234** | **NI** | **194** | **NI** |
| **MDF-3** | **226** | **NI** | **186** | **NI** |
| **MDF-4** | **700** | **NI** | **637** | **NI** |
| **MDF-5** | **652** | **NI** | **594** | **NI** |
| **TV** | **580** | **NI** | **516** | **NI** |

Although there are no actual experimental results to directly compare the B-RISK prediction. The delay in ignition of the Arm-1 and the sequence of ignition prediction are relatively similar to the amended Scenario B which is referred to as Scenario D in Chapter Three.

### 4.5.3 Summary & recommendations of multi–items in the ISO 9705 room comparison

The parameters in the DFG submodel should be further investigated and varied so the prediction capabilities could improve further. Additional sensitively analysis can be done on the radial distance between items within the compartment. This was investigated for the single items under the further calorimeter earlier in this Chapter. Other parameters could include the use of the actual HRR for each item from the experiment rather than taken from previous experiments, e.g. the single items or furniture calorimeter. Finally further exploring the FTP target ignition values in the DFG submodel, i.e. increase the value of $\dot{q}_{cr}^{"}$.

It is not possible to completely benchmark the multi-item experiments because of the large number of combinations and permutations possible from the wide range of input assumptions. The findings do not show a clear correlation between experiments and model predictions, further work is required to explore the capability of B-RISK to predict item to item ignitions within a compartment.

# Chapter Five

# CONCLUSIONS

The ignition times of mock-up armchair, TV and cabinetry furniture items exposed to a nominal 100 kW burner heat source have been measured in the furniture calorimeter and the ISO 9705 room. The items were constructed of PU foam, ABS and MDF respectively. Experiments in the cone calorimeter have been carried out to get ignition data in both the piloted- and auto-ignition modes, which was subsequently analysed using the FTP methodology. Ignition times in the furniture calorimeter were affected by the furniture item material, its orientation to the burner and the fluctuation of the burner flames. In the experiments, ignition of the MDF cube could only be achieved by having the burner in close proximity to a vertical face of the mock-up item. Ignition times for the armchairs in the ISO 9705 room experiments were shorter than the equivalent furniture calorimeter experiments.

For the armchair and TV items in which the burner was not in direct contact, an assessment of the output rate of heat release from the burner showed a better comparison between the experiments and B-RISK predictions when the measured burner data was used rather than assuming a steady-state output. Further assessment was done applying HRR output from the OCC. This was a 30 s average value which was based on Oxygen consumption and was less constant then the gas flow burner outbut.

During the armchair and TV experiments in the furniture calorimeter, fluctuation in the position of the burner flame was noticeable. It was therefore decided to adjust the ignition predictions in B-RISK by varying the radial distance parameter, as a proxy representation of the observed flame instability, but the other parameters in the mathematical formulation of the PSM and FTP method were assumed to be constant. As the radial distance increases, the

radiation received (PSM) by the object decreases, which in turn means that the time to ignition (FTP) increases at a greater rate. Hence the radial distance was varied to get a better match between experiments and predictions, and for the mock-up armchair and TV furniture calorimeter simulations, an addition of 10–30 mm to the baseline radial distance is required to get a match to the experiments to within 11% or better. For the ISO 9705 Room experiments, the B-RISK results for the armchair scenarios where much closer to the experimental results and in all but one case over-predicted the experimental time to ignition result. Therefore given the reasonable match there was not much benefit in applying the radial distance adjustment for these simulations. B-RISK is unable to predict ignition times for the MDF cube of the same order of magnitude as the experimental results. The FTP method was developed for radiant exposures in the range 0 to 100 kW/m2 (which equates to a radial distance greater than 150 mm for this burner output level). This would suggest that the FTP method is not appropriate where radiation exceeds 100 kW/m2.

Further simulations were done to replicate the multi-items ignition within the ISO 9705 room emphasised the importance of the ignition of the first and second items.

This benchmarking exercise shows that B-RISK can produce reasonable results for secondary item ignition when the source and target are not in direct contact although predicted times are affected by the assumed radial distance.

# Chapter Six

# RECOMMENDATIONS FOR FURTHER WORK

In addition to the benchmarking the DFG submodel capability and predictability for secondary item ignition via radiation within B-RISK, there is scope for further related work in this field. This may entail an extension of the work presented in this thesis or merely draw on certain aspects for a different purpose altogether.

Although the experimental programme aimed to cover a range of potential fire scenarios by varying many different factors, it would be useful to broaden the scope of the experiments even more. This could be done in the following ways (among others):

- Investigate the ignition time of secondary items by increasing the distance between the burner and each of the tested items, also include changes to the orientation of items against the burner and explore elevating the burner further up off the ground.
- Further investigate the distribution of radiant heat flux with lateral position relative to the face of the fire.

For the furniture calorimeter each experiment for each of the three items was repeated 3 times and due to the lack of time single item compartment experiments were carried out for the two armchair arrangements only.

By collecting experimental data from a wider range of scenarios there will be a better range of results. This could result in better benchmarking the DFG submodel and its limitations, assumptions and errors would be further highlighted.

There is potential for further benchmarking and validating CFD models and other zone models with the collection of data from the series of the experiments these includes (among others):

- Compare ignition times in models versus experiment
- Investigate how material properties influence ignition time
- Compare layer temperature in experiment versus models

It is also recommended that all future experiments to be video recorded this includes the single items under the furniture calorimeter and in the ISO rooms. Furthermore software such as ImageStream can be used to analyse flame shapes, volumes, pulsation frequencies and the location of ignition occurring on the tested items. Therefore video capture of the all experiments for further sensitivity analyses would be beneficial. This could help further analyse the flame orientation and movement with the location of ignition occurring on the tested items.

# REFERENCES


[1] Wade, C.A, Baker, G.B , Frank, K, Robbins, A, Harrison, R, Spearpoint, M.J. and Fleischmann, C.M (2013) B-RISK User guide and technical manual, BRANZ Study Report SR 282, Porirua, New Zealand: BRANZ Ltd.

[2] Wade, C. A. (2004). BRANZ Study Report No. 92 (revised 2004), BRANZFIRE Technical Reference Guide. Porirua, New Zealand: BRANZ Ltd.

[3] Forney, G.P.; McGrattan, K.B. 2007. User's Guide for Smokeview Version 5 - A Tool for Visualizing Fire Dynamics Simulation Data. NIST Special Publication 1017.1 Gaithersburg, MD: National Institute of Standards and Technology.

[4] Baker, G.B., Collier, P.C., Wade, C.A., Spearpoint, M.J., Fleischmann, C.M., Frank, K. and Sazegara, S. A comparison of a priori modelling predictions with experimental results to validate a design fire generator submodel. San Francisco, CA, USA: 13th International Fire and Materials Conference 2013, 28-30 Jan 2013.

[5] Wade, C.A, (2013) B-RISK 2013 Software Benchmarking Examples, BRANZ Study Report SR 292, Porirua, New Zealand: BRANZ Ltd.

[6] Shah, A. A comparison of the NIST workstations experiment with the B-RISK Desgin Fire Generator, University of Canterbury, Unpublished (2013).

[7] Madrzykowski, D., and Walton, W.D., Cook County Administration Building Fire, 69 Weat Washington, Chicago, Illinois, October 17, 2003: Heat Release Rate Experiments and FDS Simulations, National Iinstitute of Standards and Technology, Special PublicationSP-1021.

[8] Shields, T.J., Silcock, G.W. and Murray, J.J. (1994) Evaluating Ignition Data Using the Flux Time Product, Fire and Materials, Vol. 18, 243-254.

[9] Drysdale, D. (1999), An Introduction to Fire Dynamics. Second edition. John Wiley and Sons Ltd, Chichester, pp 212-222.

[10] Baker, G.B., Spearpoint, M.J., Fleischmann, C.M., and Wade, C.A., (2010) Selecting an Ignition Criterion Methodology for Use in a Radiative Fire Spread Submodel, Fire and Materials,2011.35(6):p.367-381, DOI:10.1002/fam.1059

[11] Smith, E.E., and Satija, S., (1983) Release Rate Model for Developing Fires, Journal of Heat Transfer 105(2): 281-287, http://dx.doi.org/10.1115/1.3245575

[12] Silcock, G.W.H., & Shields, T.J., "A Protocol for Analysis of Time-to-Ignition Data From Bench Scale Tests", Fire Safety Journal, Vol. 24, 75-95, 1995.

[13] Smith, E.E., and Green, T.J., Release Rates for a Mathematical Model, In Mathematical Modelling of Fires ASTM SPT 983, Mehaffey, J.R. (ed.), American Society of Testing and Materials SPT 983, Philadelphia, PA, USA, 1988, pp. 7-20.

[14] Toal, B.R., Silcock, G.W.H., and Shields, T.J., (1989) An examination of piloted ignition characteristics of cellulosic materials using the ISO Ignitability Test, Fire and Materials 14: 97-106, http://dx.doi.org/10.1002/fam.810140304

[15] Shields, T.J., Silcock, G.W., and Murray, J.J., (1993) The effect of geometry and ignition mode on ignition times obtained using the cone calorimeter and ISO Ignitability Test, Fire and Materials 17: 25-3. http://dx.doi.org/10.1002/fam.810170105

[16] Shields, T.J., Silcock, G.W., and Murray, J.J., (1994) Evaluating Ignition Data Using the Flux Time Product, Fire and Materials 18: 243-254 http://dx.doi.org/10.1002/fam.810180407

[17] Fleury R, Spearpoint M, Fleischmann C. Evaluation of thermal radiation models for fire spread analysis. Fire and Evacuation Modeling Conference 2011, Aug 15-16, Baltimore, MD, USA, 2011.

[18] Modak,A.T., Thermal Radiation From Pool Fires, Combustion and Flame, Vol.29,1977,pp.177-192, DOI:10.1016/0010-2180(77)90106-7

[19] AS/NZ 3837. Method of Test for Heat and Smoke Release Rates for Materials and Producs Using an Oxygen Consumption Calorimeter. Standards Australia and Standards New Zealand ,Homebush, Australia and Wellington, New Zealand, 1998.

[20] Piloted Ignition of Solid Materials Under Radiant Exposure, SFPE, Fire Engineering Guide: Society of Fire Protection Engineers, P.J. DiNenno, et al., Editors. 2008, National Fire Protection Association: Quincy, MA. p.

[21] Tewarson, A., Generation of Heat and Gaseous, Liquids, and Solid Products in Fires, in SFPE Handbook of Fire Protection Engineering, P.J. DiNenno, et al., Editors. 2008, National Fire Protection Association: Quincy, MA. p. 3/109 - 3/194.

[22] Janssens, M., Calorimetry, in SFPE Handbook of Fire Protection Engineering, P.J. DiNenno, et al., Editors. 2008, National Fire Protection Association: Quincy, MA. p. 3/60 - 3/89.

[23] Janssens, M.L., "Fundamental Thermophysical Characteristics of Wood and their role in Enclosure Fire Growth", PhD Dissertation, University of Gent, Belgium, 1991.

# APPENDICES

## Appendix A: Gas burner HRR derived from the OCC as input output for all the experiments used in B-RISK

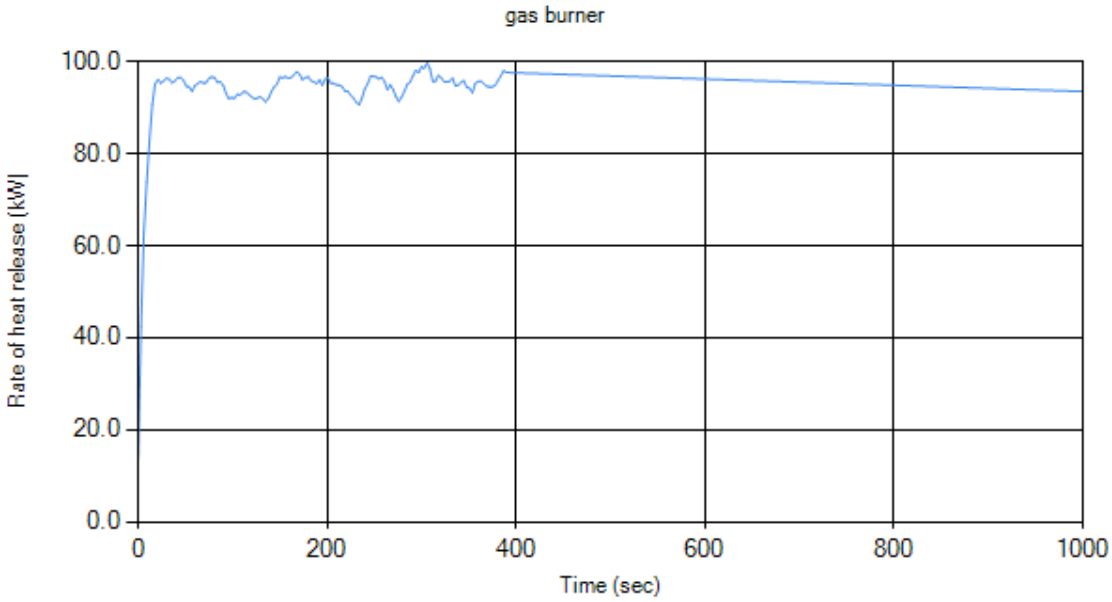


**Figure 51.** Furniture calorimeter experiment gas burner HRR for Arm–A1

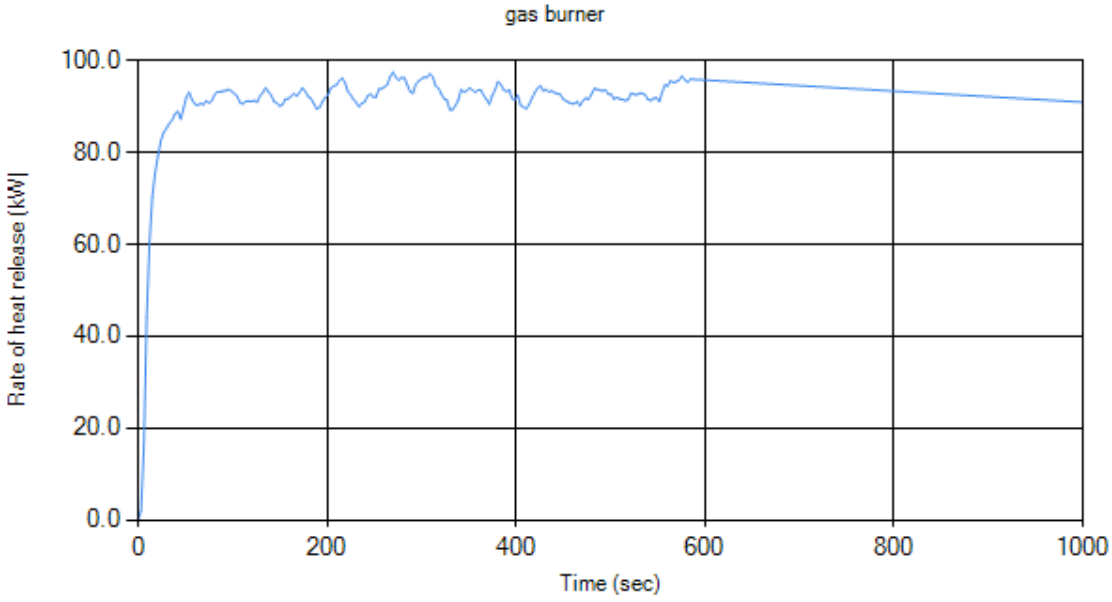


**Figure 52.** Furniture calorimeter experiment gas burner HRR for Arm–A2

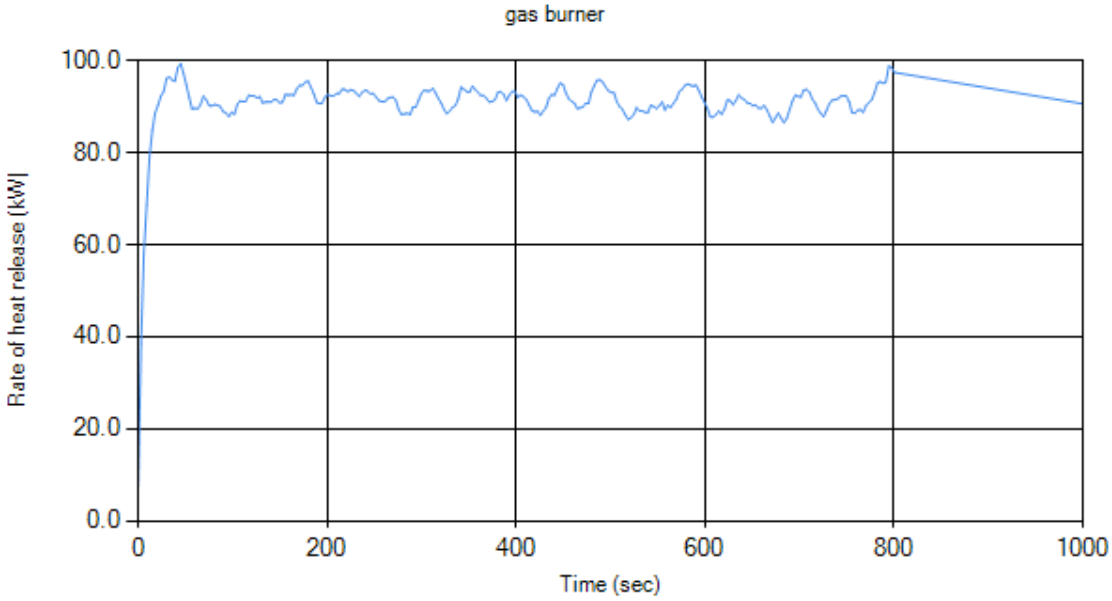


**Figure 53.** Furniture calorimeter experiment gas burner HRR for Arm–A3

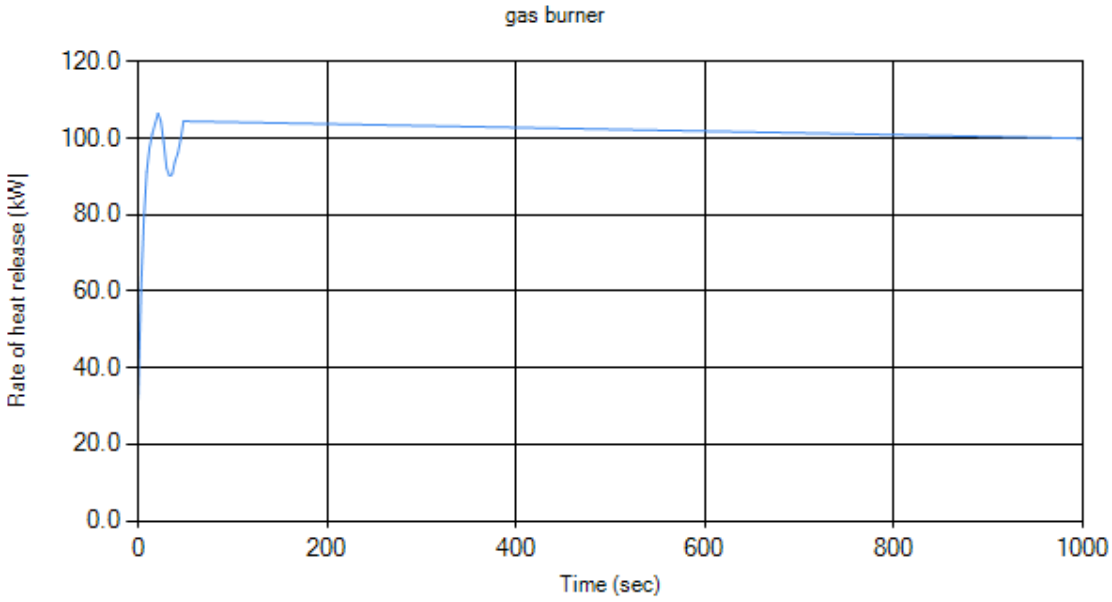


**Figure 54.** Furniture calorimeter experiment gas burner HRR for Arm–B1

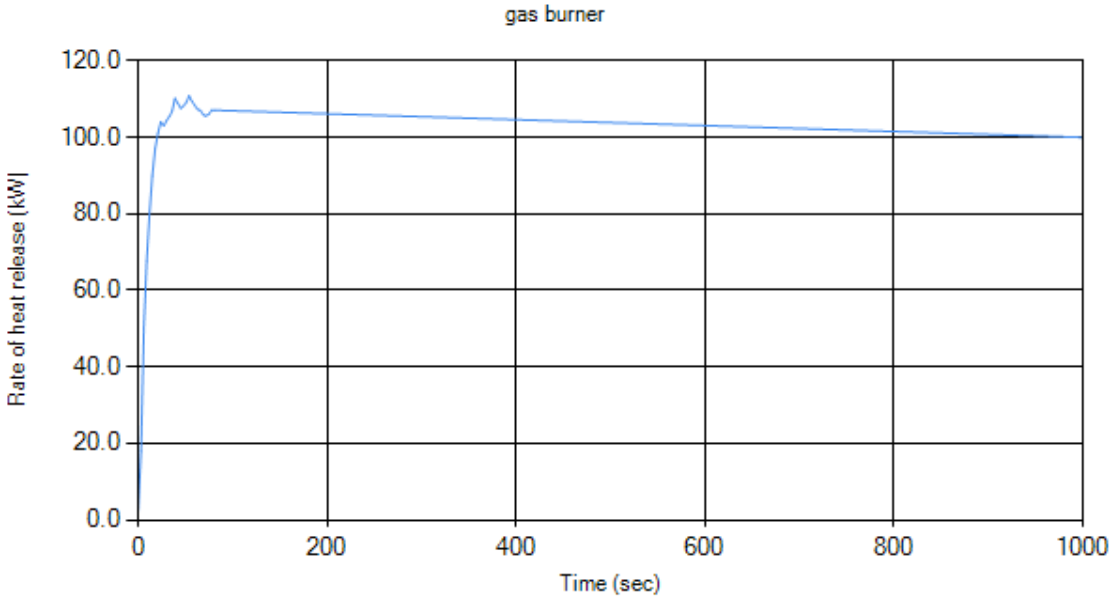


**Figure 55.** Furniture calorimeter experiment gas burner HRR for Arm–B2

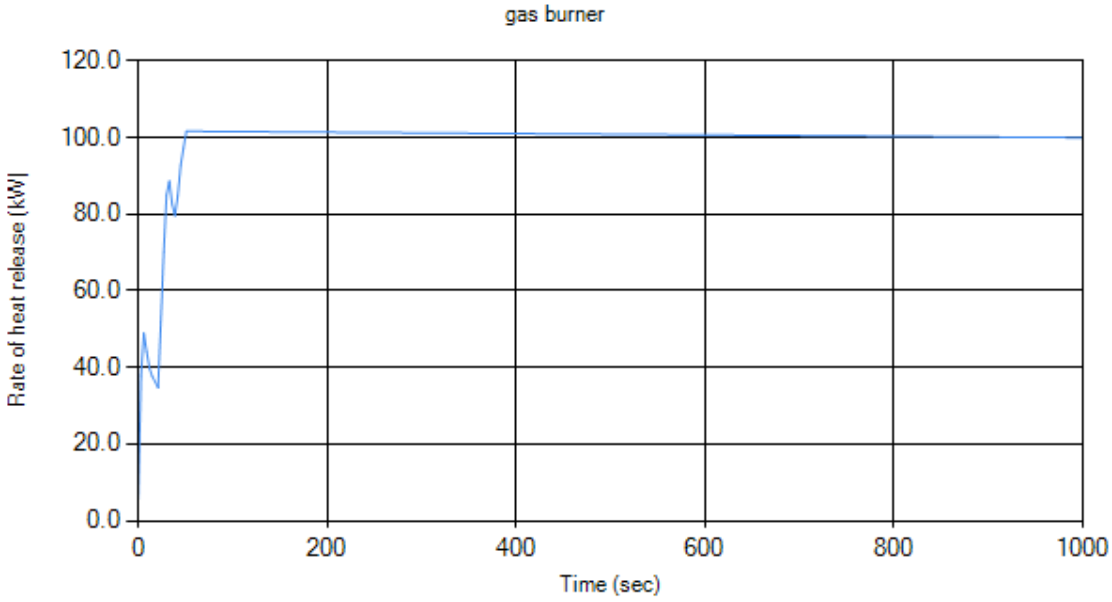


**Figure 56.** Furniture calorimeter experiment gas burner HRR for Arm–B3

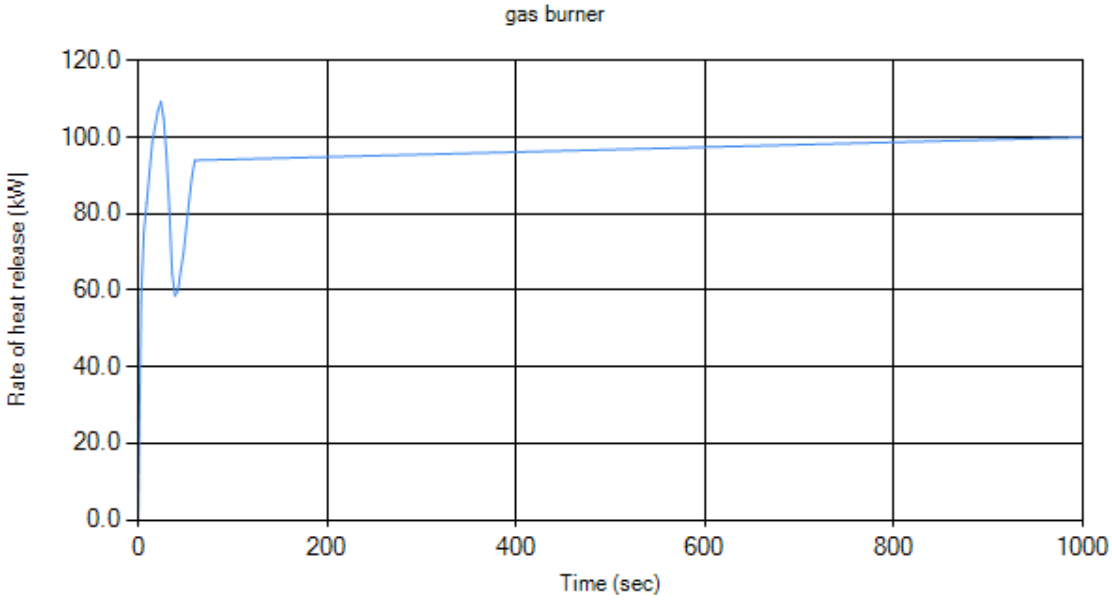


**Figure 57.** Furniture calorimeter experiment gas burner HRR for MDF–1

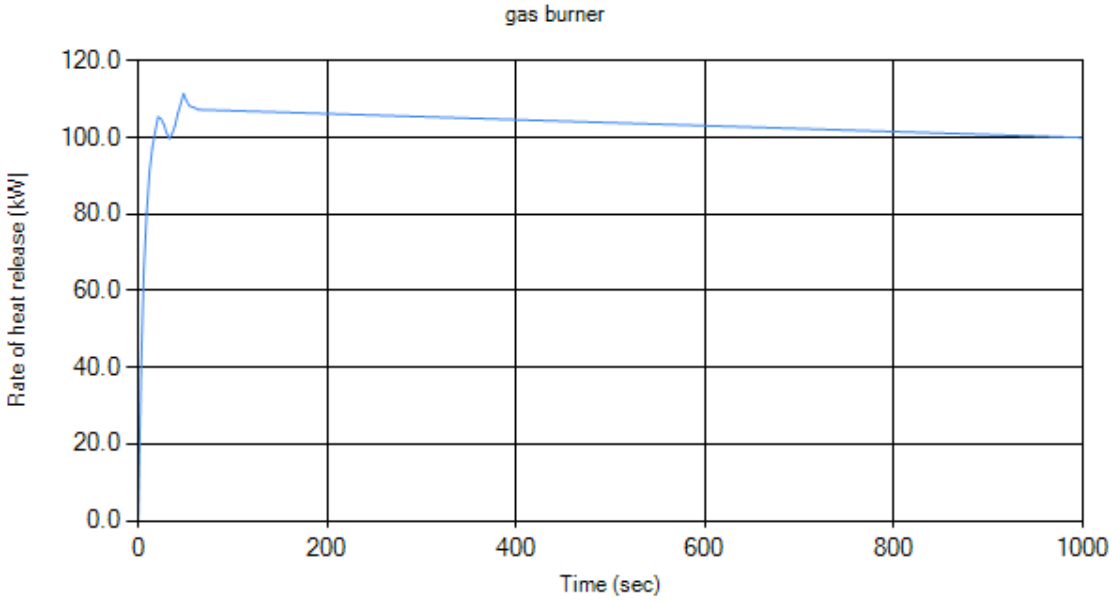


**Figure 58.** Furniture calorimeter experiment gas burner HRR for MDF–2

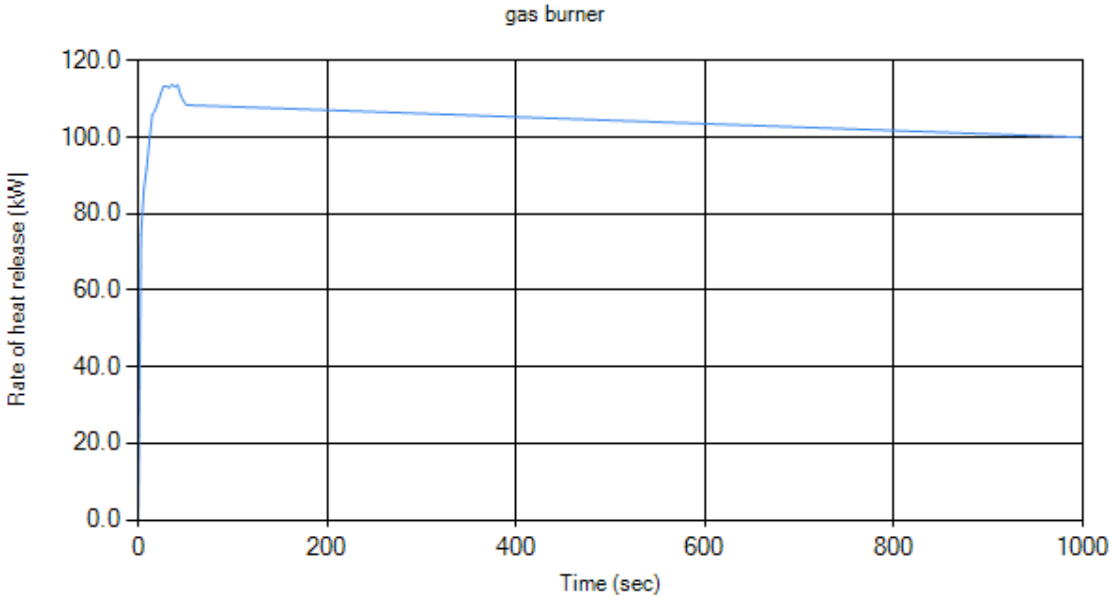


**Figure 59**. Furniture calorimeter experiment gas burner HRR for MDF–3

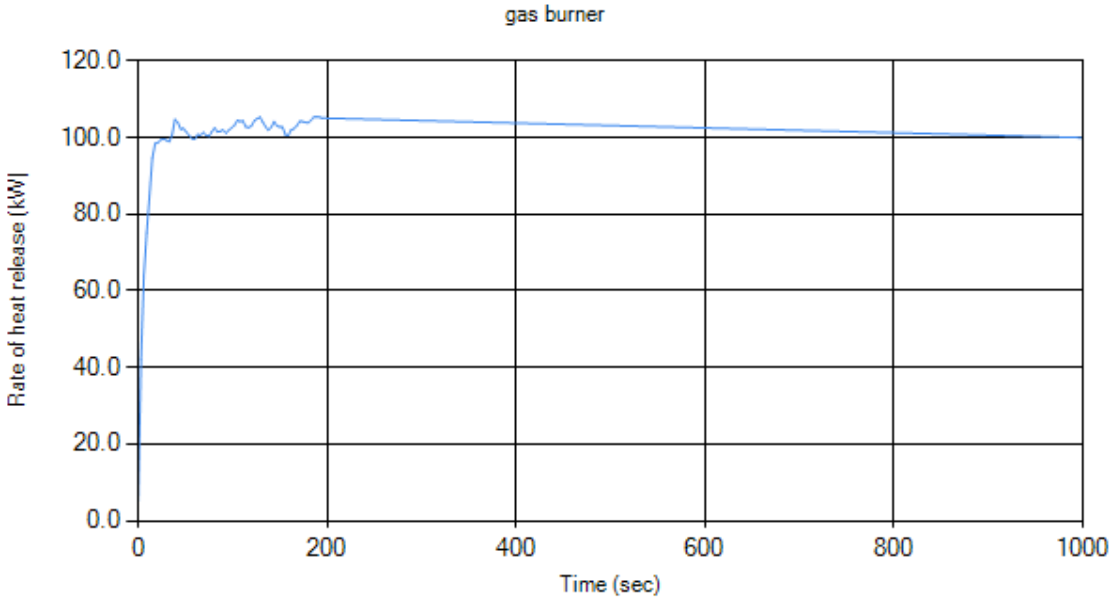


**Figure 60.** Furniture calorimeter experiment gas burner HRR for TV–1

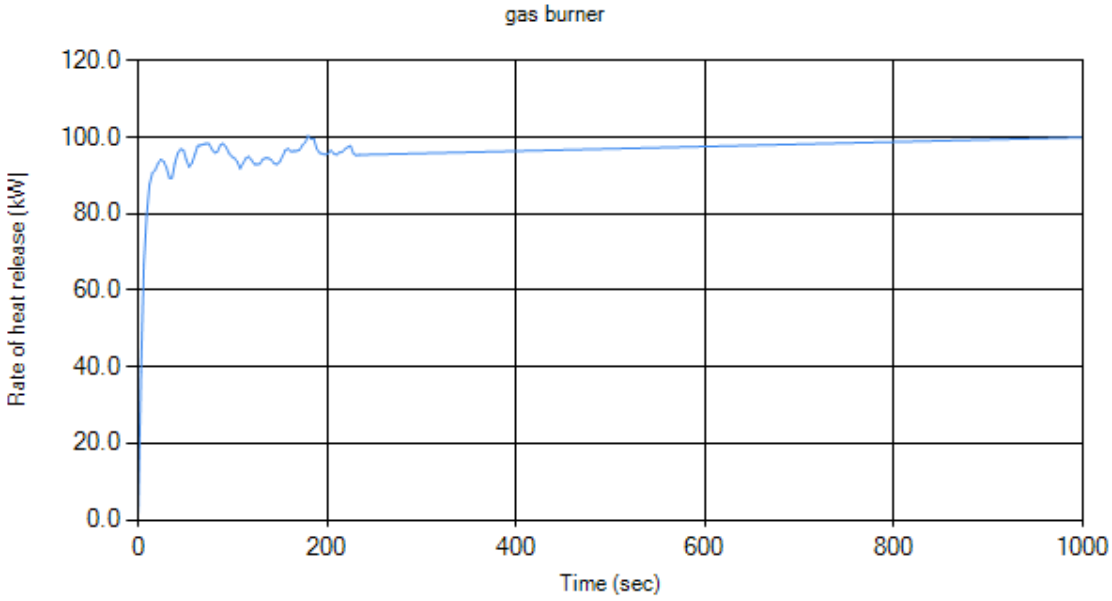


**Figure 61.** Furniture calorimeter experiment gas burner HRR for TV–2

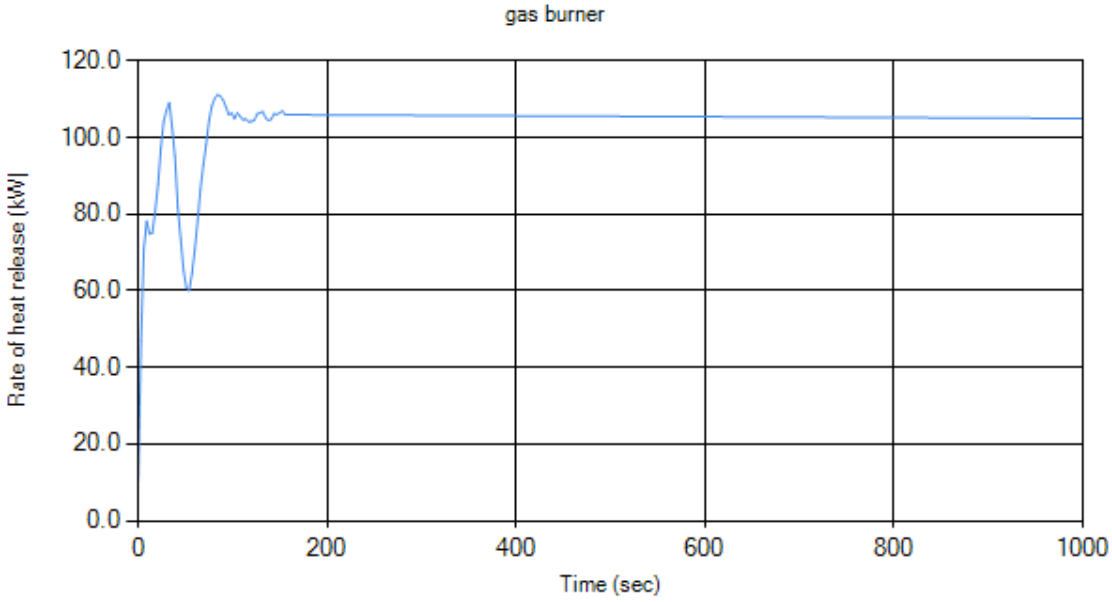


**Figure 62.** Furniture calorimeter experiment gas burner HRR for TV–3

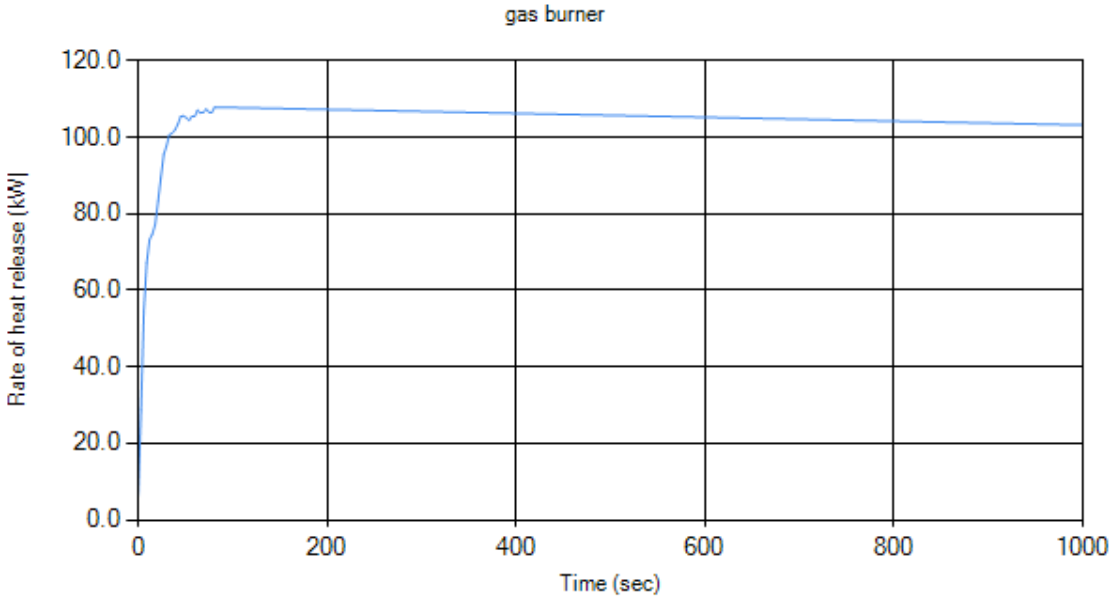


**Figure 63.** Single item in ISO 9705 room experiment gas burner HRR for Arm–A1

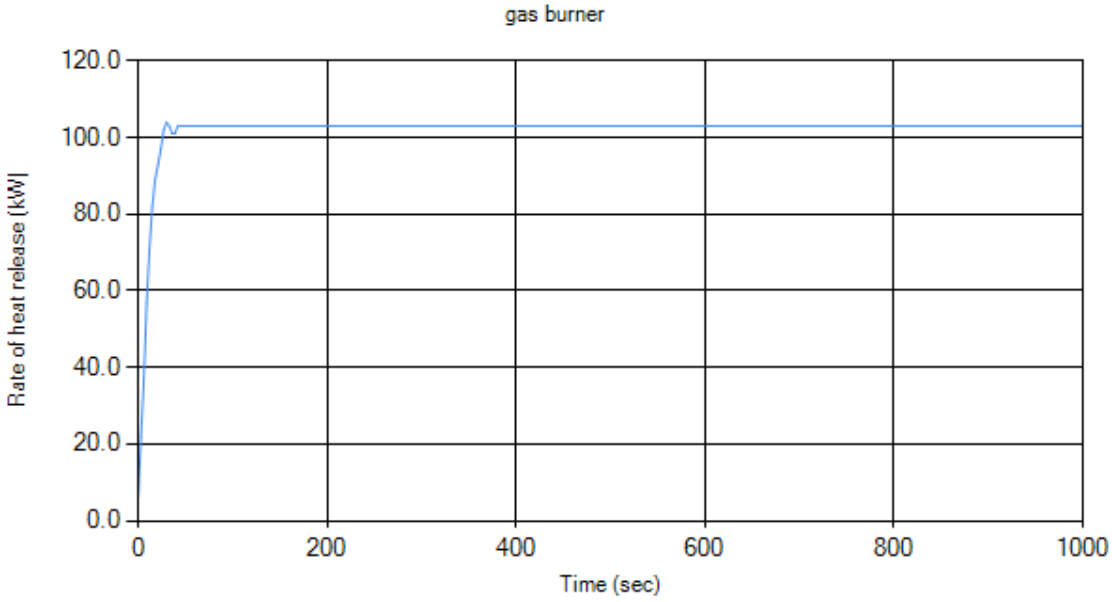


**Figure 64.** Single item in ISO 9705 room experiment gas burner HRR for Arm–A2

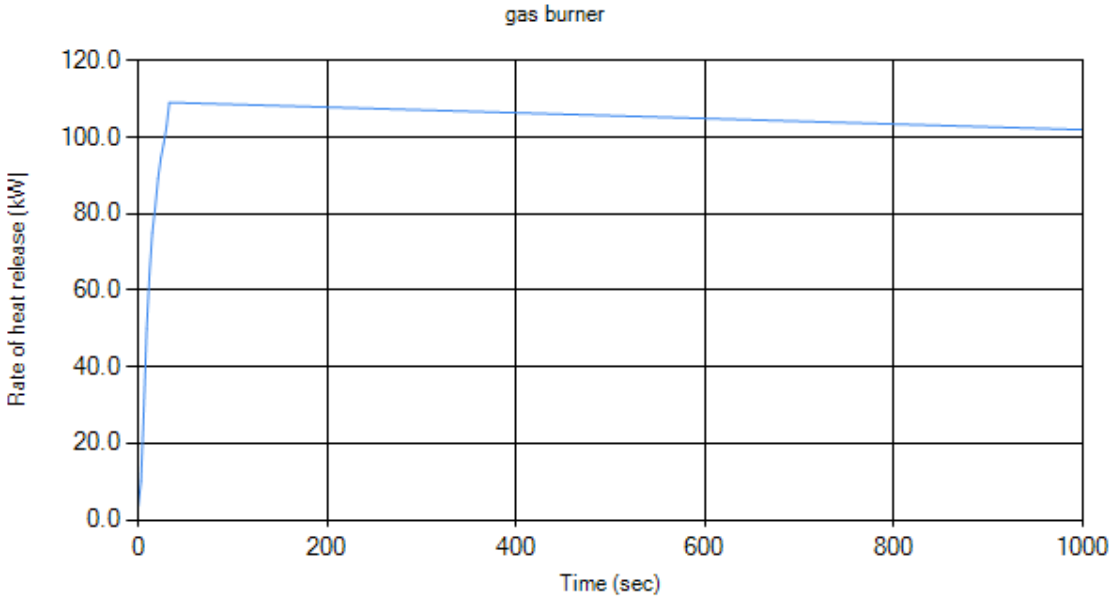


**Figure 65.** Single item in ISO 9705 room experiment gas burner HRR for Arm–A3

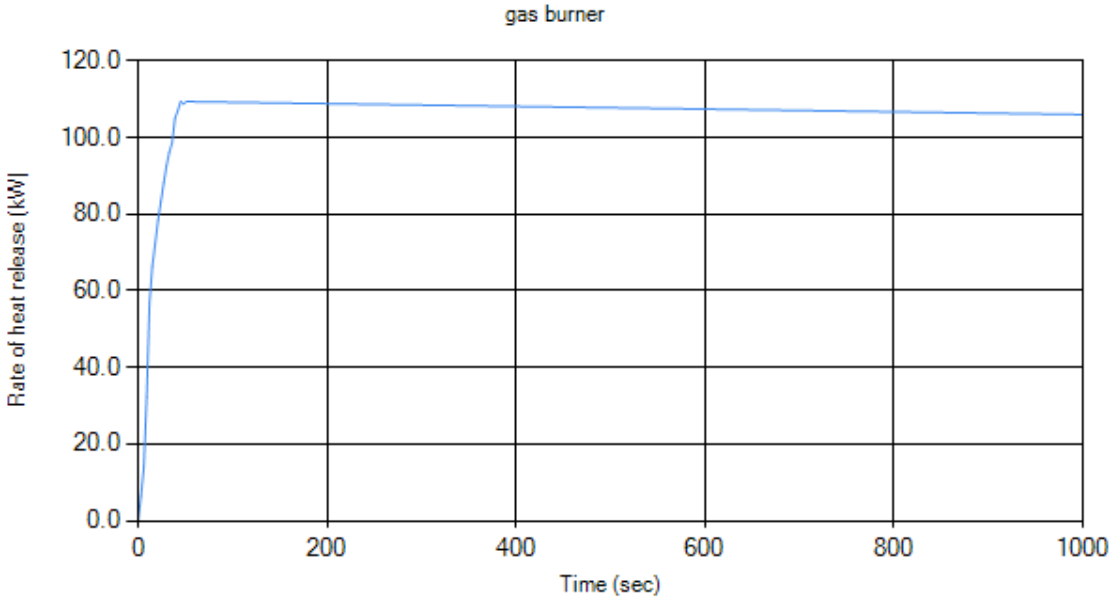


**Figure 66.** Single item in ISO 9705 room experiment gas burner HRR for Arm–B1

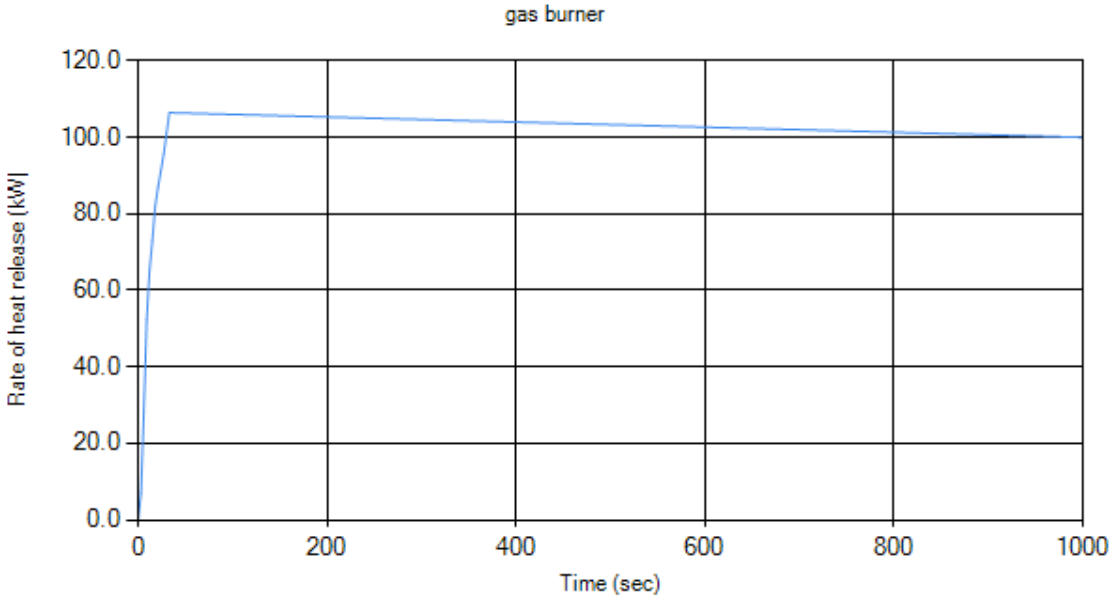


**Figure 67.** Single item in ISO 9705 room experiment gas burner HRR for Arm–B2

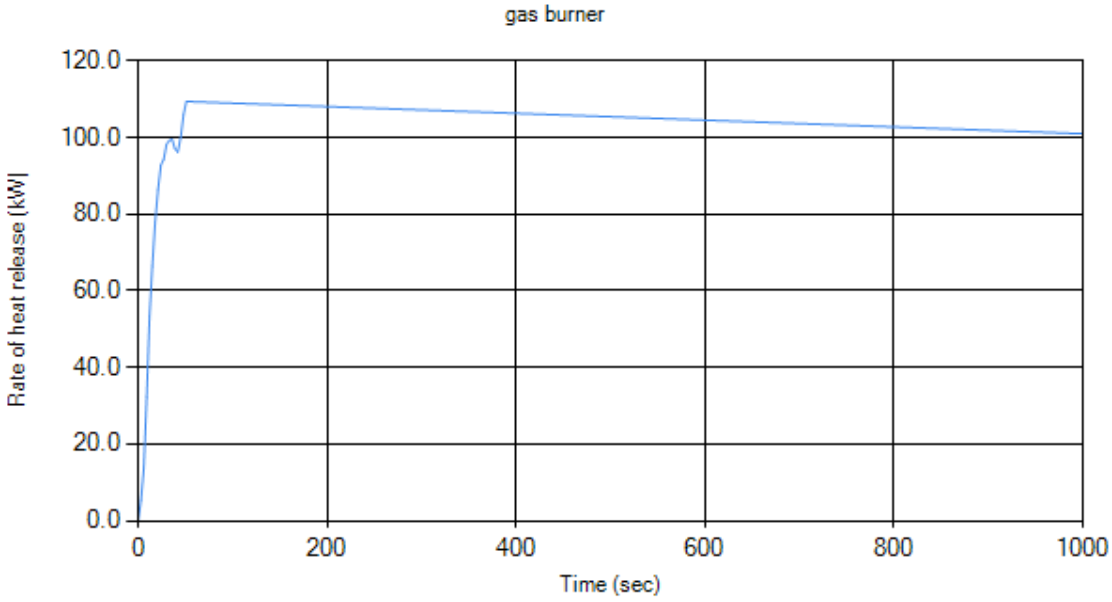


**Figure 68.** Single item in ISO 9705 room experiment gas burner HRR for Arm–B3

## Appendix B: Gas burner RHR with Oxygen consumption as input output for all the experiments used in B-RISK

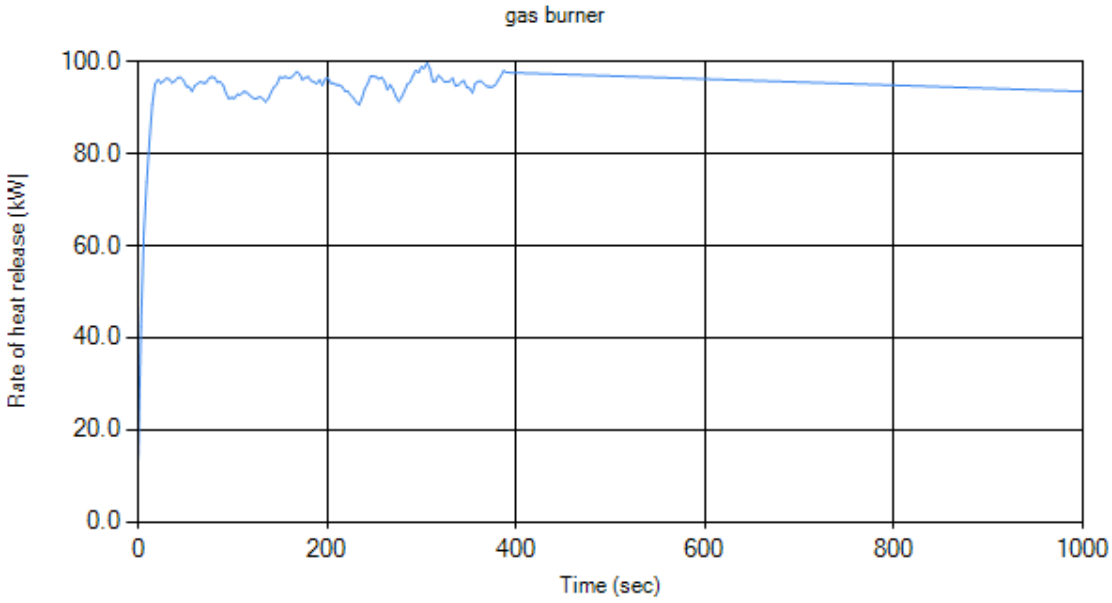


**Figure 69.** Furniture calorimeter experiment gas burner HRR for Arm–A1

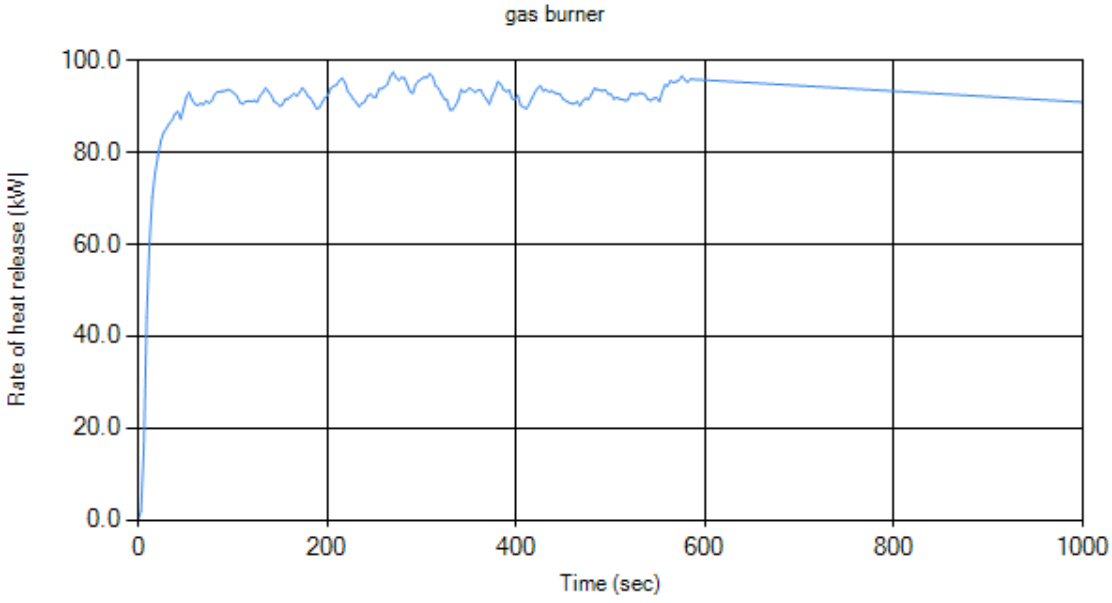


**Figure 70.** Furniture calorimeter experiment gas burner HRR for Arm–A2

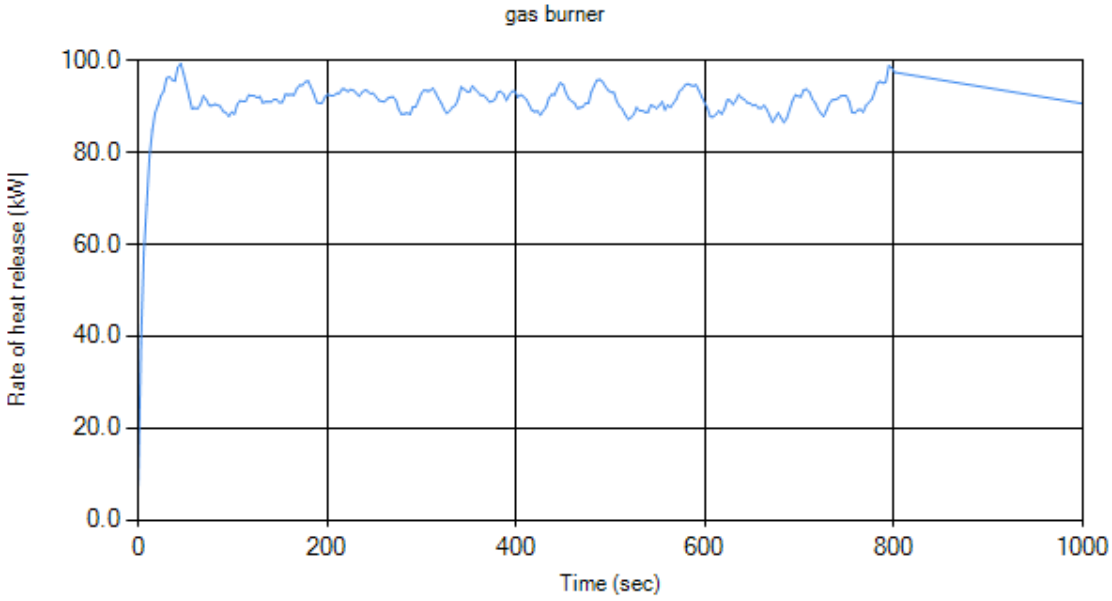


**Figure 71.** Furniture calorimeter experiment gas burner HRR for Arm–A3

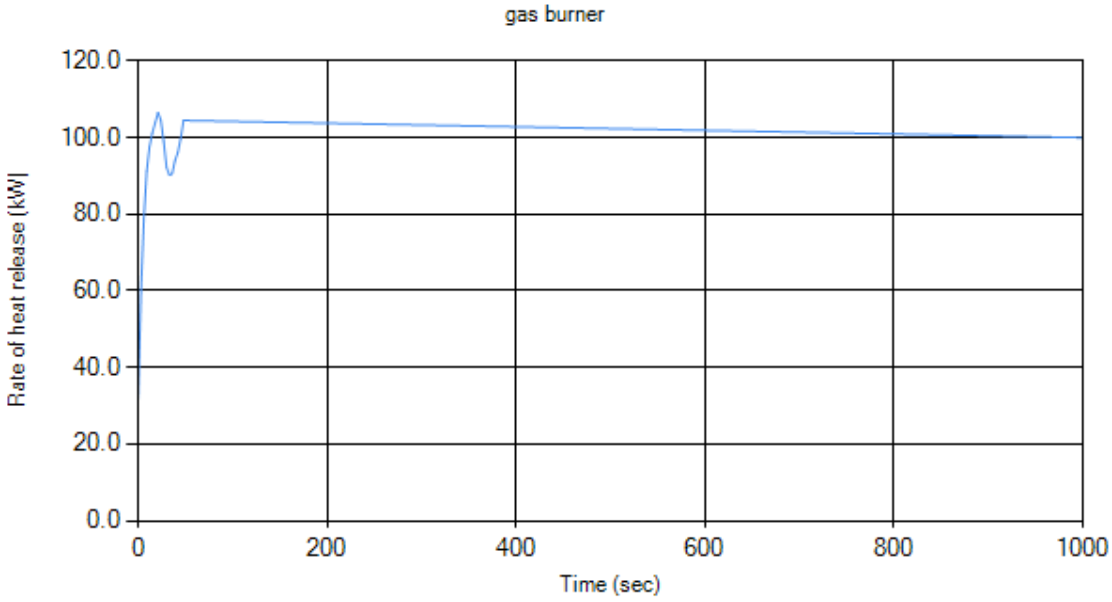


**Figure 72.** Furniture calorimeter experiment gas burner HRR for Arm–B1

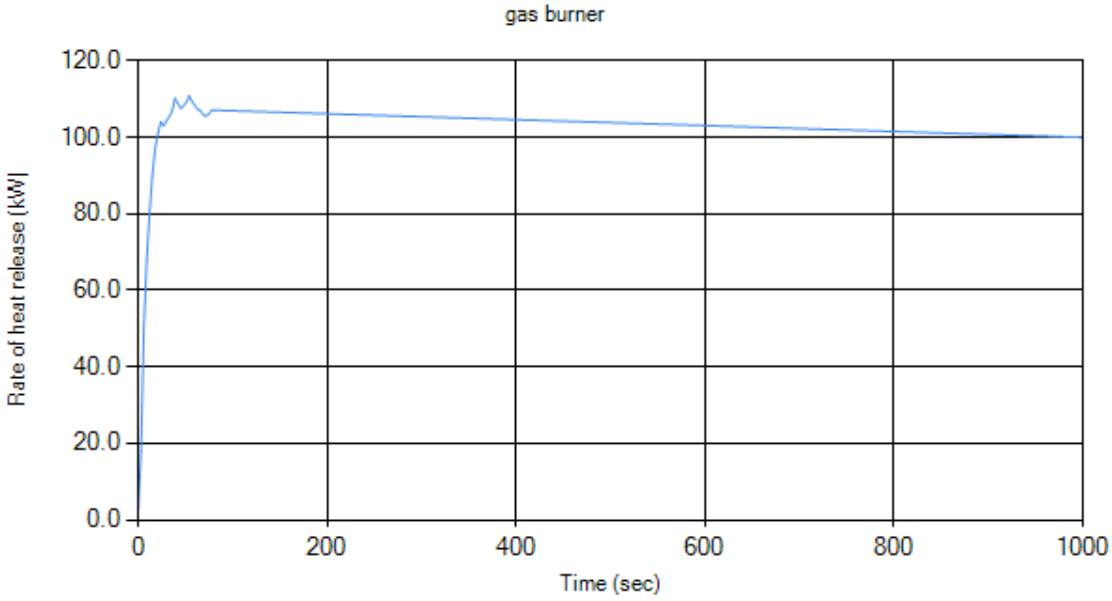


**Figure 73.** Furniture calorimeter experiment gas burner HRR for Arm–B2

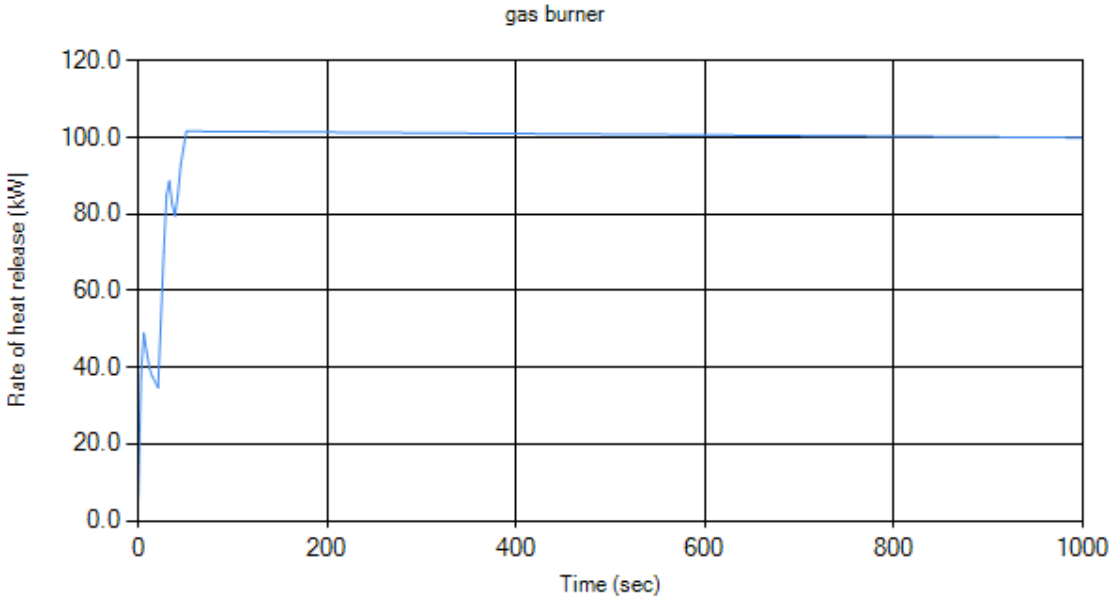


**Figure 74.** Furniture calorimeter experiment gas burner HRR for Arm–B3

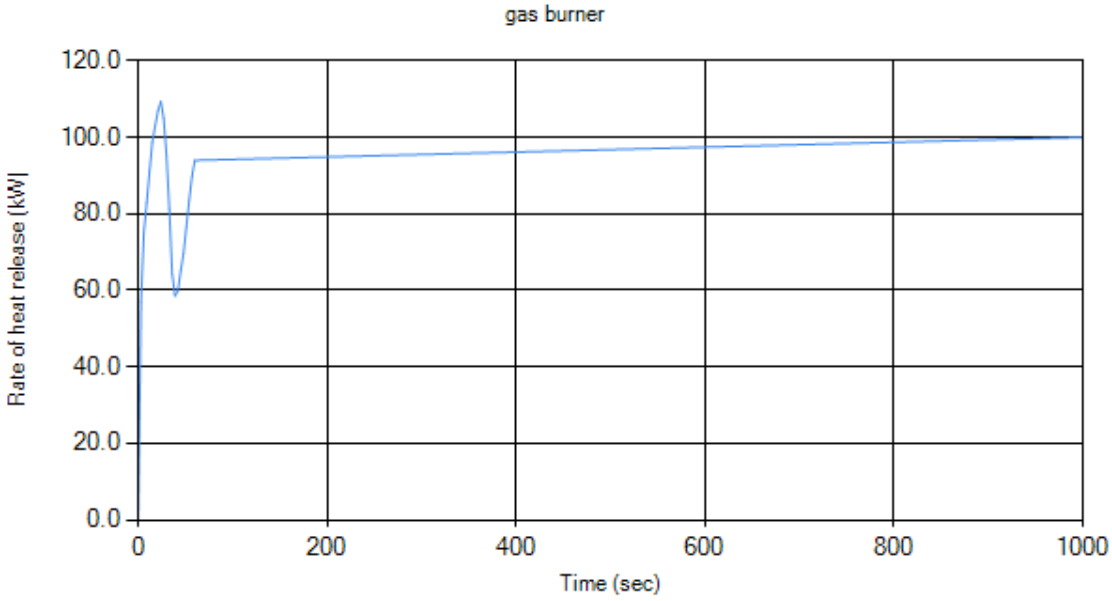


**Figure 75.** Furniture calorimeter experiment gas burner HRR for MDF–1

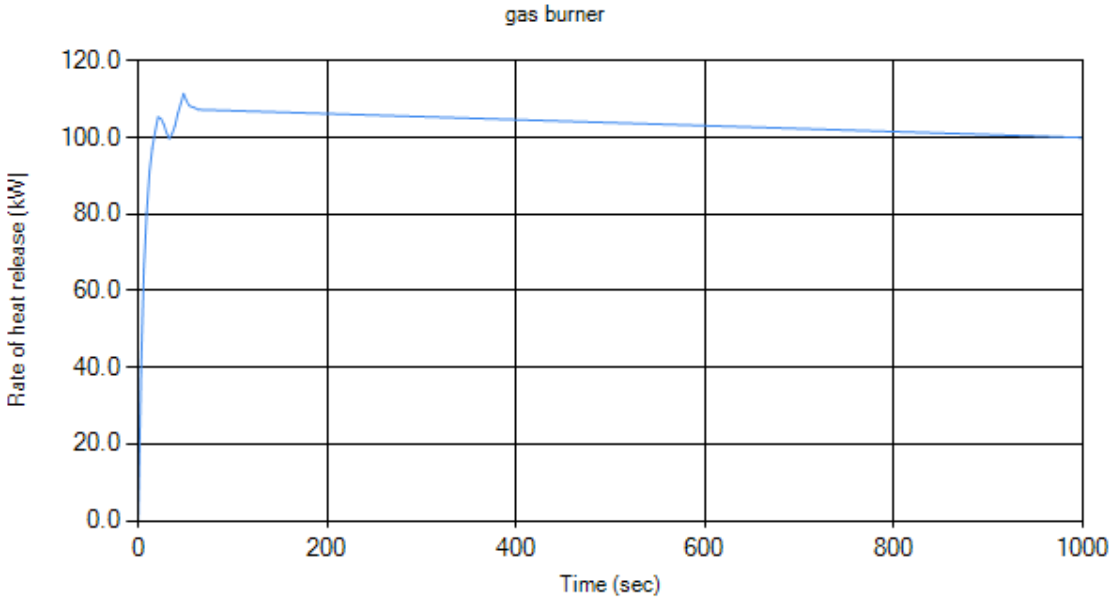


**Figure 76.** Furniture calorimeter experiment gas burner HRR for MDF–2

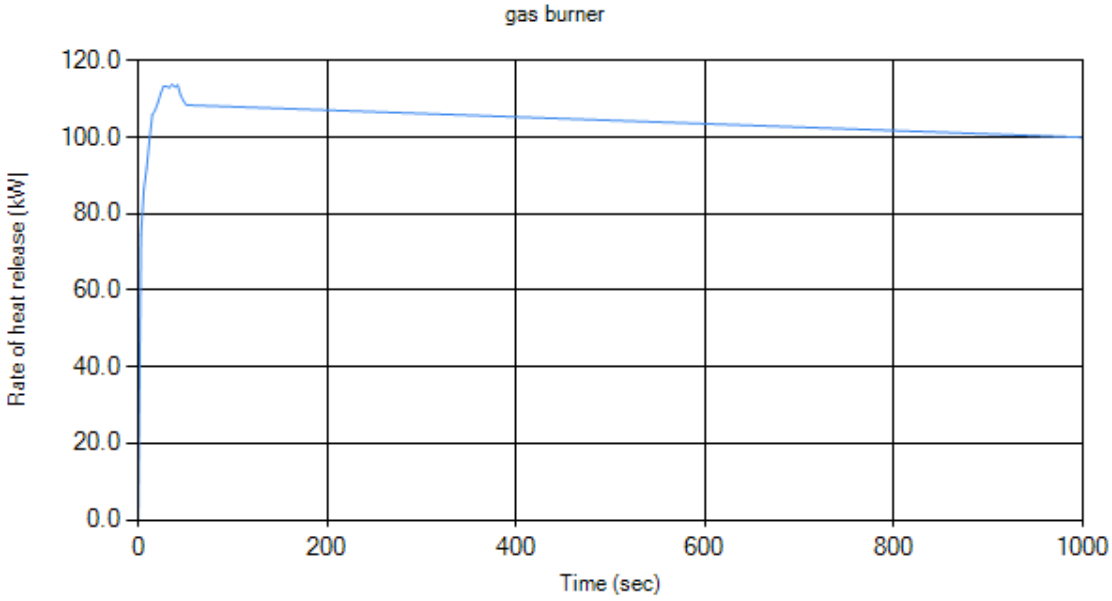


**Figure 77**. Furniture calorimeter experiment gas burner HRR for MDF–3

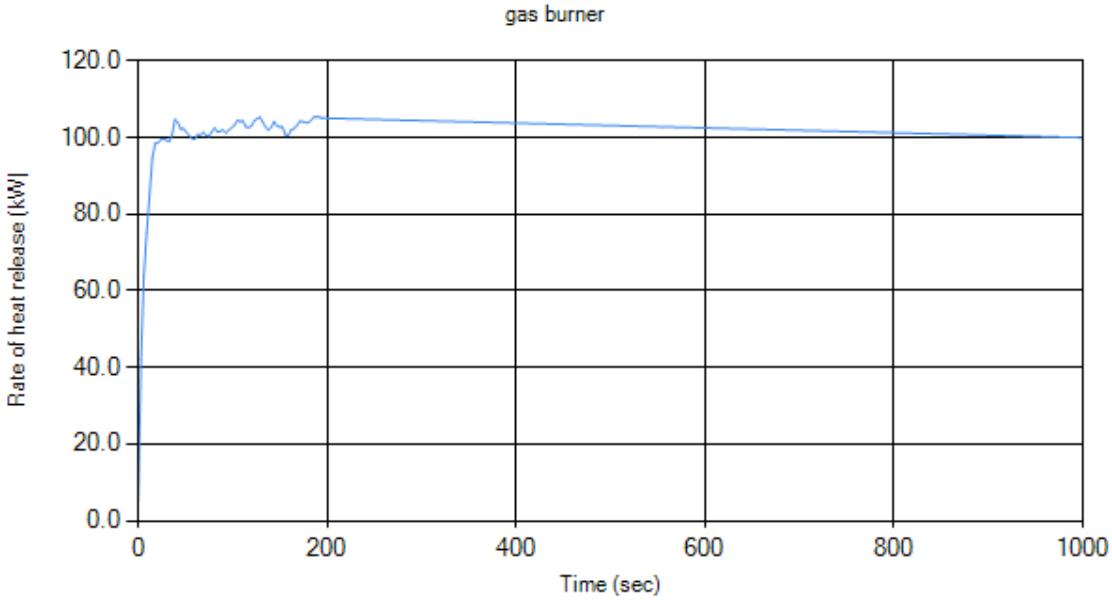


**Figure 78.** Furniture calorimeter experiment gas burner HRR for TV–1

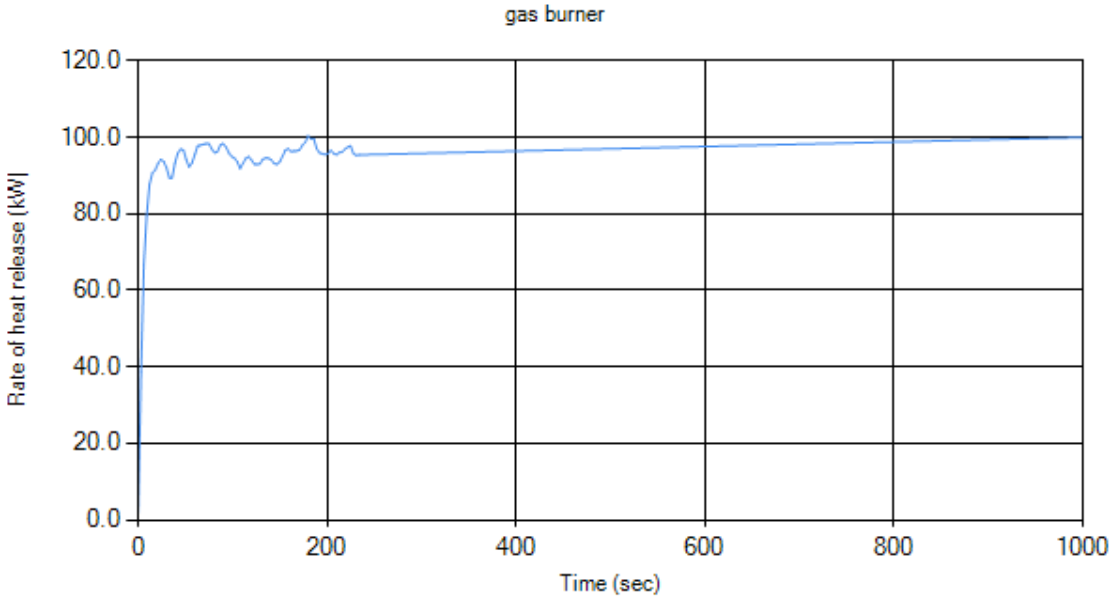


**Figure 79.** Furniture calorimeter experiment gas burner HRR for TV–2

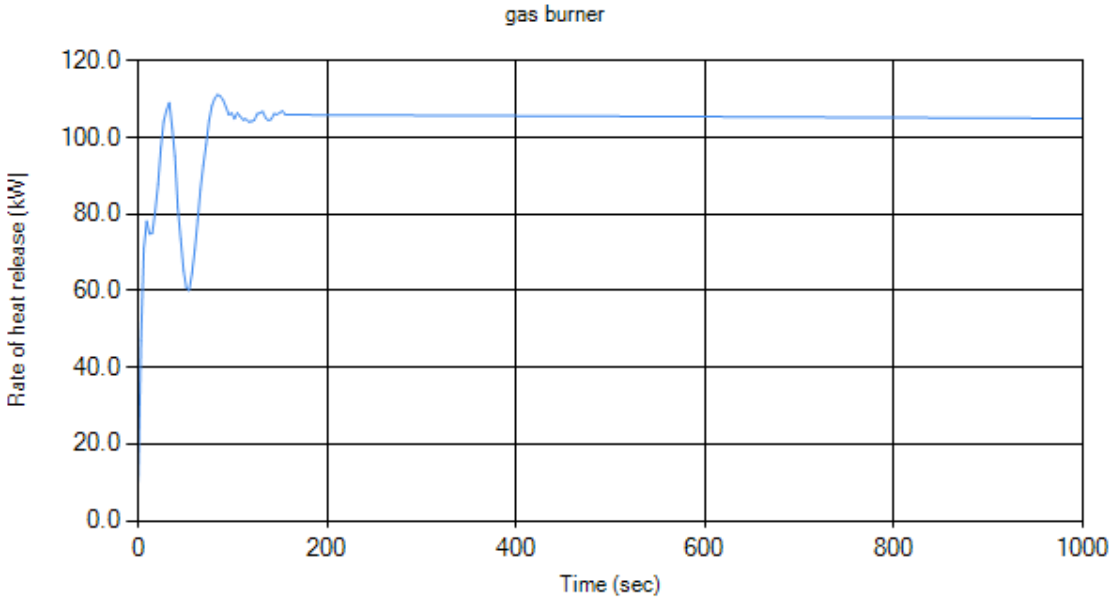


**Figure 80.** Furniture calorimeter experiment gas burner HRR for TV–3

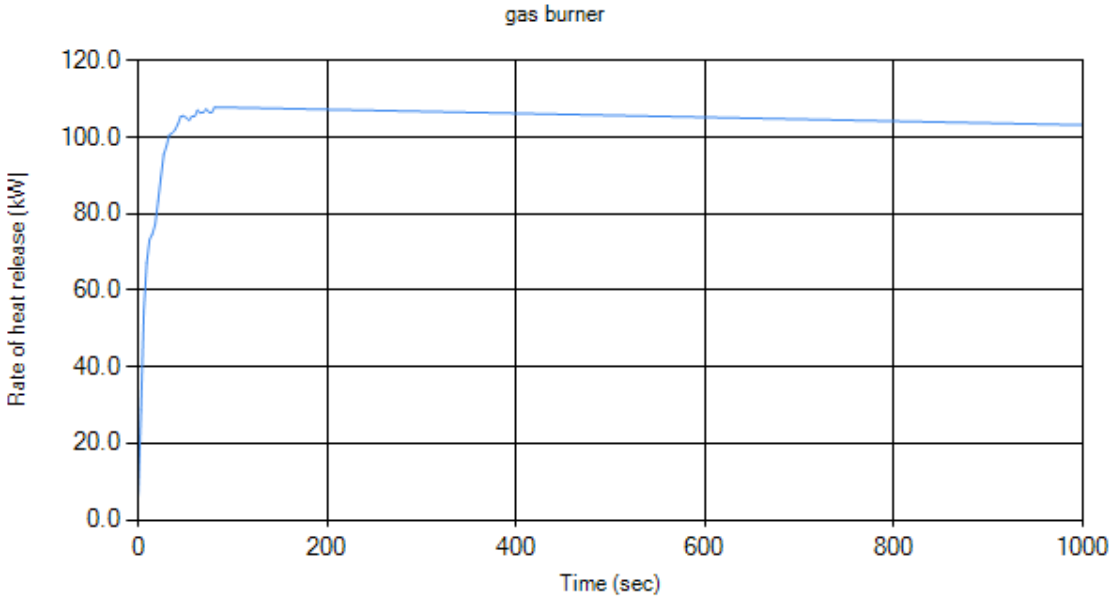


**Figure 81.** Single item in ISO 9705 room experiment gas burner HRR for Arm–A1

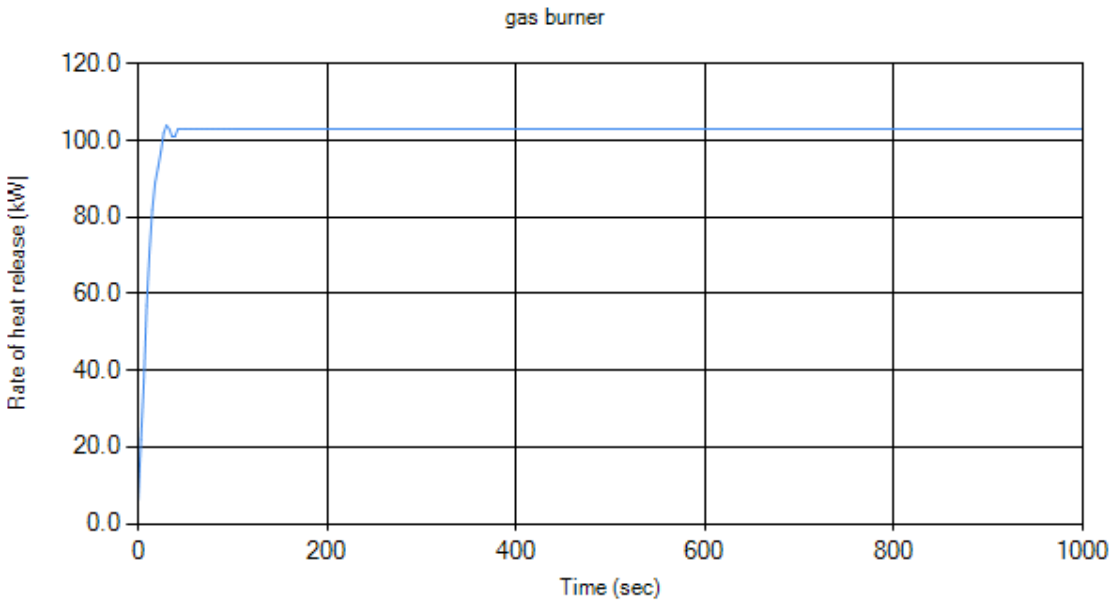


**Figure 82.** Single item in ISO 9705 room experiment gas burner HRR for Arm–A2

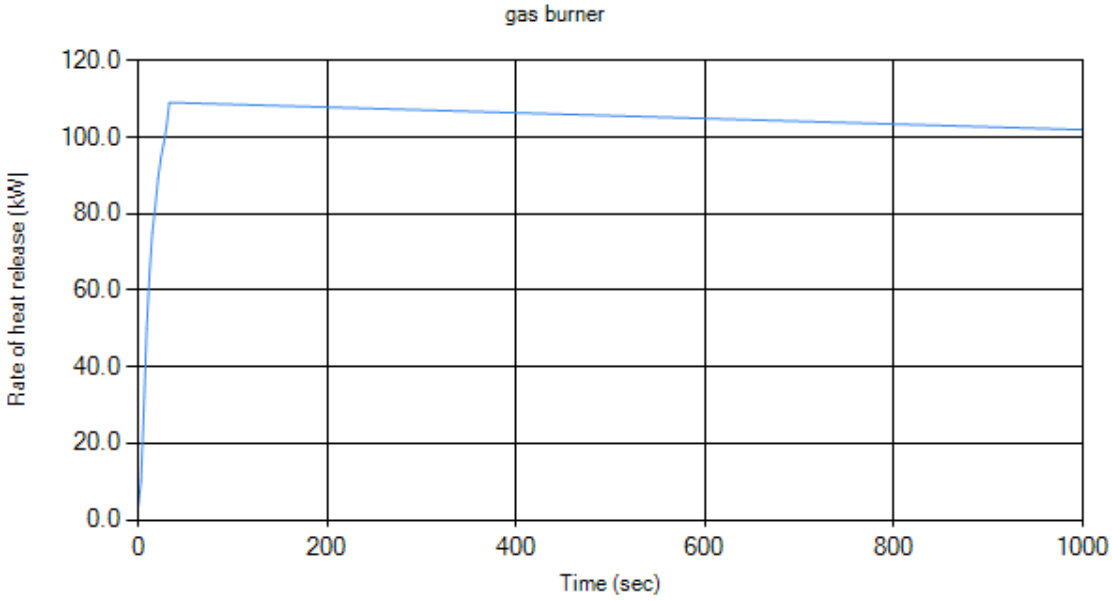


**Figure 83.** Single item in ISO 9705 room experiment gas burner HRR for Arm–A3

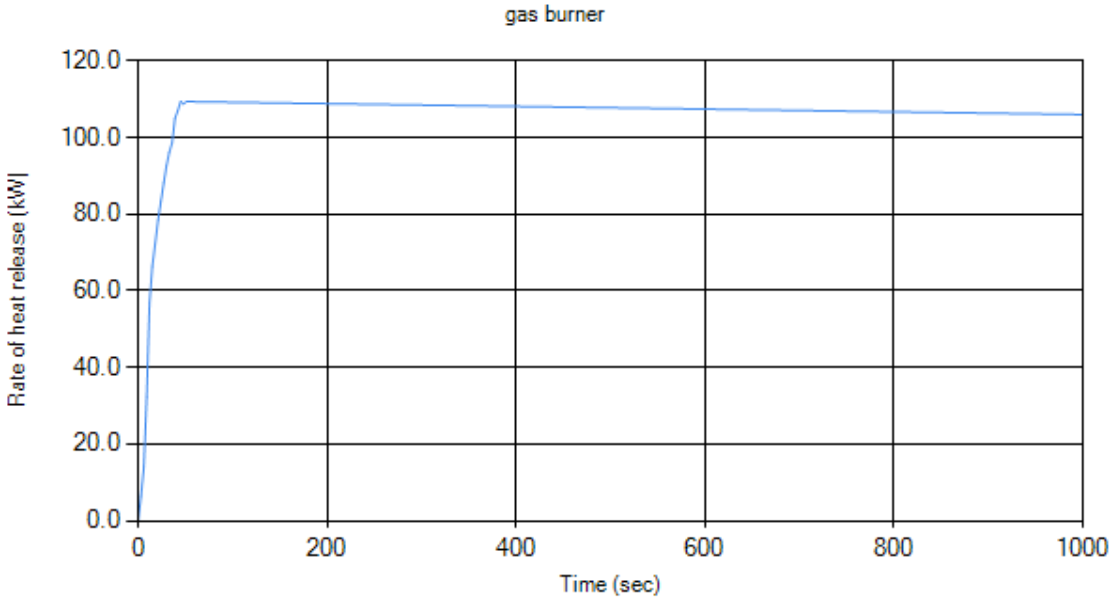


**Figure 84.** Single item in ISO 9705 room experiment gas burner HRR for Arm–B1

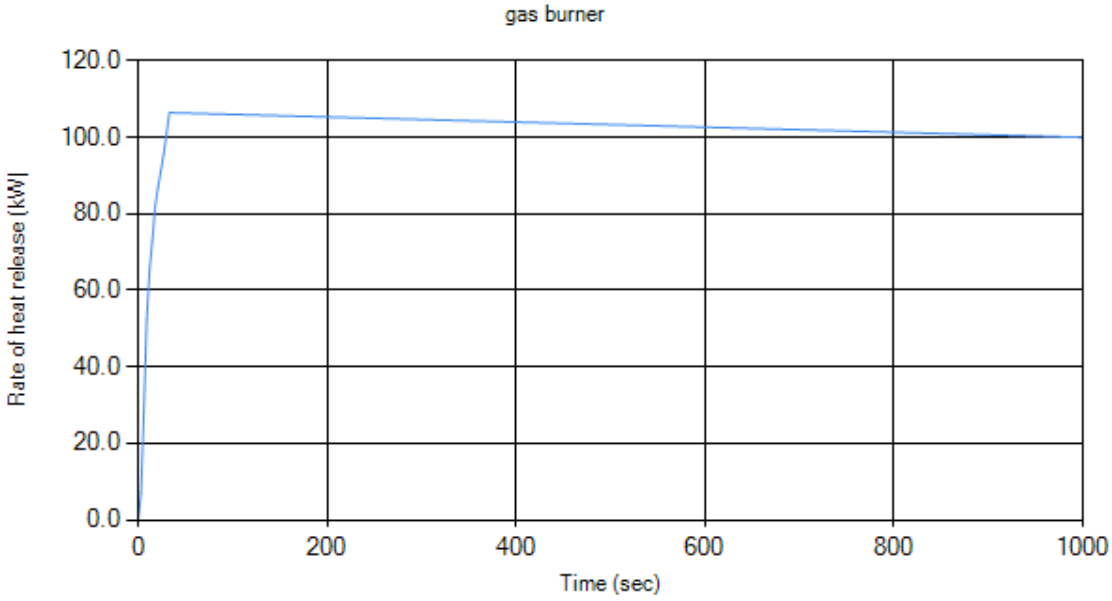


**Figure 85.** Single item in ISO 9705 room experiment gas burner HRR for Arm–B2

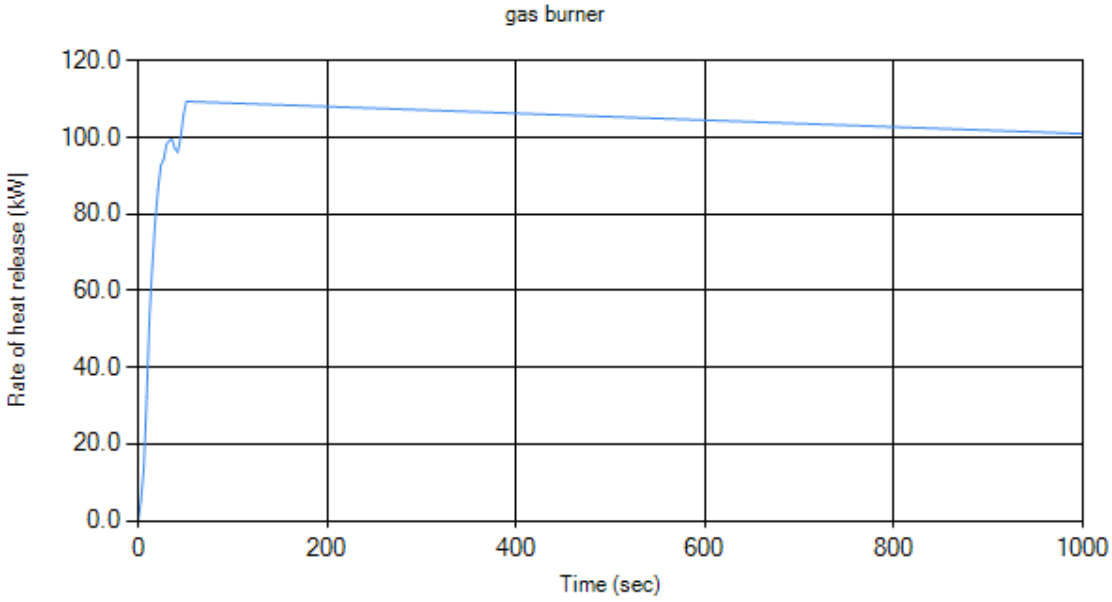


**Figure 86.** Single item in ISO 9705 room experiment gas burner HRR for Arm–B3

**Appendix C: Ignition times of item in B-RISK with the radial distance sensitivity analysis.**

| Arm-A<br>Scenario A<br>(Furniture Calorimeter) | Experiment ignition time (s) | | |
|---|---|---|---|
| | Arm-A1 | Arm-A2 | Arm-A3 |
| | 278 | 582 | 789 |
| | B-RISK ignition time (s) | | |
| | Arm-A1 | Arm-A2 | Arm-A3 |
| Assumed HRR 100kW at 300 mm | 44 | 44 | 44 |
| Gas burner at 300 mm | 72 | 119 | 93 |
| Redial distance at 310 mm | 151 | 231 | 206 |
| Redial distance at 315 mm | 214 | 333 | 355 |
| Best fit redial distance at 320 mm | 354 | 602 | 798 |
| Redial distance at 325 mm | 591 | 1022 | 1109 |

| Arm-B<br>Scenario B<br>(Furniture Calorimeter) | Experiment ignition time (s) | | |
|---|---|---|---|
| | Arm-B1 | Arm-B2 | Arm-B3 |
| | 75 | 105 | 85 |
| | B-RISK ignition time (s) | | |
| | Arm-B1 | Arm-B2 | Arm-B3 |
| Assumed HRR 100kW at 300 mm | 44 | 44 | 44 |
| Gas burner at 300 mm | 51 | 43 | 79 |
| Redial distance at 310 mm | 72 | 57 | 106 |
| Best fit redial distance at 315 mm | 90 | 68 | 131 |
| Redial distance at 320 mm | 117 | 86 | 170 |
| Redial distance at 325 mm | 161 | 114 | 239 |

| TV (Furniture Calorimeter) | Experiment ignition time (s) | | |
|---|---|---|---|
| | TV-1 | TV-2 | TV-3 |
| | 225 | 276 | 303 |
| | B-RISK ignition time (s) | | |
| | TV-1 | TV-2 | TV-3 |
| Assumed HRR 100kW at 300 mm | 64 | 64 | 64 |
| Gas burner at 300 mm | 70 | 85 | 91 |
| Redial distance at 310 mm | 98 | 129 | 115 |
| Redial distance at 315 mm | 117 | 163 | 132 |
| Redial distance at 320 mm | 142 | 203 | 153 |
| Redial distance at 325 mm | 176 | 226 | 181 |
| Best fit redial distance at 330 mm | 218 | 366 | 219 |

| MDF (Furniture Calorimeter) | Experiment ignition time (s) | | |
|---|---|---|---|
| | MDF-1 | MDF-2 | MDF-3 |
| | 57 | 62 | 51 |
| | B-RISK ignition time (s) | | |
| | MDF-1 | MDF-2 | MDF-3 |
| Assumed HRR 100kW at 300 mm | 7 | 7 | 7 |
| Gas burner at 300 mm | 7 | 9 | 6 |
| Redial distance at 310 mm | 9 | 10 | 7 |
| Redial distance at 315 mm | 10 | 11 | 8 |
| Redial distance at 320 mm | 11 | 12 | 9 |
| Redial distance at 325 mm | 12 | 13 | 10 |

| | | | |
|---|---|---|---|
| **Best fit redial distance at 390 mm** | **58** | **41** | **33** |

| **Arm-A** **Scenario A** **(Single Item in the ISO room)** | **Experiment ignition time (s)** | | |
|---|---|---|---|
| | **Arm-A1** | **Arm-A2** | **Arm-A3** |
| | **75** | **42** | **30** |
| | **B-RISK ignition time (s)** | | |
| | **Arm-A1** | **Arm-A2** | **Arm-A3** |
| **Assumed HRR 100kW at 300 mm** | **44** | **44** | **44** |
| **Gas burner at 300 mm** | **57** | **53** | **47** |
| **Redial distance at 310 mm** | **76** | **77** | **61** |
| **Redial distance at 315 mm** | **92** | **97** | **71** |
| **Redial distance at 320 mm** | **116** | **129** | **86** |

| **Arm-B** **Scenario B** **(Single Item in the ISO room)** | **Experiment ignition time (s)** | | |
|---|---|---|---|
| | **Arm-B1** | **Arm-B2** | **Arm-B3** |
| | **45** | **27** | **42** |
| | **B-RISK ignition time (s)** | | |
| | **Arm-B1** | **Arm-B2** | **Arm-B3** |
| **Assumed HRR 100kW at 300 mm** | **44** | **44** | **44** |
| **Gas burner at 300 mm** | **55** | **51** | **57** |
| **Redial distance at 310 mm** | **68** | **68** | **71** |
| **Redial distance at 315 mm** | **78** | **82** | **82** |
| **Redial distance at 320 mm** | **92** | **102** | **97** |

## Appendix D: photos from ISO room experiments


**Figure 87.** Scenario A-2 the gas burner was turned on and the experiment begin.

**Figure 88.** Scenario A-2 experiment showed the ignition of Arm-1.


**Figure 89.** Scenario A-2 pre flash-over in the ISO room.

**Figure 90.** Scenario A-2 after the experiments is ended in the ISO room.


**Figure 91.** Scenario A-3


**Figure 92.** Scenario A-3

**Figure 93.** Scenario A-3


**Figure 94.** Scenario B-2


**Figure 95.** Scenario B-2


**Figure 96.** Scenario B-2


**Figure 97.** Scenario D-2

.


**Figure 98.** Scenario D-2


**Figure 99.** Scenario D-2

**Figure 100.** Scenario D-2